

FE

Report 4708

ADA019417

EXPERIMENTAL INVESTIGATION OF THE HIGH VELOCITY COANDA WALL JET APPLIED TO BLUFF TRAILING EDGE CIRCULATION CONTROL AIRFOILS

DAVID W. TAYLOR
NAVAL SHIP RESEARCH AND DEVELOPMENT CENTER

Bethesda, Md. 20084



12

EXPERIMENTAL INVESTIGATION OF THE HIGH VELOCITY
COANDA WALL JET APPLIED TO BLUFF TRAILING EDGE
CIRCULATION CONTROL AIRFOILS

by

Robert J. Englar

APPROVED FOR PUBLIC RELEASE: DISTRIBUTION UNLIMITED

AVIATION AND SURFACE EFFECTS DEPARTMENT ✓
RESEARCH AND DEVELOPMENT REPORT

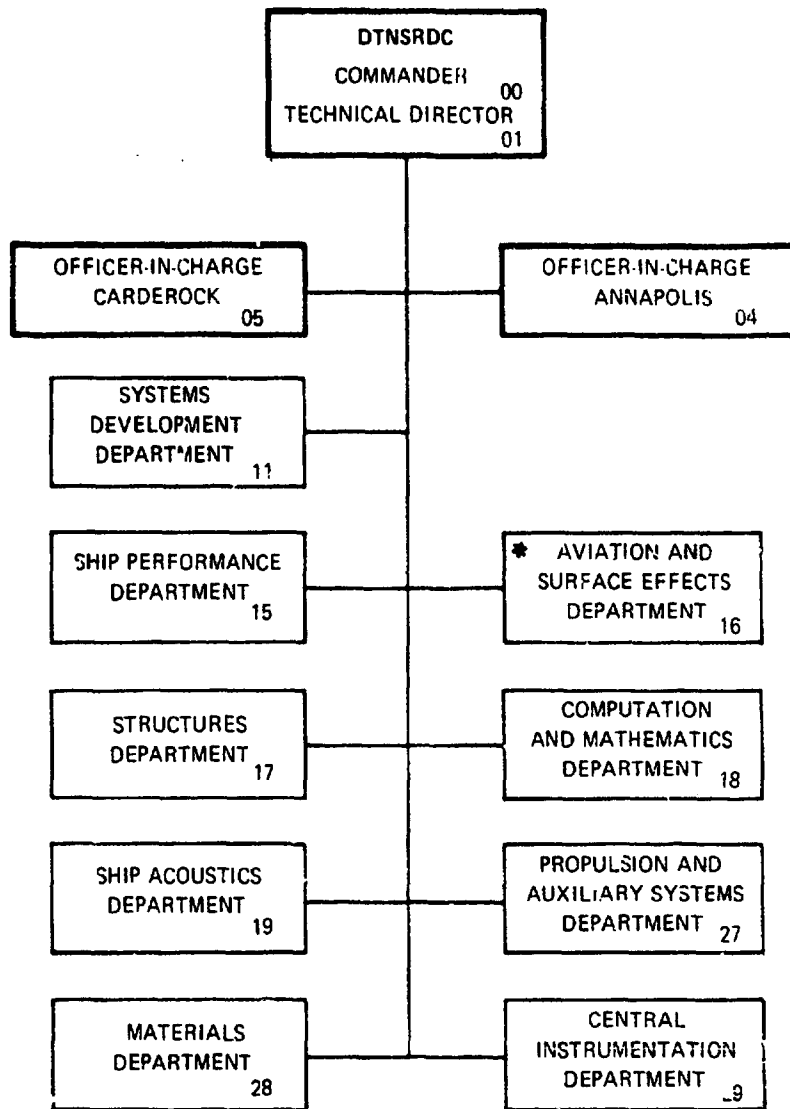
DDC
RECEIVED
JAN 14 1976
RECEIVED

September 1975

Report 4708

A

MAJOR DTNSRDC ORGANIZATIONAL COMPONENTS



UNCLASSIFIED

SECURITY CLASSIFICATION OF THIS PAGE (When Data Entered)

19 REPORT DOCUMENTATION PAGE		READ INSTRUCTIONS BEFORE COMPLETING FORM
1. REPORT NUMBER 18 DTNSRDC 4708	2. GOVT ACCESSION NO.	3. RECIPIENT'S CATALOG NUMBER
4. TITLE (and Subtitle) 6 EXPERIMENTAL INVESTIGATION OF THE HIGH VELOCITY COANDA WALL JET APPLIED TO BLUFF TRAILING EDGE CIRCULATION CONTROL AIRFOILS	5. TYPE OF REPORT & PERIOD COVERED 4 Aero Report 1213 ✓	
7. AUTHOR(s) 10 Robert J. Englar	8. CONTRACT OR GRANT NUMBER(s) 12 115 p.	
9. PERFORMING ORGANIZATION NAME AND ADDRESS David W. Taylor Naval Ship Research and Development Center Bethesda, Maryland 20084	10. PROGRAM ELEMENT, PROJECT, TASK AREA & WORK UNIT NUMBERS Project Order 3-0152, NR-215-215X Work Unit 1-1690-130	
11. CONTROLLING OFFICE NAME AND ADDRESS Office of Naval Research, Code 461 Arlington, Virginia 22217	12. REPORT DATE 11 September 75	13. NUMBER OF PAGES 115
14. MONITORING AGENCY NAME & ADDRESS (if different from Controlling Office) 16 ONR-PC-3-0152, NR-215-215X	15. SECURITY CLASS. (of this report) UNCLASSIFIED	
15a. DECLASSIFICATION/DOWNGRADING SCHEDULE		
16. DISTRIBUTION STATEMENT (of this Report) APPROVED FOR PUBLIC RELEASE: DISTRIBUTION UNLIMITED		
17. DISTRIBUTION STATEMENT (of the abstract entered in Block 20, if different from Report) 9 Research and development rept. Sep 75-Apr 73		ACCEPTION NO. DTIC DLC
18. SUPPLEMENTARY NOTES Supersedes AD-771690		
19. KEY WORDS (Continue on reverse side if necessary and identify by block number) (See reverse side)		
20. ABSTRACT (Continue on reverse side if necessary and identify by block number) A two-dimensional experimental investigation, intended to probe the mechanism for reduction in performance of circulation control elliptic airfoils in compressible flow, was conducted subsonically on a 20-percent-thick modified elliptic profile employing high Coanda wall jet velocities. The results include detailed pressure distributions (both normal and chordwise) and trailing edge shear stress measurements made with a hot film anemometer. (Continued on reverse side)		

DD FORM 1 JAN 73 1473

EDITION OF 1 NOV 68 IS OBSOLETE
S/N 0102-014-6601

UNCLASSIFIED

SECURITY CLASSIFICATION OF THIS PAGE (When Data Entered)

387 695

UNCLASSIFIED

SECURITY CLASSIFICATION OF THIS PAGE(When Data Entered)

(Block 19)

Circulation Control Airfoils
Coanda Wall Jet
Bluff Trailing Edge
Two-Dimensional High Lift Investigation
Elliptic Airfoil
Jet Detachment
Jet Separation
High Velocity Coanda Jet

Shear Stress Distribution
Hot Film Anemometer
Hot Film Probe Calibration
Transonic Wind Tunnel Blockage
Jet Normal Static Pressure Variation
Choked Wall Jet Velocity
Chordwise Static Pressure Distribution

(Block 20 Continued)

for a range of jet slot heights and jet total pressures corresponding to high subsonic, sonic, and supersonic jet velocities. Jet Mach numbers of almost 1.3 were found to have no adverse effects on the airfoil performance, and the degrading jet detachment phenomenon was never encountered. Significant differences in the jet flow field with and without an external free stream were noted, as was the deviation of the static pressure across the jet from a constant value as assumed in conventional boundary layer analysis. Airfoil lift performance was found to vary with slot height, and the detailed shear stress measurement enabled location of the jet separation point. Also discussed is the calibration and use of the hot film shear stress probe.

UNCLASSIFIED

SECURITY CLASSIFICATION OF THIS PAGE(When Data Entered)

PREFACE

This project was initiated in February 1971 to provide basic understanding into the aerodynamics of circulation control airfoils as part of an ongoing program of the Rotary Wing Division of the David W. Taylor Naval Ship Research and Development Center (DTNSRDC) to apply these airfoils to rotary wing aircraft. The author wishes to express his appreciation to the Office of Naval Research (Aeronautics, Code 461) for funding of the research and to the Aviation and Surface Effects Department of the DTNSRDC for use of its wind tunnels and computerized data reduction facilities. Additional appreciation is expressed to the Rotary Wing Division electronic technician, Mr. M. B. Stone, for setup and checkout of the electronic equipment and to Miss Rose M. McCrossin for typing of the manuscript.

The transonic blockage tests were conducted in September 1971, the hot film probe calibrations were done in the period December 1972–January 1973, and the subsonic two-dimensional wall jet investigations were performed from February through April 1973.

TABLE OF CONTENTS

ABSTRACT
ADMINISTRATIVE INFORMATION
INTRODUCTION
BACKGROUND AND LITERATURE REVIEW
TRANSONIC TESTS OF THIN CC SECTIONS
JET DETACHMENT LITERATURE REVIEW
INITIAL APPROACH
TRANSONIC AIRFOIL TRAILING EDGE INVESTIGATIONS
PROBLEM AREAS
TRANSONIC BLOCKAGE TESTS
MODELS AND TEST APPARATUS
TEST SECTION SURVEY
BLOCKAGE TESTS, NO BLOWING
FLOW FIELD DETAILS
EFFECTS OF MODEL BLOWING
CONCLUSIONS FROM BLOCKAGE TESTS
ALTERNATIVE TEST
HOT FILM SHEAR STRESS PROBE CALIBRATION
SHEAR STRESS MEASURING DEVICES
CALIBRATION TECHNIQUE
CALIBRATION APPARATUS AND PROCEDURE
CALIBRATION RESULTS AND DISCUSSION
SUBSONIC TWO-DIMENSIONAL INVESTIGATIONS
MODEL
TEST APPARATUS AND TECHNIQUE
RESULTS AND DISCUSSION OF SUBSONIC INVESTIGATIONS
STATIC TESTS (NO FREE STREAM) AND DYNAMIC
TESTS WITH STATIC PROBE INSTALLED
DYNAMIC TESTS WITH SLOT HEIGHT VARIATION
DETAILED TRAILING EDGE INVESTIGATIONS
CONCLUSIONS AND RECOMMENDATIONS
REFERENCES

LIST OF FIGURES

	Page
1 - Basic Circulation Control Aerodynamics	3
2 - Two-Dimensional Lift Characteristics of Blown Elliptic Airfoils	4
3 - Transonic Model Geometries	7
4 - Lift Variation with Mach Number at $\alpha = -1.2$ Degrees for Rounded Ellipse	8
5 - Lift Variation with Mach Number at $\alpha = -1.2$ Degrees for Pure Ellipse	9
6 - Comparison of CC Ellipses with Lift Performance of NACA 0012	10
7 - Comparative Lift Characteristics of the Three Transonic Models with $\alpha = -1.2$ Degrees	11
8 - Comparison of Maximum Equivalent Lift-to-Drag Ratio for the Three Configurations with $\alpha = -1.2$ Degrees	12
9 - Jet Detachment Limits for Coanda Wall Jet	14
10 - Choked and Unchoked Jet Static Pressure Distributions on a 90-Degree Deflection Surface with No Free Stream	16
11 - Comparison of Compressible Flow Results with Static and Subsonic Flow Jet Detachment Criteria	17
12 - Two-Dimensional Transonic Test Configuration	21
13 - Blockage Models and Test Setup	23
14 - Static Wall Tap Locations in 18- x 18-Inch Tunnel for CC Cylinder Test	24
15 - Blockage Test Setup	25
16 - Free-Stream Mach Number as a Function of Butterfly Valve Setting for Various Blocked Areas	26
17 - Choking Mach Number-Comparison of Theory and Experiment	28
18 - Mach Number Distributions, Tunnel Unchoked	29
19 - Mach Number Distributions, Tunnel Choked	30

	Page
20 – Mach Number Variation at Selected Taps with Butterfly Valve Variation, 1.5-Inch Cylinder	32
21 – Mach Number Variation at Selected Taps with Butterfly Valve Variation, 2.0-Inch Cylinder	33
22 – Effect of Model Blowing on Corrected Free-Stream Mach Number	34
23 – Effect of Model Blowing on Two Local Taps, 2-Inch Cylinder	35
24 – Details of Anemometer Circuitry	39
25 – Details of Annular Calibration Tunnel	43
26 – Annular Calibration Tunnel Setup	45
27 – Velocity, Dynamic Pressure, and Reynolds Number at the Calibration Station as a Function of Blower RPM	46
28 – Static Pressure Drop in Annulus Channel	47
29 – Sensor Voltage as a Function of Shear Stress, $R/R_0 = 1.2$ (3-Inch OD Pipe)	49
30 – Sensor Voltage as a Function of Shear Stress, $R/R_0 = 1.6$ (3-Inch OD Pipe)	51
31 – Sensor Voltage as a Function of Shear Stress for Five Overheat Ratios (3-Inch OD Pipe)	52
32 – Sensor Voltage as a Function of Shear Stress (4-Inch OD Pipe)	53
33 – Variation of Probe Cold Resistance with Temperature	54
34 – Comparison of Voltage-Shear Stress Relationship for 3- and 4-Inch OD Pipes, $R/R_0 = 1.8$	55
35 – Sensor Dissipated Power versus Shear Stress, $R/R_0 = 1.6$ (3-Inch OD Pipe)	56
36 – Comparison of Sensor Power-Shear Stress Relationship for 3- and 4-Inch OD Pipes, $R/R_0 = 1.8$	58
37 – Details of Two-Dimensional Subsonic Model	61
38 – Trailing Edge Cylinder and Static Probe Detail	62
39 – Model Installation in the 15- x 20-Inch Tunnel	64

	Page
40 - Subsonic Two-Dimensional Test Setup and Equipment	65
41 - Trailing Edge Static Pressure Distribution with No Free Stream, $h = 0.100$ Inch, $q_{\infty} = 0$	68
42 - Trailing Edge Static Pressure Distributions for Choked and Unchoked Slot with No Free Stream, $h = 0.100$ Inch, $q_{\infty} = 0$	70
43 - Trailing Edge Static Pressure Distributions with No Free Stream, $h = 0.050$ Inch, $q_{\infty} = 0$	71
44 - Normal Static Pressure Variation across Jet, $h = 0.100$ Inch, $q_{\infty} = 0$	73
45 - Normal Static Pressure Variation across Jet, $h = 0.100$ Inch, $q_{\infty} = 22$ PSF	74
46 - Wall Shear Stress as a Function of Duct Pressure, $h = 0.050$ Inch, $q_{\infty} = 0$	77
47 - Skin Friction as a Function of Blowing for Various Slot Heights, $\theta_{HF} = 48$ Degrees	78
48 - Airfoil Lift as a Function of Blowing, $\alpha = 0$ Degree, $\theta_{HF} = 0$ Degree	79
49 - Airfoil Static Pressure Distributions, $h = 0.050$ Inch, $q_{\infty} = 27.5$ PSF, $\alpha = 0$ Degree	81
50 - Airfoil Static Pressure Distributions, $h = 0.013$ Inch, $q_{\infty} = 27.5$ PSF, $\alpha = 0$ Degree	82
51 - Trailing Edge Pressure Distributions, $h = 0.013$ Inch, $q_{\infty} = 27.5$ PSF	84
52 - Trailing Edge Pressure Distributions, $h = 0.032$ Inch, $q_{\infty} = 27.0$ PSF	85
53 - Shear Stress Distributions for Five Duct Pressures, $h = 0.013$ Inch, $q_{\infty} = 27.5$ PSF	87
54 - Shear Stress Distributions for Four Duct Pressures, $h = 0.032$ Inch, $q_{\infty} = 27.5$ PSF	88
55 - Oscilloscope Traces for $h = 0.032$ Inch, $P_d = 10$ In. Hg, $q_{\infty} = 27.5$ PSF	90
56 - Skin Friction Coefficient Distributions for Five Momentum Coefficients, $h = 0.013$ Inch, $q_{\infty} = 27.5$ PSF	93

	Page
57 - Skin Friction Coefficient Distributions for Four Momentum Coefficients, $h = 0.032$ Inch, $q_{\infty} = 27.5$ PSF	94
58 - Skin Friction as a Function of Blowing for Constant Angular Position, $h = 0.032$ Inch, $q_{\infty} = 27.5$ PSF	95
59 - Location of Jet Separation Point for Two Slot Heights as a Function of Blowing, $q_{\infty} = 27.5$ PSF	96

NOTATION

A_b	Model blocked area, ft ²
A_j	Model slot area, ft ²
b	Model span, ft
C_d	Profile drag coefficient
C_{d_e}	Equivalent drag coefficient (Equation (2))
C_f	Skin friction coefficient
C_l	Section lift coefficient
C_p	Pressure coefficient
C'_p	Pressure coefficient, no free-stream flow
C_μ	Momentum coefficient (Equation (1))
c	Model chord, ft
d_3	Effective annulus height, 3-inch OD inner pipe
d_4	Effective annulus height, 4-inch OD inner pipe
E_b	Anemometer bridge voltage, volts
E_s	Sensor operating voltage, volts
g	Gravitational acceleration, ft/sec ²
h	Model slot height, ft
I, I_b	Anemometer bridge current, amps
i	Current, amps
L_s	Hot film sensor length, ft
M_∞	Free-stream Mach number
M_j	Jet Mach number

m	Mass flux, slug/sec
P_d, p_d	Duct (plenum) total pressure, lb/ft ²
P_{ij}	Static pressure at inside jet boundary, lb/ft ²
P_{oj}	Static pressure at outside jet boundary, lb/ft ²
P_R	Prandtl number
P_s	Sensor operating power, watts
P_t	Free stream total pressure, lb/ft ²
P_{∞}, p_{∞}	Free stream static pressure, lb/ft ²
p	Local static pressure, lb/ft ²
Q_w	Hot film heat loss
q_{∞}	Free stream dynamic pressure, lb/ft ²
R	Model trailing edge radius, ft
R	Sensor operating resistance, ohms
R_c	Reynolds number based on model chord
R_{c_d}	Reynolds number based on effective annulus height (d_3 or d_4)
R_{leads}	Resistance of hot film leads, ohms
R_p	Probe operating resistance, ohms
R_{pipe}	Pipe radius, ft
R_{P0}	Probe cold resistance, ohms
R_0	Sensor cold resistance, ohms
R_1	Universal gas constant, ft lb/lb/°R
R_3	Anemometer fixed resistance, ohms

R_a	Anemometer adjustable resistance, ohms
S	Model planform area, ft^2
s	Arc distance from slot, ft
T	Probe operating temperature, $^{\circ}\text{C}$
T_d	Duct (plenum) total temperature, $^{\circ}\text{R}$
T_s	Sensor operating temperature, $^{\circ}\text{C}$
T_w	Wall temperature, $^{\circ}\text{C}$
T_0	Free stream reference temperature, $^{\circ}\text{C}$
t	Model thickness, ft
U_τ	Friction velocity $(\tau_w/\rho)^{1/2}$
u, v	Local velocity, ft/sec
V_j	Jet velocity, ft/sec
V_∞	Free stream velocity, ft/sec
x	Distance from airfoil leading edge or annular tunnel entrance, ft
y	Normal distance from surface, ft
α, α_g	Geometric incidence, deg
α_T	Temperature coefficient of resistance, per $^{\circ}\text{C}$
γ	Ratio of specific heats
δ	Vertical displacement of cambered mean line from chord line, ft
η	Incremental radial distance, ft
θ	Angular position from slot, deg
θ_{HF}	Hot film angular location from slot, deg
θ_{SP}	Static probe angular location from slot, deg
$\theta_{s,p}$	Location of jet separation from slot, deg

λ	Thermal conductivity
μ	Coefficient of viscosity, lb sec/ft ²
ν	Kinematic viscosity, ft ² /sec
ρ_j	Jet density, slug/ft ³
ρ_∞	Free stream density, slug/ft ³
τ_w	Wall shear stress, lb/ft ²

ABSTRACT

A two-dimensional experimental investigation, intended to probe the mechanism for reduction in performance of circulation control elliptic airfoils in compressible flow, was conducted subsonically on a 20-percent-thick modified elliptic profile employing high Coanda wall jet velocities. The results include detailed pressure distributions (both normal and chordwise) and trailing edge shear stress measurements made with a hot film anemometer for a range of jet slot heights and jet total pressures corresponding to high subsonic, sonic, and supersonic jet velocities. Jet Mach numbers of almost 1.3 were found to have no adverse effects on the airfoil performance, and the degrading jet detachment phenomenon was never encountered. Significant differences in the jet flow field with and without an external free stream were noted, as was the deviation of the static pressure across the jet from a constant value as assumed in conventional boundary layer analysis. Airfoil lift performance was found to vary with slot height, and the detailed shear stress measurement enabled location of the jet separation point. Also discussed is the calibration and use of the hot film shear stress probe.

ADMINISTRATIVE INFORMATION

The work presented herein was conducted for the Office of Naval Research (Aeronautics, Code 461) as Project Order 3-0152, NR215-215X and was accomplished in the time period September 1971 to April 1973. Preparation of this report was funded under Work Unit 4-1600-001.

The material was issued earlier as NSRDC Technical Note AL-308 in June 1973, and had previously been submitted in partial fulfillment of requirements for the degree of Master of Science, Aerospace Engineering, from the University of Maryland. Thus in some details it deviates from traditional format of the David W. Taylor Naval Ship Research and Development Center (DTNSRDC).

INTRODUCTION

The application of tangential blowing over the bluff trailing edge of elliptic airfoil profiles offers very high lift generation at relatively low blowing rates, in addition to the phenomenon of lift production essentially independent of angle of attack. These properties make circulation control (CC) airfoils, as they have come to be known, quite desirable for application to helicopter rotors, where the necessary cyclic pitch variation around the blade

azimuth can now be achieved by cyclic blowing on blades of fixed incidence.¹⁻³ This offers a large payoff in reduction of the mechanical complexity presently associated with cyclic variation in the blade pitch as well as the capability for high blade lift at aerodynamic efficiencies similar to conventional rotor airfoils.*

The basis of operation of the circulation control airfoil section is dependent on the well known "Coanda effect" where a low pressure sheet of air remains attached to the curved trailing edge of the airfoil primarily due to the balance between centrifugal force in the jet and the reduced pressure at the wall due to the jet velocity (Figure 1). Initially, the device is a very effective boundary layer control (BLC) due to entrainment of flow from the upper surface; at higher blowing rates, however, BLC yields to supercirculation (large stagnation point movement and greater circulation than that obtained solely by entraining the boundary layer). When this occurs, the jet controls the location of the aft stagnation point (and thus the forward one as well) and the airfoil experiences an increase in effective camber and the associated lift. As the typical lift versus momentum coefficient curve of Figure 1 shows, maximum lift augmentation ($\Delta C_l/C_{\mu}$) occurs in the BLC region whereas higher lift is associated with higher blowing and supercirculation. Figure 2 presents some characteristic two-dimensional lift data typical of low speed performance.⁴⁻⁶

Practical application of these CC airfoils to a helicopter rotor implies that their operation at high subsonic or transonic speeds must be established since the tip section of the advancing blade would have to operate at these velocities. In addition to the compressible flow field which will be experienced, the airfoil must operate with considerably higher jet velocities in order to have any effect on the high speed surroundings. A two-dimensional transonic test of two thin CC airfoil sections was run over a Mach number range from 0.3 to 0.9 to investigate the properties of these blown airfoils at higher operational speeds.⁷ These results indicated

¹Cheeseman, I. C. and A. R. Seed, "The Application of Circulation Control Blowing to Helicopter Rotors," Journal of the Royal Aeronautical Society, Feb and Jul 1966. A complete listing of references is given on pages 99 through 101.

²Wilkerson, J. B., K. R. Reader, and D. W. Linck, "The Application of Circulation Control Aerodynamics to a Helicopter Rotor Model," Paper 704, 29th Annual National Forum of the American Helicopter Society, Washington, D. C., May 1973.

³Williams, R. M. and E. O. Rogers, "Design Considerations of Circulation Control Rotors," Paper 603, 28th Annual National Forum of the American Helicopter Society, Washington, D. C., May 1972.

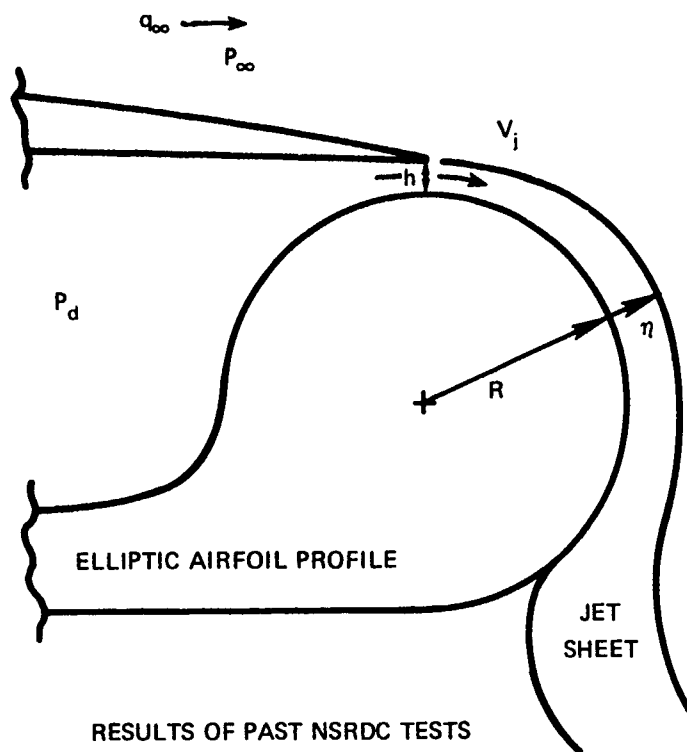
⁴Englar, R. J., "Two-Dimensional Subsonic Wind Tunnel Tests of Two 15-Percent Thick Circulation Control Airfoils," Aug 1971, Naval Ship Research and Development Center Tech Note AL-211. (AD 900 210L)

⁵Englar, R. J., "Two-Dimensional Subsonic Wind Tunnel Tests of a Cambered 30-Percent Thick Circulation Control Airfoil," May 1972, Naval Ship Research and Development Center Tech Note AL-201. (AD 913-411L)

⁶Williams, Robert M. and Harvey J. Howe, "Two-Dimensional Subsonic Wind Tunnel Tests on a 20-Percent Thick, 5-Percent Cambered Circulation Control Airfoil," Washington, D.C., Aug 1970, Naval Ship Research and Development Center Tech Note AL-176. (AD 877-764)

⁷Englar, R. J., "Two-Dimensional Transonic Wind Tunnel Tests of Three 15-Percent Thick Circulation Control Airfoils," Dec 1970, Naval Ship Research and Development Center Tech Note AL-182. (AD 882-075)

*This latter property of high lift may be extended to fixed wing aircraft for STOL application.



TANGENTIAL BLOWING OVER
ROUNDED COANDA SURFACE

PRESSURE-CENTRIFUGAL
FORCE BALANCE:

$$\frac{dP}{d\eta} = \frac{\rho V_j^2}{R + \eta}$$

RESULTS OF PAST NSRDC TESTS

1. $C_l > 6.5$ FOR $C_\mu < 0.25$
2. $\Delta C_l / C_\mu = 70$
3. LIFT INDEPENDENT OF INCIDENCE

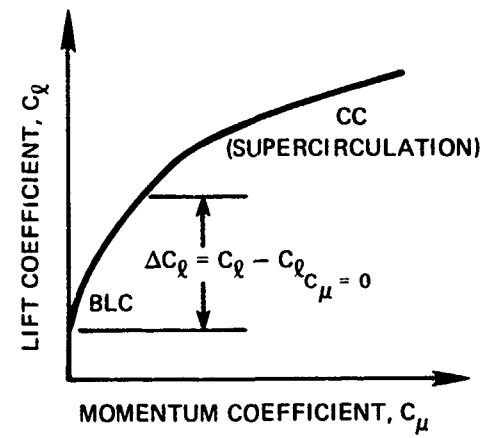


Figure 1 - Basic Circulation Control Aerodynamics

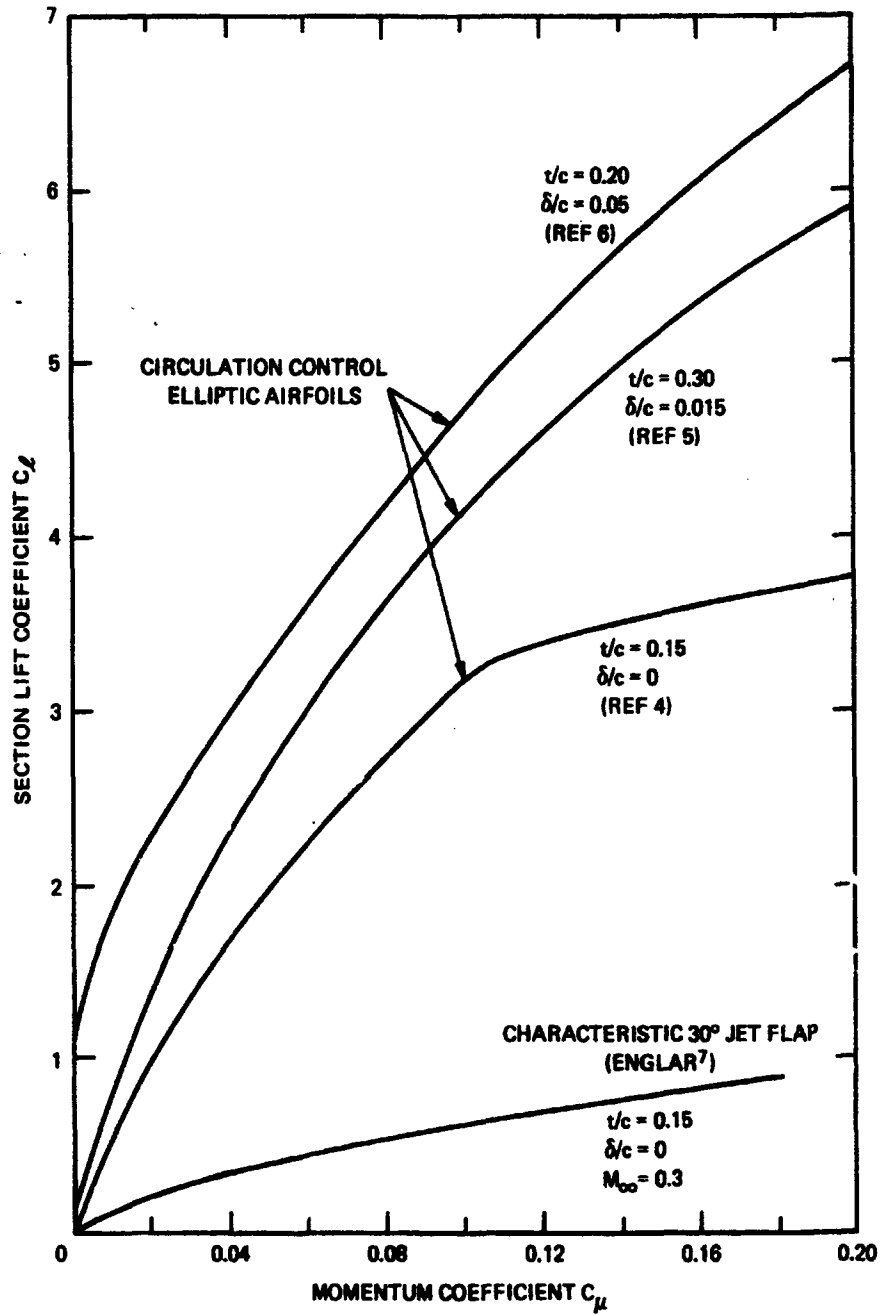


Figure 2 - Two-Dimensional Lift Characteristics of Blown Elliptic Airfoils

that airfoil performance is heavily dependent on the Coanda turning of the high velocity trailing edge wall jet and that certain phenomena are present, especially in the case of the choked or underexpanded jet, which may lead to premature separation (detachment) of the jet and subsequent loss of lift augmentation. It is, therefore, the purpose of this paper to experimentally investigate the characteristics of this high velocity Coanda wall jet on a CC airfoil with external flow and the resulting performance of the airfoil below, at, and above the choked nozzle flow condition.

BACKGROUND AND LITERATURE REVIEW

The Coanda principle has found many and varied uses in the field of aerodynamics as a flow turning device and its application as a lift augmentor has been well documented. (Stone and Englar⁸ provide a partial bibliography.) Its application to elliptic airfoil sections was patented by Griswold⁹ in 1959, and subsonic tests of this and similar devices have been plentiful. However, application of the device to transonic airfoils has only been considered more recently (for example, Kizilos and Rose¹⁰) and it was because of the lack of information that Englar conducted two-dimensional tests earlier.⁷ The results of these tests displayed performance trends that were, in certain respects, considerably different from the subsonic airfoil characteristics, and they identified a degradation of lift performance that was apparently caused by premature separation (or detachment) of the jet from the trailing edge at higher speeds.

TRANSONIC TESTS OF THIN CC SECTIONS

Compressible flow considerations dictate a thin section for blade tip operation, but the CC section must be thicker than conventional high-speed airfoils in that the blunt trailing edge must be sufficiently thick to yield good Coanda turning. (Englar and Williams¹¹ provide constraints on subsonic trailing edge design parameters to achieve this effect.) A potential flow investigation of the critical Mach numbers of various thickness ellipses over the required range of transonic lift coefficients indicated that an ellipse of 15-percent thickness-to-chord ratio was a sufficient compromise with regards to critical Mach number and trailing edge

⁸Stone, M. B. and R. J. Englar, "Circulation Control—A Bibliography with Selected References," Jul 1973, Naval Ship Research and Development Center Report 4108.

⁹Griswold, R. W., "Circulatory Jet Airfoils," United States Patent 2,885,160, 5 May 1959.

¹⁰Kizilos, A. P. and R. E. Rose, "Experimental Investigations of Flight Control Surfaces Using Modified Air Jets," St. Paul, Minn., Nov 1969, Honeywell, Inc. Document 12055-FR1, (DDC AD 864-2716).

¹¹Englar, R. J. and R. M. Williams, "Design of a Circulation Control Stern Plane for Submarine Applications," Mar 1971, Naval Ship Research and Development Center Tech Note AL-200. (AD 901-198)

geometry. As a result, the three geometric ellipse models of Figure 3 were constructed. The jet flap configuration was included as a reference airfoil whose lift augmentation ability had already been established. Coanda blowing over a cylindrical trailing edge with the slot located at 96-percent chord composed one of the CC sections while blowing over a pure elliptic trailing edge comprised the other. The "rounded ellipse," as the first was called, was of the general geometry known to yield high lift augmentation at subsonic speeds (this was later verified by Englar in subsonic tests⁴). The "pure ellipse," with the slot at the same distance from the leading edge as that of the rounded ellipse, had a much larger local radius of curvature downstream of the slot; it was expected to produce less turning but also smaller trailing edge suction peaks and reduced adverse pressure gradients. Figures 4 and 5 present the resulting lift coefficients as a function of Mach number for the two CC ellipses at a constant $\alpha = -1.2$ degrees and constant momentum coefficient, defined as

$$C_{\mu} = \frac{\dot{m}V_j}{q_{\infty}S} = \frac{2\rho_j A_j V_j^2}{\gamma p_{\infty} M_{\infty}^2 S} \quad (1)$$

The lift coefficient for the rounded ellipse shows a strong decrease with increasing Mach number at constant blowing rate, a trend that is definitely opposite to the normal compressibility-produced lift increase with M_{∞} . The pure ellipse shows the conventional trend up to a certain value of M_{∞} for constant C_{μ} ; then a sharp lift decrease is experienced also. Airfoil performance relative to a standard rotor tip section, the NACA 0012, is shown in Figure 6, where substantial lift at low or negative incidence is apparent. The maximum C_l values obtained over the test range of $C_{\mu} \leq 0.08$ for the three airfoils including the jet flap are compared in Figure 7. A similar comparison for maximum equivalent efficiency (C_l/C_{d_e}) is shown in Figure 8. (In this latter parameter, the equivalent drag coefficient in the denominator is defined as

$$C_{d_e} = C_d + C_{\mu} \frac{V_j}{2V_{\infty}} + C_{\mu} \frac{V_{\infty}}{V_j} \quad (2)$$

where, as the detailed derivation by Englar⁵ points out, the second and third terms account for the energy required to produce the blowing and thus allow direct comparison to the efficiency of conventional airfoils.) Maximum efficiency for the rounded ellipse occurs at $M_{\infty} = 0.4$, while the pure ellipse extends the maximum to $M_{\infty} = 0.7$. These comparative results, plus similar trends presented in Kizilos and Rose,¹⁰ suggest that the reduction in performance at higher subsonic speeds may be strongly dependent on one or more of the following:

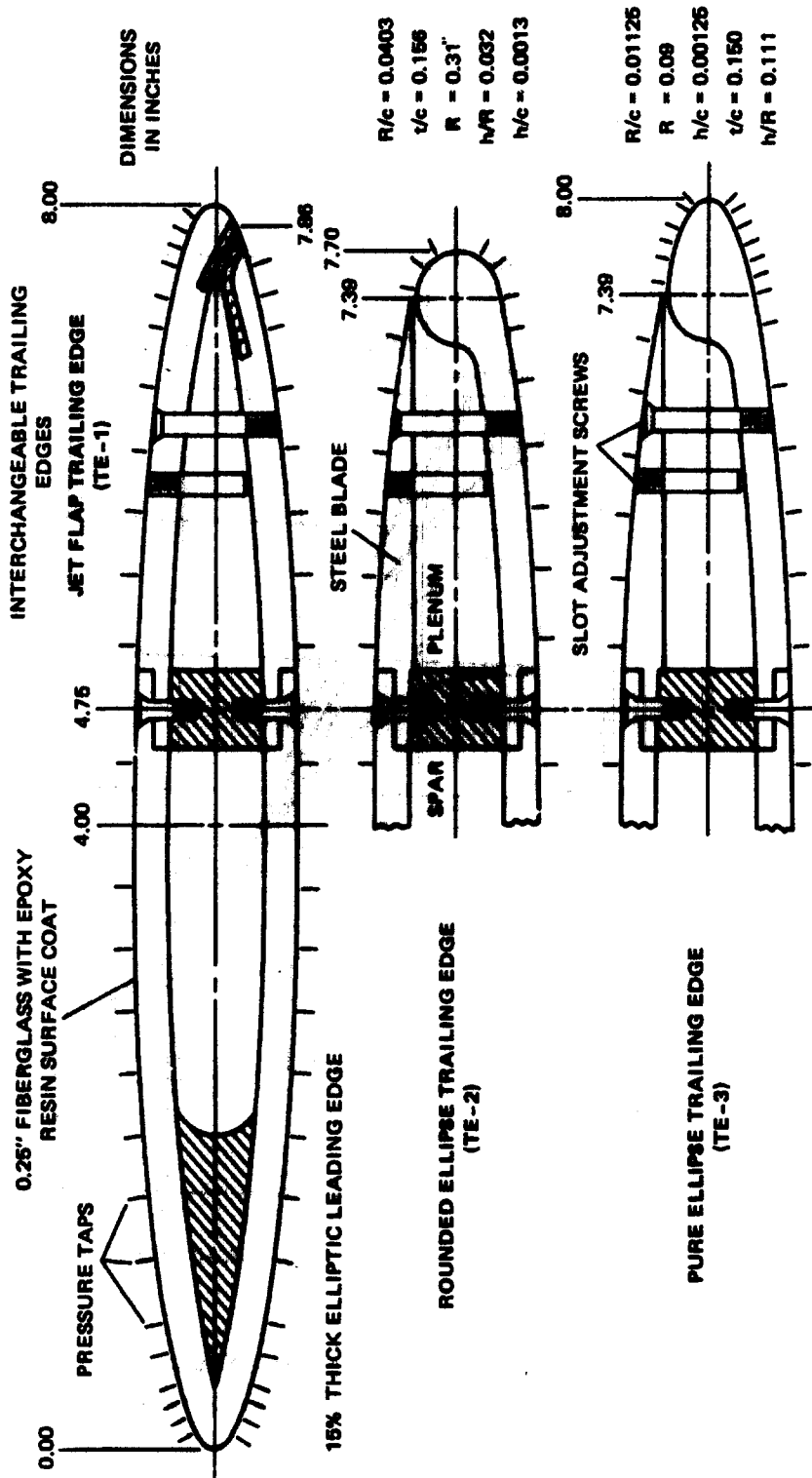


Figure 3 -- Transonic Model Geometries
(From Englar⁷)

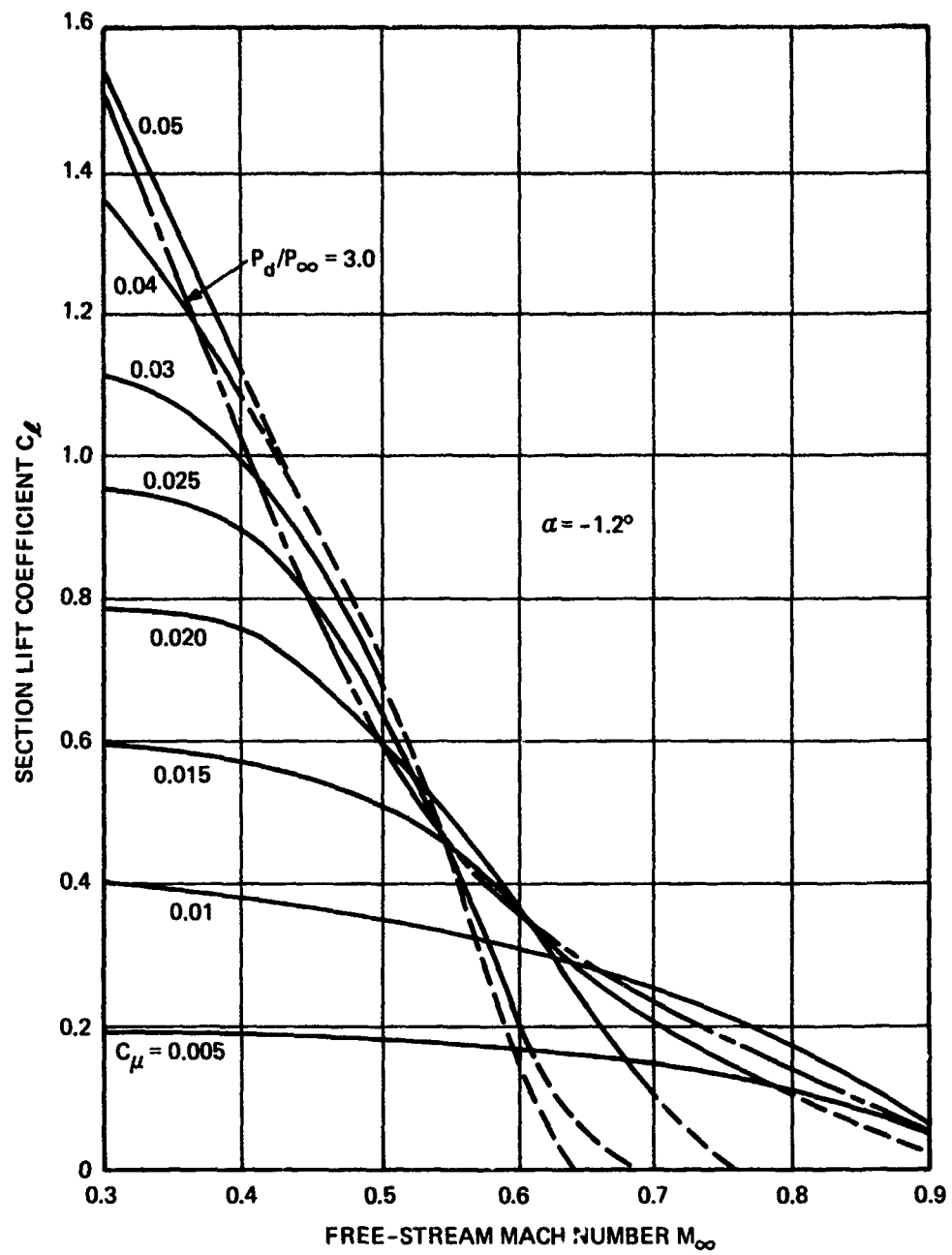


Figure 4 - Lift Variation with Mach Number at $\alpha = -1.2$ Degrees for Rounded Ellipse
(Model TE-2 in Englar⁷)

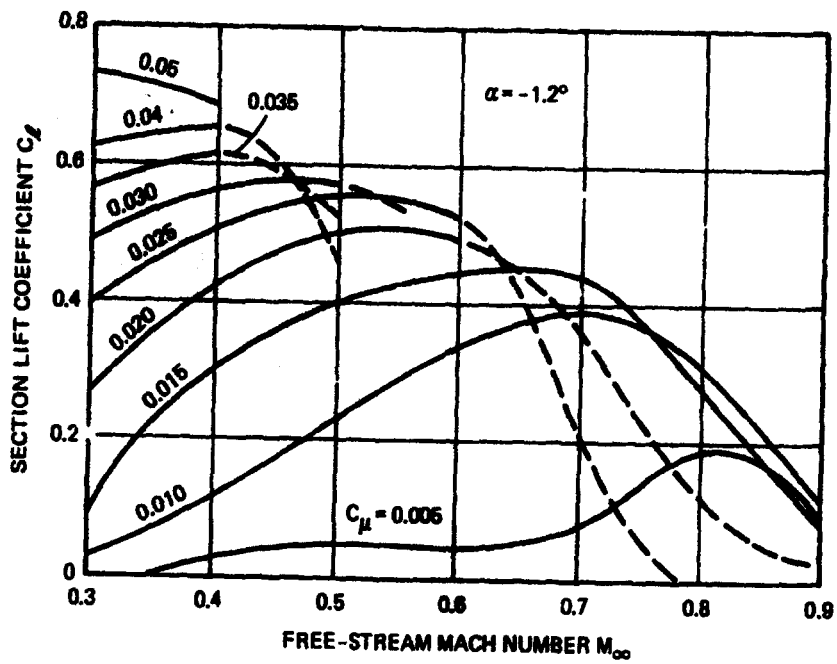


Figure 5 - Lift Variation with Mach Number at $\alpha = -1.2$ Degrees for Pure Ellipse
(Model TE-3 in Englar⁷)

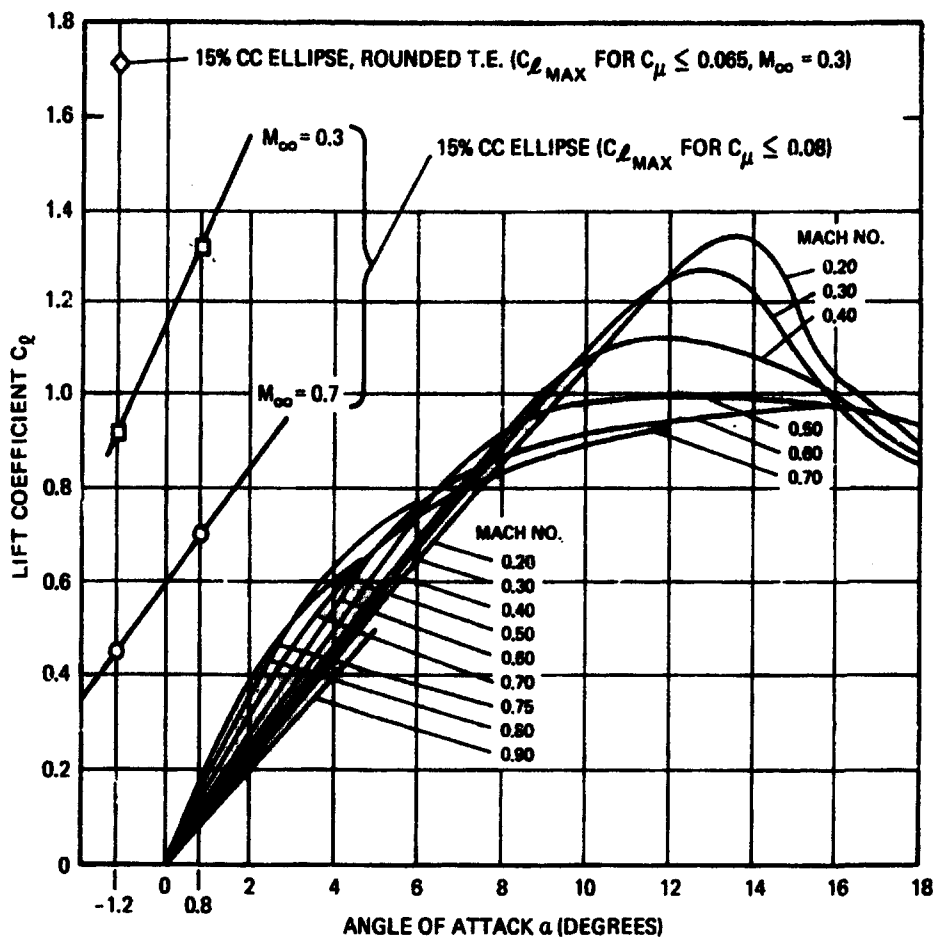


Figure 6 - Comparison of CC Ellipses with Lift Performance of NACA 0012
 (CC data from Eagle⁷; NACA data from NASA CR-114)

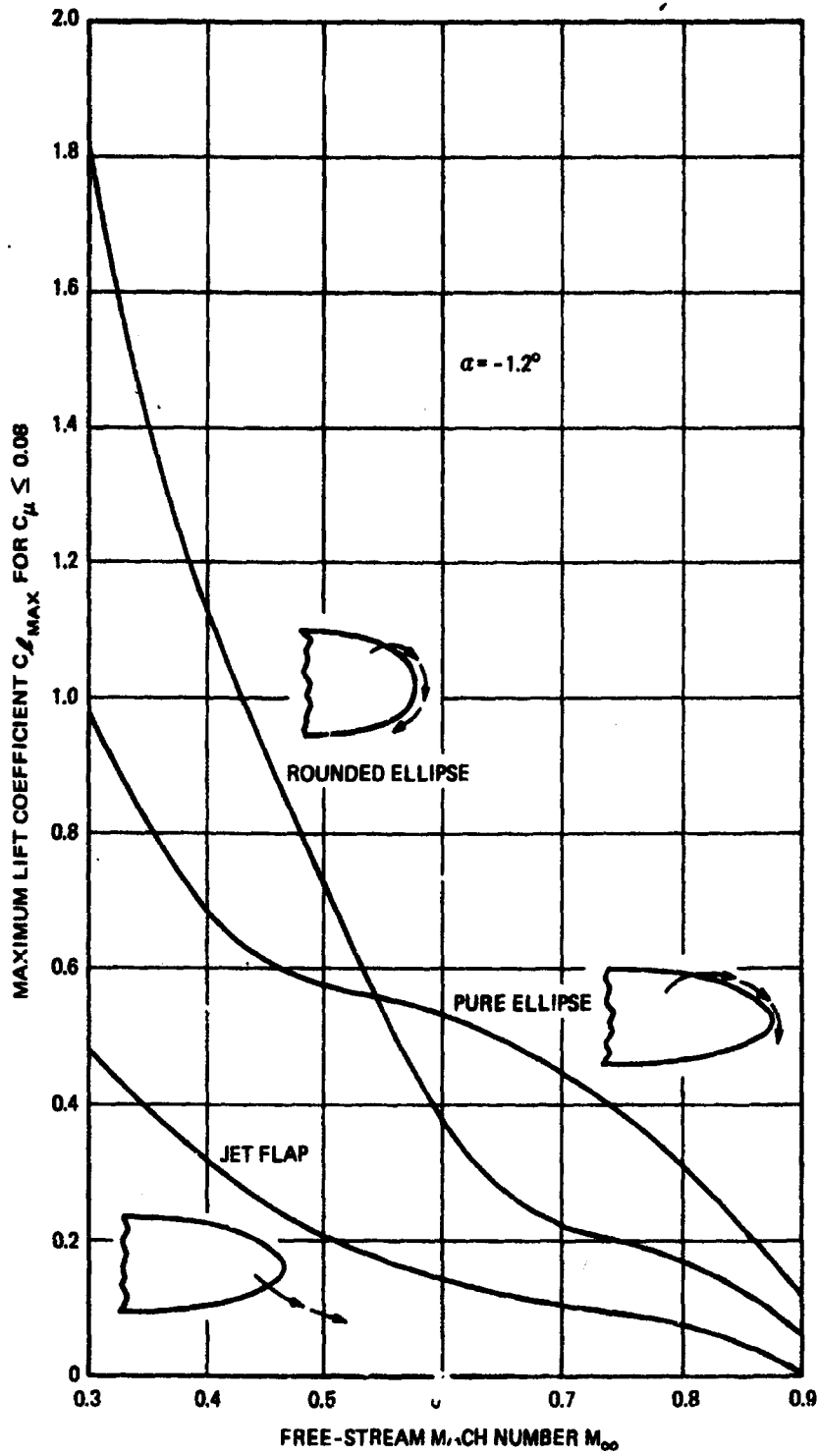


Figure 7 - Comparative Lift Characteristics of the Three Transonic Models
with $\alpha = -1.2$ Degrees
(Characteristics from Engler⁷)

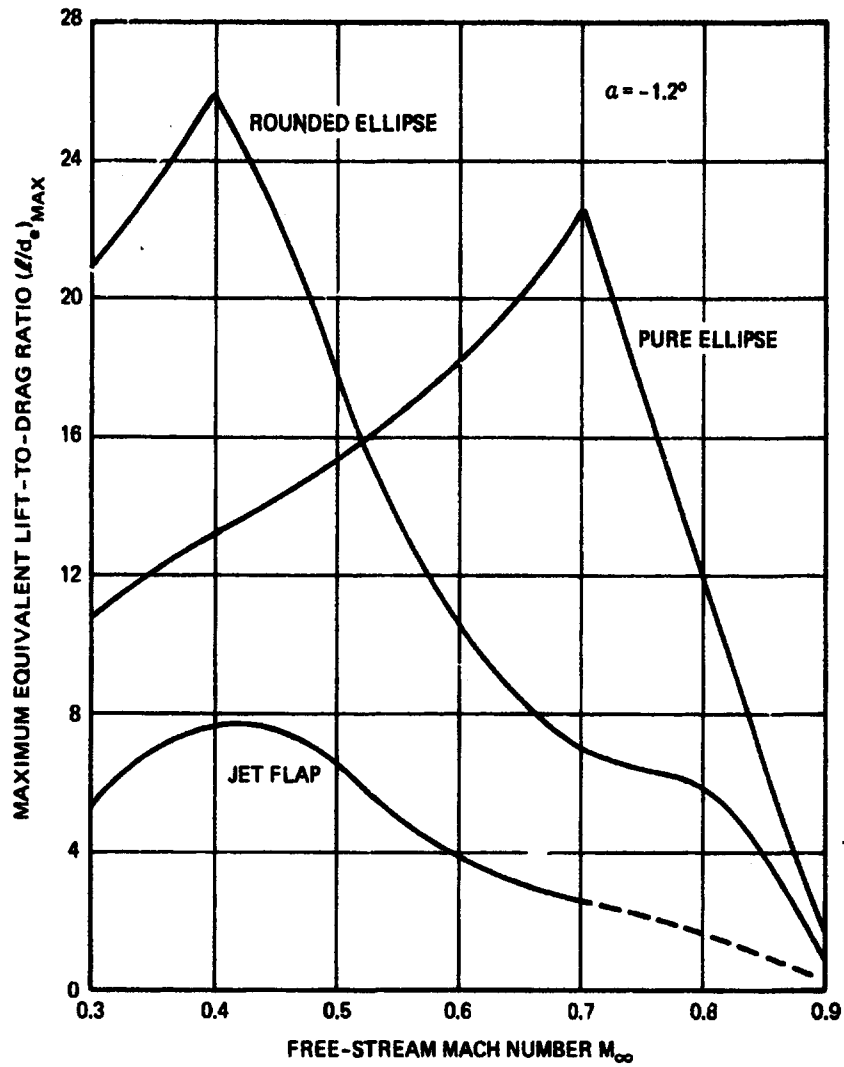


Figure 8 - Comparison of Maximum Equivalent Lift-to-Drag Ratio for the Three Configurations with $\alpha = -1.2$ Degrees
(Configurations from Eagle⁷)

1. Trailing edge geometry (local radius downstream of slot, slot height-to-radius ratio, radius-to-chord ratio).
2. External pressure distribution caused by the compressible flow field.
3. Jet pressure ratio P_d/p_∞ and thus jet Mach number and velocity.
4. Jet detachment (complete jet separation resulting in no Coanda turning and little lift augmentation).

Since the jet detachment phenomenon is apparently directly related to the other three factors, it was thus decided to undertake an experimental investigation of all four, with particular emphasis on the jet detachment problem and its causes. The basic problem to be examined is the effect of high wall jet velocity and variations in trailing edge geometry on both wall jet turning and on the separation (or detachment) characteristics of the jet in a compressible flow field. It is suspected that due to the high jet to free stream velocity ratios, the significance of Reynolds number and upstream boundary layer characteristics will be less than for the low-speed case, where their importance is strongly felt.

JET DETACHMENT LITERATURE REVIEW

The presence of a jet attachment limit for Coanda-type devices was already realized during research on the generation of high lift devices preceding CC airfoils, that is, the tangentially blown flap (noncircular trailing edge). Both Tararine and Dorand¹² and Lowry¹³ report that detachment is brought about by large slot heights, high pressure ratios across the nozzle, and small radii on the Coanda surface. Lowry defines the experimentally determined limiting pressure ratio as

$$P_d/p_\infty = 1.40/(h/R)^{1/3} \quad (3)$$

Both this curve and the experimental curve from Tararine and Dorand¹² are plotted in Figure 9, where only conditions to the left and below the curves represent attached Coanda jets. It should be noted that the Lowry data are for static ambient conditions (i.e., no external free stream) and, as such, are not indicative of any effects which might be produced by an external pressure distribution. More recent studies were conducted by Kizilos and Rose¹⁰ on cylindrical Coanda surfaces after their transonic tests on a modified CC-type control surface

¹²Tararine, S. and R. Dorand, "Determination Through Wind Tunnel Tests and Analytical Methods of the Optimum Deflection Devices Suitable for Use on Jet Flap Helicopter Rotor Blades," Dec 1960, European Research Office, U. S. Dept. of the Army, Report DE2013.

¹³Lowry, J. G., J. M. Riebe, and J. P. Campbell, "The Jet-Augmented Flap," Paper 715, 25th Annual Meeting of the Institute of the Aeronautical Sciences, New York, Jan 1957.

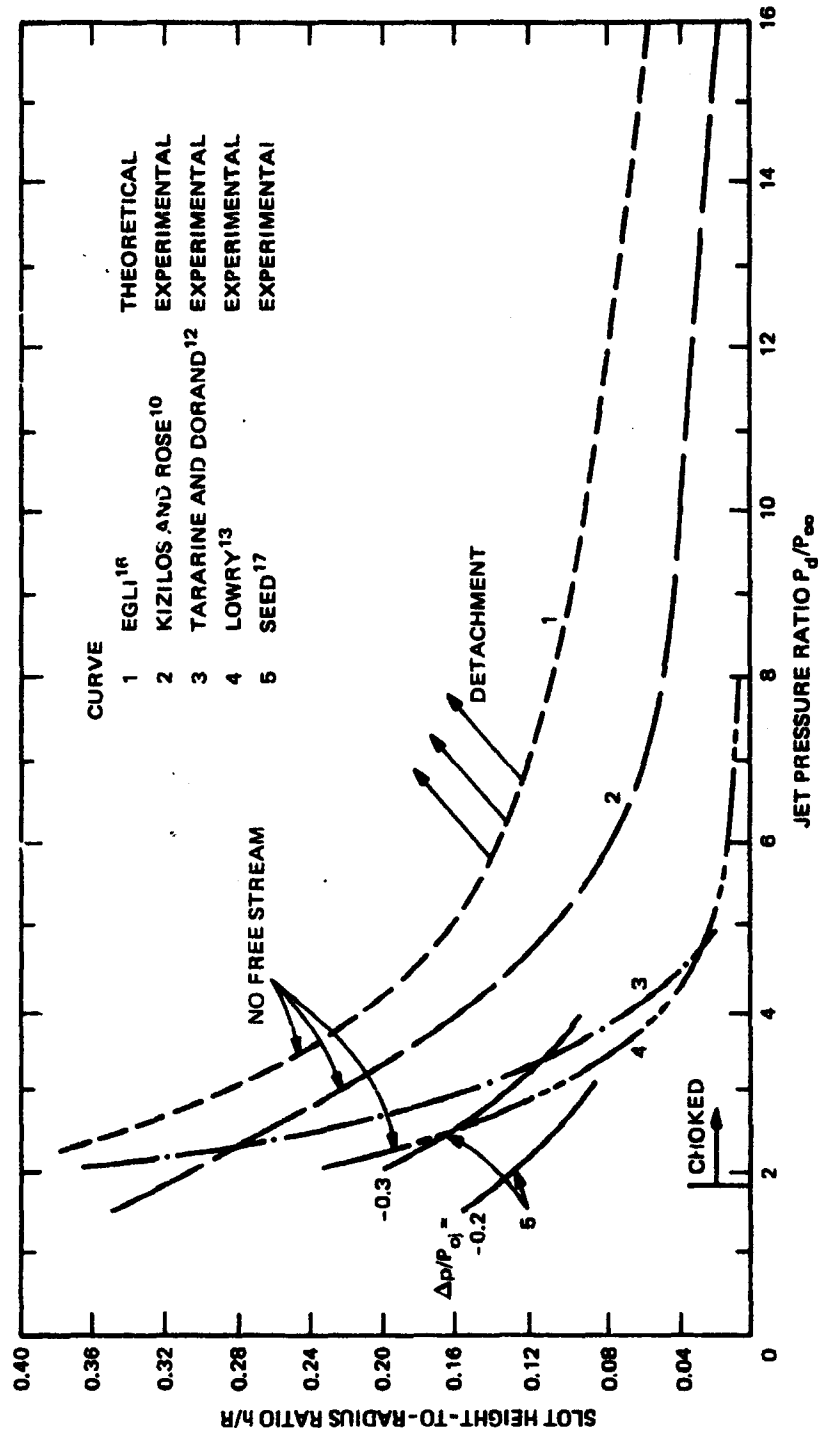


Figure 9 -- Jet Detachment Limits for Coanda Wall Jet

indicated detachment problems at high subsonic speeds. Their static experimental variation of both slot height and radius for varying jet pressure ratio is also shown in Figure 9. This curve is considerably more conservative than the previous two, indicating that a much larger pressure ratio is allowable for a given configuration before jet detachment occurs. Also presented in this reference are shadowgraph pictures of the Coanda surface, clearly showing the compression and expansion waves characteristic of an underexpanded jet. Strong compression waves occur in the supersonic jet at a pressure ratio just below that at which the jet detaches. These same patterns were also evident in Schlieren photographs from Bailey.¹⁴ Surface pressure distributions from this and other studies^{10,15} confirm large fluctuations between positive and negative pressure coefficients for underexpanded jets (see Figure 10). It was postulated from these data that the detachment phenomenon was related to a sufficiently large pressure rise due to recompression of the supersonic jet. A theoretical formulation of this flow field (with no external flow) was done by Egli¹⁶ who used a Prandtl-Meyer expansion technique to calculate the pressure rise produced by a shock of sufficient strength to cause detachment. As can be seen in Figure 9, this analysis is quite conservative.

Attempts to use any of the above criteria to explain the transonic loss in lift performance for those CC airfoils which had been tested lead to the conclusion that the airfoil geometries and jet flow parameters were usually safely below any of the detachment curves of Figure 9. This was attributed to the fact that none of these curves included the effects of the pressure field produced on the airfoil by the compressible external flow, nor the usual drop in free-stream static pressure which occurs in downdraft tunnel tests with increase in Mach number. This is verified in Figure 11 which compares the static detachment curves of Kizilos and Rose¹⁰ and those of Tararine and Dorand¹² with detachment data from the former¹⁰ for a CC airfoil with $h/R = 0.021$ at high subsonic Mach numbers. The detachment limit clearly drops to a lower pressure ratio with increased M_{∞} , i.e., decreased free-stream static pressure. Another attempt to correlate the detachment limits with dynamic data was published by Seed¹⁷ who integrated the pressure-centrifugal force balance across the jet, $dp/d\eta = \rho V_j^2/(R + \eta)$, to obtain for incompressible inviscid flow with no flow entrainment, mixing, of jet growth:

¹⁴Bailey, A. B., "Use of the Coanda Effect for the Deflection of Jet Sheets over Smoothly Curved Surfaces, Part I," Aug 1961, University of Toronto Institute of Aerophysics Tech Note 51.

¹⁵Roderick, W. E. B., "Use of the Coanda Effect for the Deflection of Jet Sheets over Smoothly Curved Surfaces, Part II," Sep 1961, University of Toronto Institute of Aerophysics Tech Note 49.

¹⁶Egli, W. H., "An Approximate Analysis of the Criterion for Detachment of a Supersonic Jet from the Surface of a Right Circular Cylinder," Feb 1968, Honeywell, Inc., Memorandum MR 10235.

¹⁷Seed, A. R., "Detachment of Wall Jets from Curved Surfaces," Apr 1969, Paper published by the National Gas Turbine Establishment, Pyestock, Hants, England.

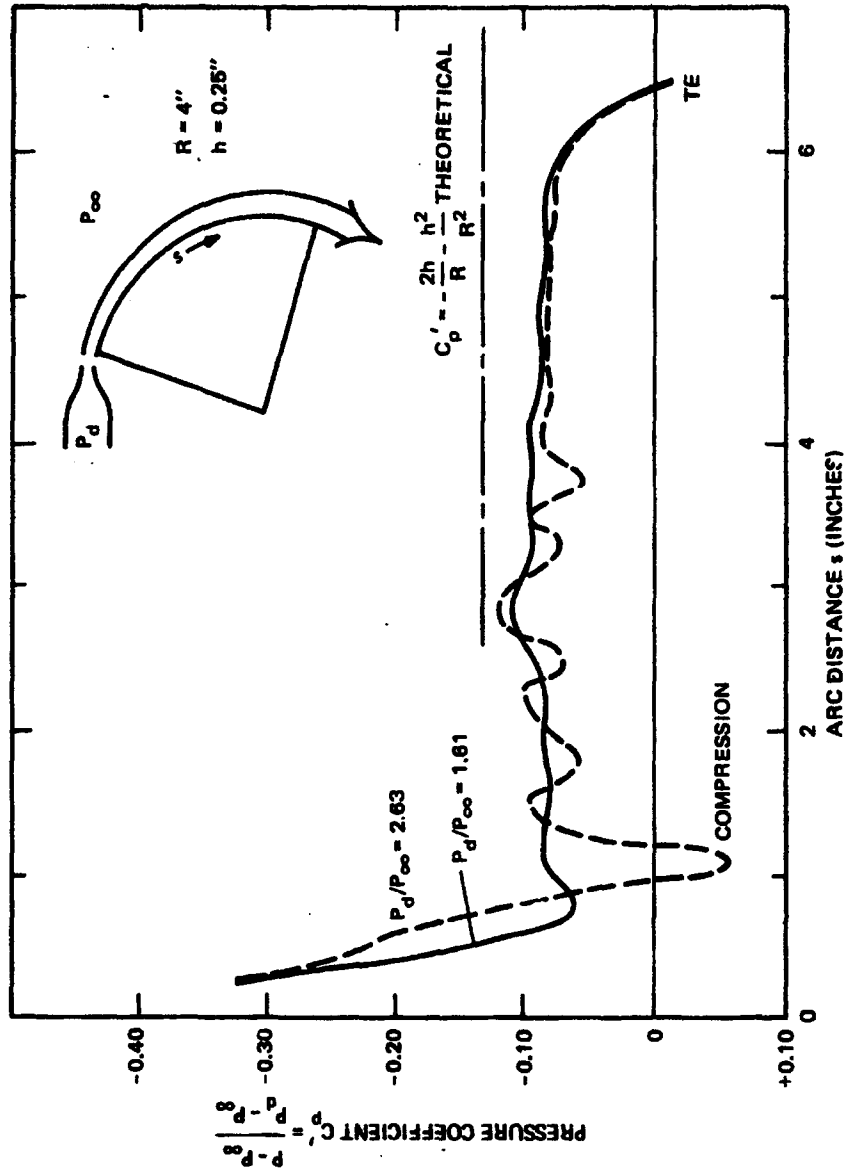


Figure 10 - Choked and Unchoked Jet Static Pressure Distributions on a 90-Degree Deflection Surface with No Free Stream
 (From Rodetick 15)

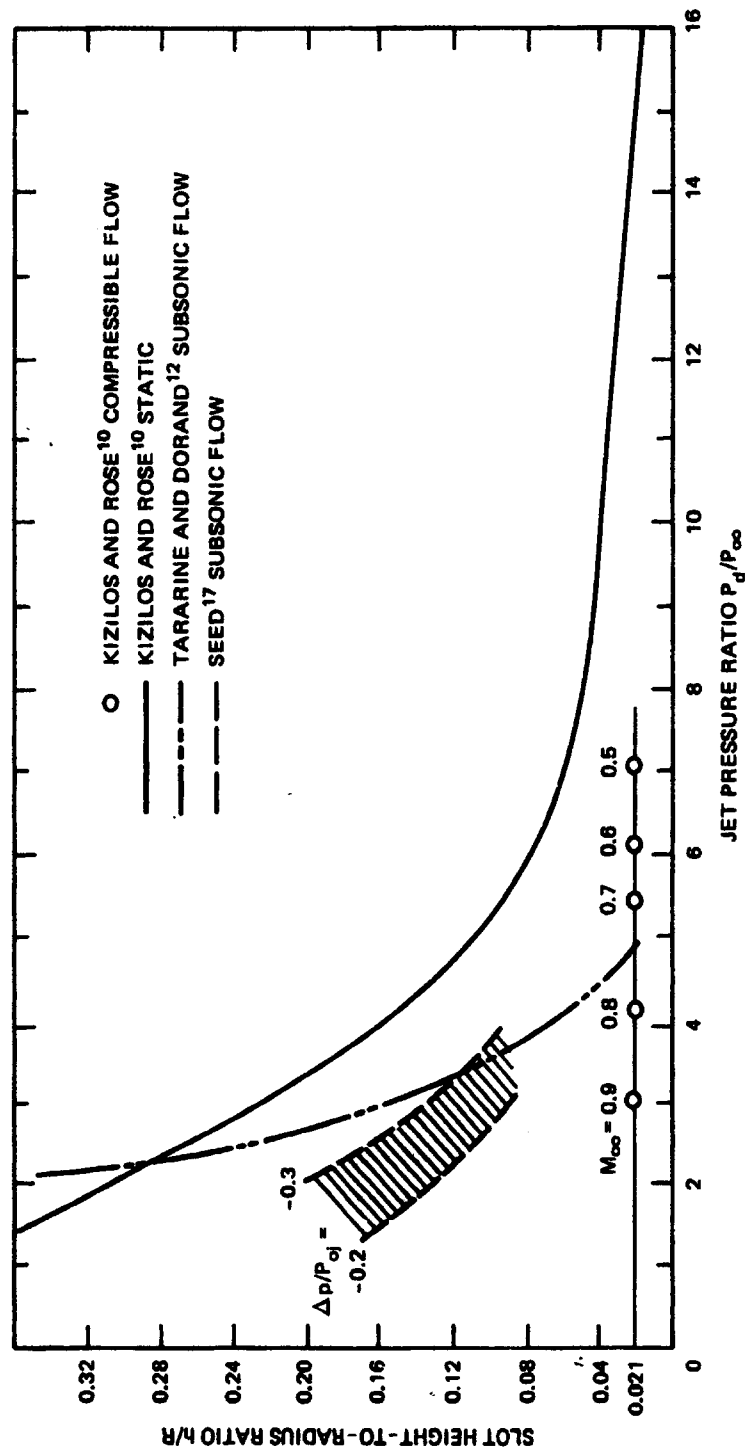


Figure 11 - Comparison of Compressible Flow Results with Static and Subsonic Jet Detachment Criteria

$$\frac{\Delta p}{P_{0j}} = \frac{P_{ij} - P_{0j}}{P_{0j}} = -\frac{\gamma}{2} M_j^2 \left(\frac{2h}{R} + \frac{h^2}{R^2} \right) \quad (4)$$

or for compressible flow

$$\frac{\Delta p}{P_{0j}} = \left[1 - \frac{\gamma - 1}{2} M_j^2 \left(\frac{2h}{R} + \frac{h^2}{R^2} \right) \right]^{\frac{\gamma}{\gamma - 1}} - 1 \quad (5)$$

where the subscripts on pressure refer to the inside wall (sub ij) and outside boundaries of the jet. On the basis of results for several elliptic airfoils tested up to $M_\infty = 0.6$, Seed concluded that jet detachment would occur for

$$-0.2 \leq \frac{P_{ij} - P_{0j}}{P_{0j}} \leq -0.3 \quad (6)$$

The external pressure P_{0j} was predicted by potential flow and was not assumed to be free-stream static pressure. In certain of the Seed results, detachment was actually produced only at the very small local radius at the lip of the slot, and then reattachment occurred downstream along the larger trailing edge radius proper. Whereas the Seed work thus introduced dependence on normal static pressure gradient across the slot, his limiting values needed verification for more general shapes at higher Mach numbers.

INITIAL APPROACH

The preceding studies indicate that the compressible flow performance of CC sections is probably dependent not only on local trailing edge geometry and characteristics of the under-expanded jet but also is quite strongly influenced by the external free stream. It was thus decided to construct enlarged versions of the two elliptic CC sections used earlier⁷ and to thoroughly instrument them so that detailed trailing edge characteristics could be measured in a compressible free stream.

TRANSONIC AIRFOIL TRAILING EDGE INVESTIGATIONS

Of particular interest in the proposed transonic test was the effect of changes in trailing edge geometry with respect to the high-speed Coanda jet and the effect of recompression in

the jet on the detachment criteria curves of Figure 9. Instrumentation was to include the following:

1. Chordwise static pressure taps to record midspan pressure distribution and lift.
2. Spanwise static taps to monitor two-dimensionality.
3. Flush hot film shear stress probe mounted in the positionable cylindrical trailing edge to determine the location of the jet separation point.
4. Pitot-static pressure traverse probe mounted in the trailing edge to obtain jet velocity profiles and normal static pressure gradients across the jet.
5. Closely spaced static taps in the trailing edge.
6. Total pressure and temperature sensors to deduce jet velocity and mass flow.
7. Schlieren or shadowgraph optical system to locate recompression waves, jet separation points, and jet outer surface.

With the above equipment, it was desired to install enlarged duplicates of the original transonic CC ellipses⁷ in the 18- x 18-inch NSRDC transonic tunnel and to run a range of Mach numbers from 0.3 to 0.9 at several values of C_{μ} corresponding to choked flow and higher velocity underexpanded jets. Detailed measurements of the trailing edge variables would then be compared for the two trailing edge geometries in order to explain the differing performance and effects of geometry and recompression on jet detachment.

PROBLEM AREAS

The desire to duplicate the original transonic ellipses was supplemented by the need to make the trailing edges as large as possible in order to increase the accuracy of the data-measuring procedures. The slot height should also be as large as possible, but since the parameter slot height-to-radius ratio was an important geometric consideration, it was desired to maintain the same values as the original models. This would mean slot heights no larger than 0.02 inch even if the original models were doubled in size. The required size of pitot probe for jet profile investigation would thus have to be quite small. Bradfield and Yale¹⁸ set forth a procedure for constructing probes with only a 0.001-inch opening and 0.003-inch thickness, with pressure response times of 5 to 20 seconds. Even with these small probes, pressure measurements in the sonic or greater velocity jet would still prove difficult because of the mixed nonisentropic flow. Bow shock formation would occur on any probe downstream of a choked nozzle, and whereas total pressure could be obtained by using the Rayleigh pitot formula, the static pressure at any point in the supersonic field would be practically impossible to determine. Probe total pressure measurements could be supplemented

¹⁸Bradfield, W. S. and G. E. Yale, "Small Pitot Tubes with Fast Pressure Response Time," *Journal of the Aeronautical Sciences*, Oct 1951.

by a density measurement (say, by interferometry) to arrive at static pressure, but this would require knowledge of total conditions ahead of the probe; these would be practically unobtainable because of the nonisentropic regions caused by compression waves and turbulent mixing with the entrained boundary layer. It thus appeared doubtful that valid data within the jet could be recorded in the supersonic region of the jet. However, meaningful pitot and static data should be obtainable downstream of the final recompression wave—the original tests indicated a subsonic region before the occurrence of separation. In any case, shear stress and surface static measurements could be made in either flow regime.

Sturek and Danberg¹⁹ offered an alternative for measuring the static pressure gradient across the jet through use of a bevelled flat plate probe in a $M_\infty = 3.5$ boundary layer survey. Proper alignment of that probe yielded a zero degree wedge angle on the flat side and negligible pressure disturbance. A possible problem could arise in the proposed application should any corner flow between the plate probe and the trailing edge result (see Figure 12 for proposed installation). If present, this effect should be small since the boundary layer development on the probe will be thin.

An additional problem area was that of model size relative to tunnel size. The maximum thickness for the 15-percent rounded ellipse was roughly twice the diameter of the trailing edge. Increasing the diameter would also mean increasing the model thickness and thus encountering tunnel blockage limitations. It was decided that replacing the elliptic contour aft of midchord with parallel walls of no curvature would allow the trailing edge radius to be doubled with no change in model frontal area. (See Figure 12.) In addition, the upstream boundary layer would then be developing on a flat plate and thus not be dependent on upper surface curvature distribution. It was then a question of whether an enlarged model thickness would allow transonic testing for a Mach number range up to 0.9 without appreciable tunnel choking, wall interference effects, or jet impingement on the tunnel floor. The series of tests described in the next section was undertaken to resolve these questions.

TRANSONIC BLOCKAGE TESTS

The proposed transonic CC ellipse test required as large a model as possible for detailed trailing edge flow field surveys over a Mach number range up to 0.9. These two requirements are counteracting with regards to a transonic tunnel of a given size, and it was thus necessary to determine the maximum model size which could be run in the 18- x 18-inch NSRDC

¹⁹Sturek, W. B. and J. E. Danberg, "Experimental Measurements of the Supersonic Boundary Layer in a Region of Moderate Adverse Pressure Gradient," Paper 71-162, AIAA 9th Aerospace Sciences Meeting, New York, Jan 1971.

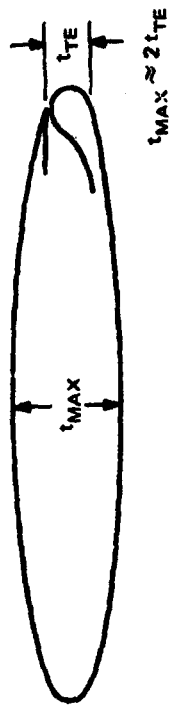


Figure 12a - Original 15-Percent Ellipse with Rounded Trailing Edge

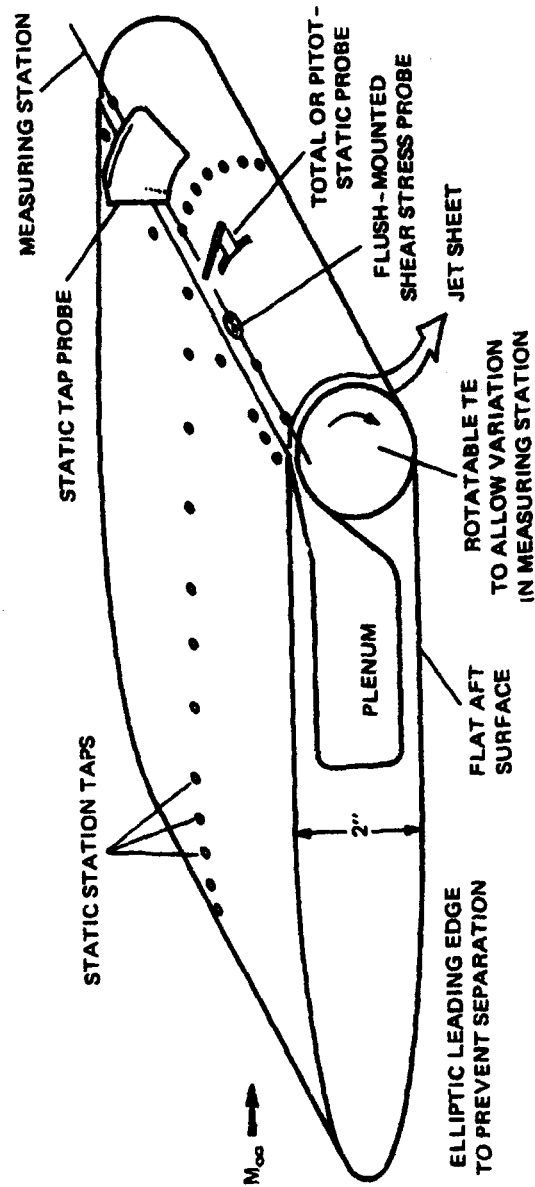


Figure 12b - Proposed Two-Dimensional Transonic Test Configuration

Figure 12 - Two-Dimensional Transonic Test Configuration

transonic tunnel at the desired $M_\infty = 0.9$ without tunnel choking. Thom²⁰ gives a theoretical prediction, but it was uncertain how this would be affected by model blowing and its corresponding flow entrainment. A set of preliminary tests was thus run to determine maximum model thickness for an unchoked test section at $M_\infty = 0.9$ or, conversely, the maximum Mach number attainable for a given model thickness.

MODELS AND TEST APPARATUS

Two circular cylinder models (diameters 1.5 and 2.0 inches) were built with tangential slots as shown in Figure 13 (the 2-inch model is identical to the 1.5-inch-diameter model, with the exception of the enlarged diameter and a 0.032-inch slot). Cylinders were chosen as simple models to provide the necessary *projected* blocked area. It is realized that their critical Mach number (≈ 0.42) is quite low, and it is *not* suggested that these sections be considered as transonic CC airfoils. The models spanned the tunnel horizontally and were supported by wall mounts, one of which was connected to a 2-inch-diameter air supply line. Static pressures on the model were measured at surface taps at the upper and lower crests (i.e., 50-percent chord station). Thirty-six static taps were located in the tunnel wall to yield a Mach number survey of the flow field. (See Figure 14.) All pressures were recorded on a multiple scannivalve readout system, with atmospheric total pressure. Figure 15 shows photographs of the test setup. It should also be noted that with the transonic nozzle blocks installed, the test section height was reduced from 18 to 16.2 inches.

TEST SECTION SURVEY

With models removed from the tunnel and transonic nozzle blocks installed, a series of empty test section runs was made to determine whether there were longitudinal variations in Mach number. A reference tap 24 inches upstream from the centerline (see Figure 14) was used to record uncorrected free-stream Mach number. The survey showed that within the velocity range of interest, the greatest variation in Mach number from this reference value was 1.78 percent. Figure 16 depicts Mach number at the reference tap resulting from various butterfly valve settings (BFVS, in counts) by which the velocity is set. Note that $M_\infty = 1.0$ was not reached in the empty test section even with the valve fully opened. This is attributed to the fact that the boundary layer buildup caused the minimum area throat ($M = 1.0$) to form downstream of the test section.

²⁰Thom, A., "Blockage Corrections in a Closed High-Speed Tunnel," Nov 1943, Aeronautical Research Council R & M 2033.

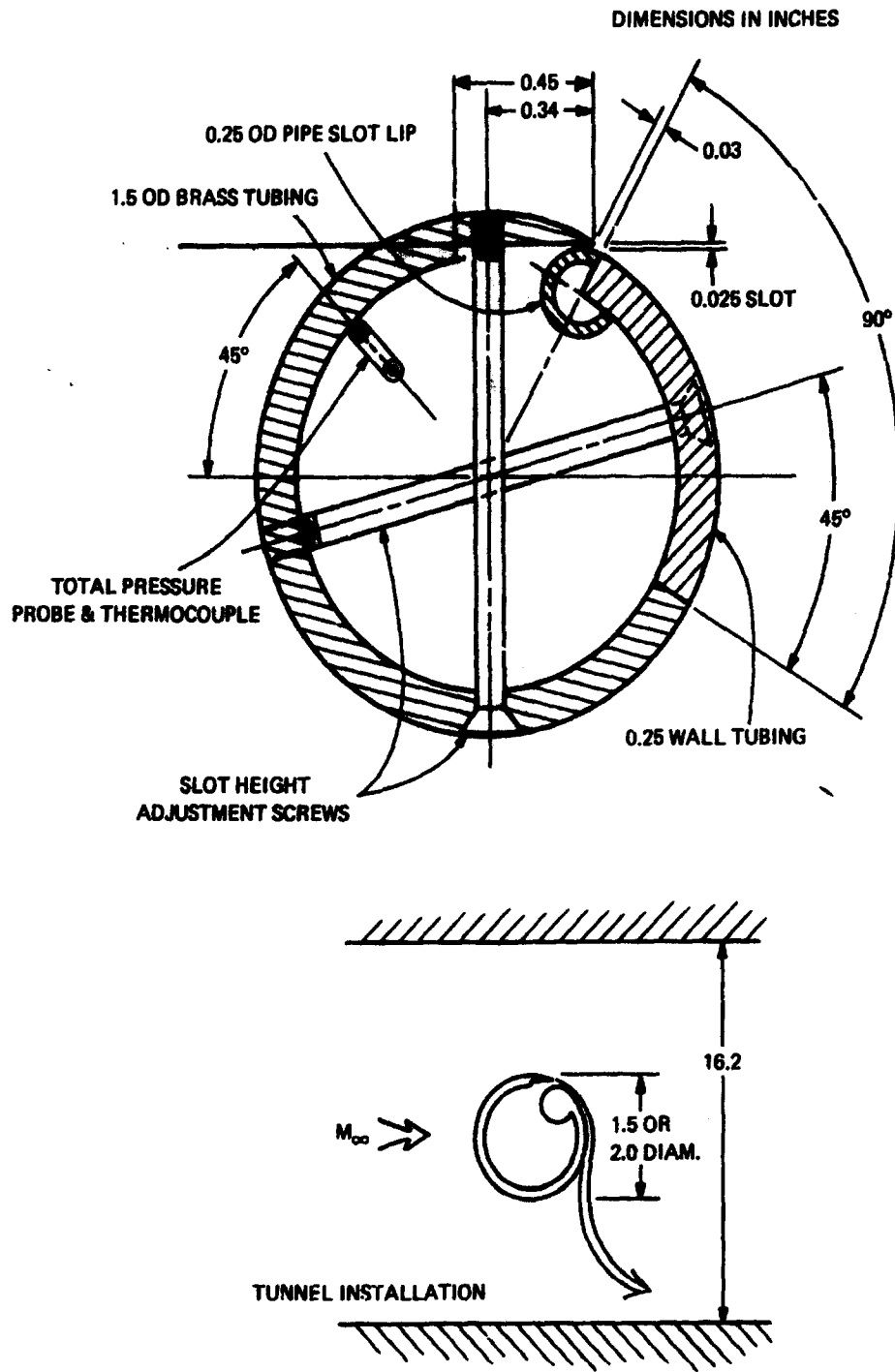


Figure 13 - Blockage Models and Test Setup

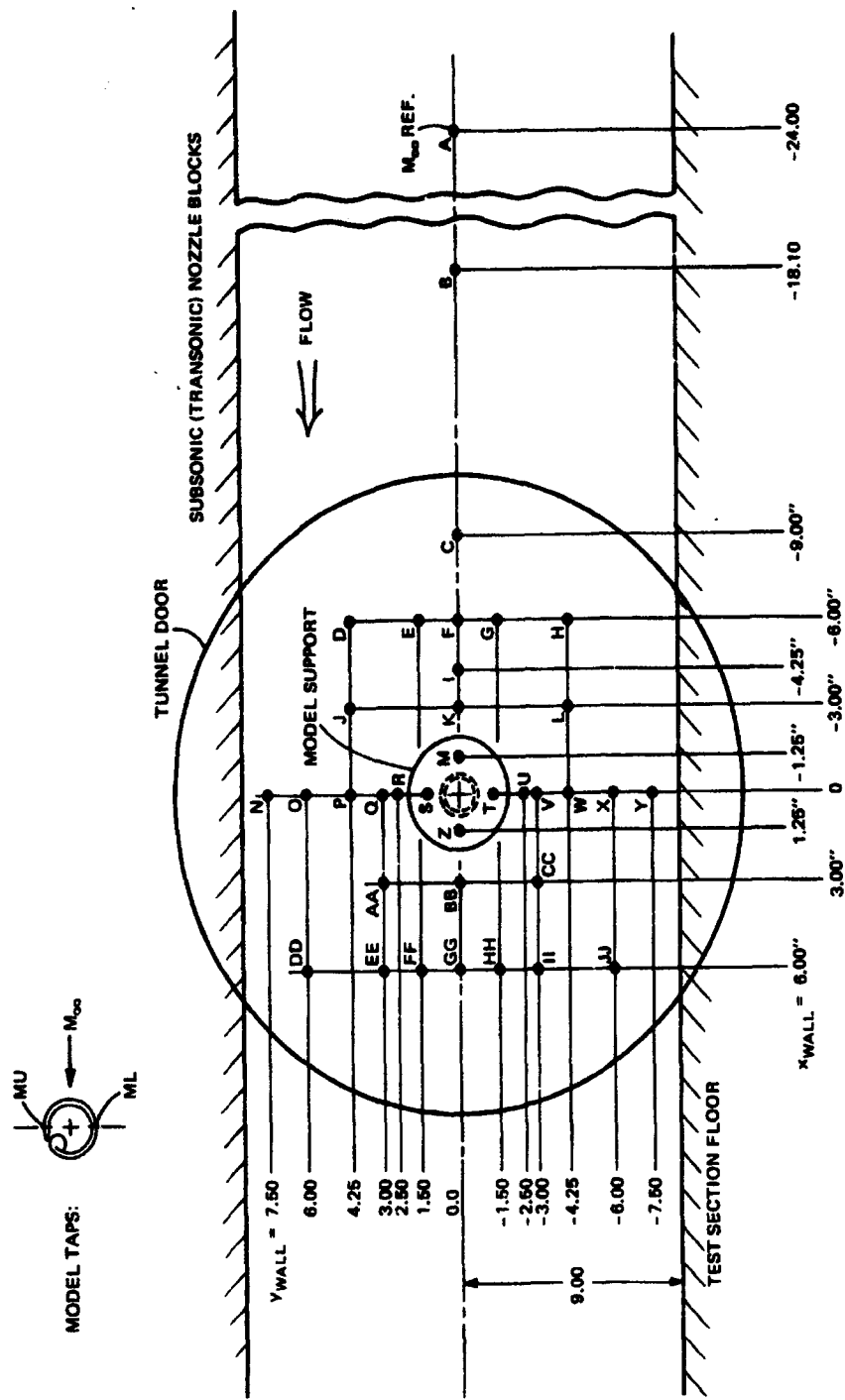
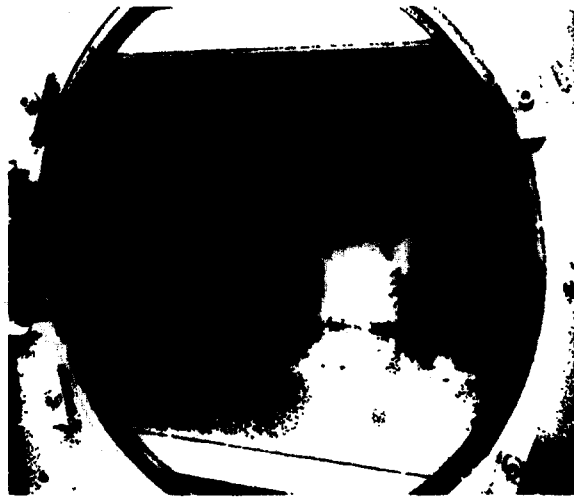


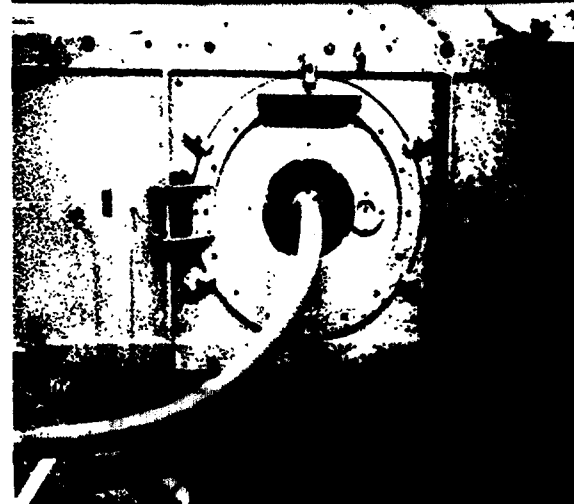
Figure 14 — Static Wall Tap Locations in 18 - x 18 Inch Tunnel for CC Cylinder Test



MODEL MOUNTED IN WALL,
TEST SECTION OPEN

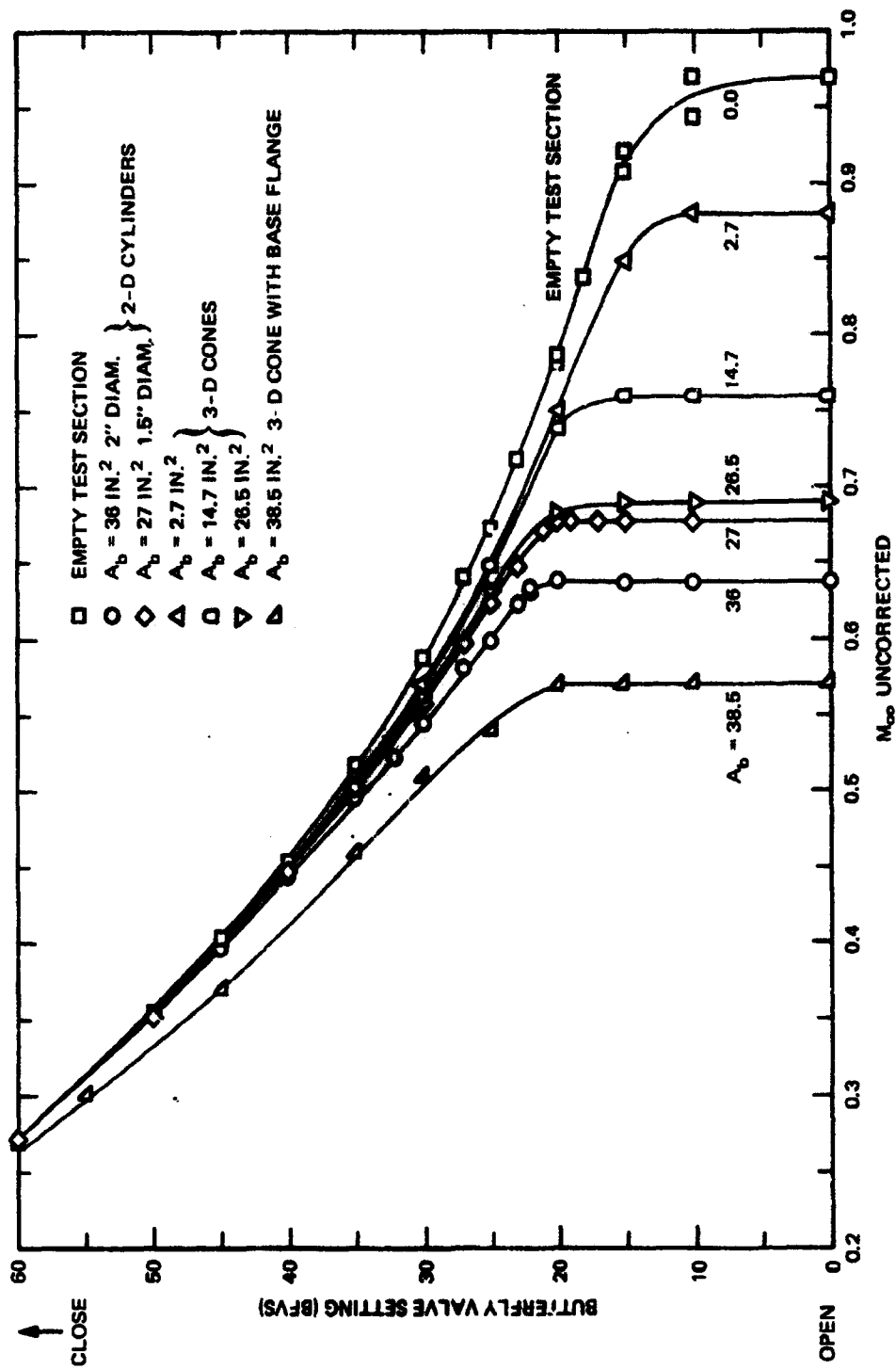


TUNNEL DOOR INSTALLATION OF
STATIC WALL TAPS (SEE FIGURE 14)



2-INCH AIR SUPPLY LINE

Figure 15 – Blockage Test Setup



BLOCKAGE TESTS, NO BLOWING

In turn, each model was installed in the tunnel and a series of butterfly valve settings was run without model blowing. Choking of the tunnel was recognized when an increase in butterfly valve setting was accompanied by no further increase in test section Mach number; this was caused by a Mach number of unity at the effective minimum area throat produced by the model. The free-stream Mach number thus obtained was the maximum for a given model thickness; conversely, for that Mach number, the associated model thickness (proportional to blocked area) was the upper limit to avoid choking. Figure 16 depicts very clearly that this choking phenomenon occurred for both models at a butterfly setting between 20 and 22, which corresponds to a Mach number (uncorrected) of about 0.637 for the larger cylinder and 0.676 for the smaller. Also shown in this figure are the results of similar tests run in the same tunnel by Eastman and Gilmore of NSRDC (undocumented) on cones with a variety of base (projected) areas. The only comparison of similar blocked areas that can be made is between the 27-in.² cylinder and the 26.5-in.² cone. The additional 0.014 increment in choking Mach number for the cone appears to be due to a "relaxing" of the tunnel wall constrictions for a round-base area located in the middle of the tunnel, as compared to a two-dimensional area spanning it. This same trend is seen more clearly in Figure 17 where agreement with theory is slightly better for the cones than for the two-dimensional cylinders.

All mention of Mach number thus far has been of "indicated" M_{∞} recorded at the reference tap supposedly far enough upstream to be unaffected by the presence of the model. These values must be corrected for tunnel wall restrictions in the form of solid and wake blockage corrections (see Thom²⁰). Unfortunately, wake blockage, which should be rather significant behind the cylinder, cannot be calculated here because it depends on drag coefficient, which was not recorded (a wake drag rake would have produced additional blockage). Figure 17 thus also shows the choking Mach numbers corrected for solid blockage only: 0.684 for the small cylinder and 0.647 for the 2-inch model.

FLOW FIELD DETAILS

Recorded (uncorrected) Mach numbers at each wall and model tap are shown in Figures 18 and 19 for two sample cases for the 1.5-inch cylinder: unchoked (Figure 18, BFVS = 30) and after tunnel choking (Figure 19, BFVS = 19). The taps are labeled and their locations can be seen in Figure 14. Taps at the same longitudinal station are connected by faired curves. It should be noted that certain downstream taps are located in the model wake, and thus total pressure at these points (which was not measured) is no longer the same as the free-stream total pressure in which the Mach number calculations are based. ($M = \sqrt{1 - P_t/P_\infty}$ where P_∞ is the free-stream value measured in the settling chamber.) Thus, these points should be invalid. The important factor to observe in Figure 19 is the effect of choking on

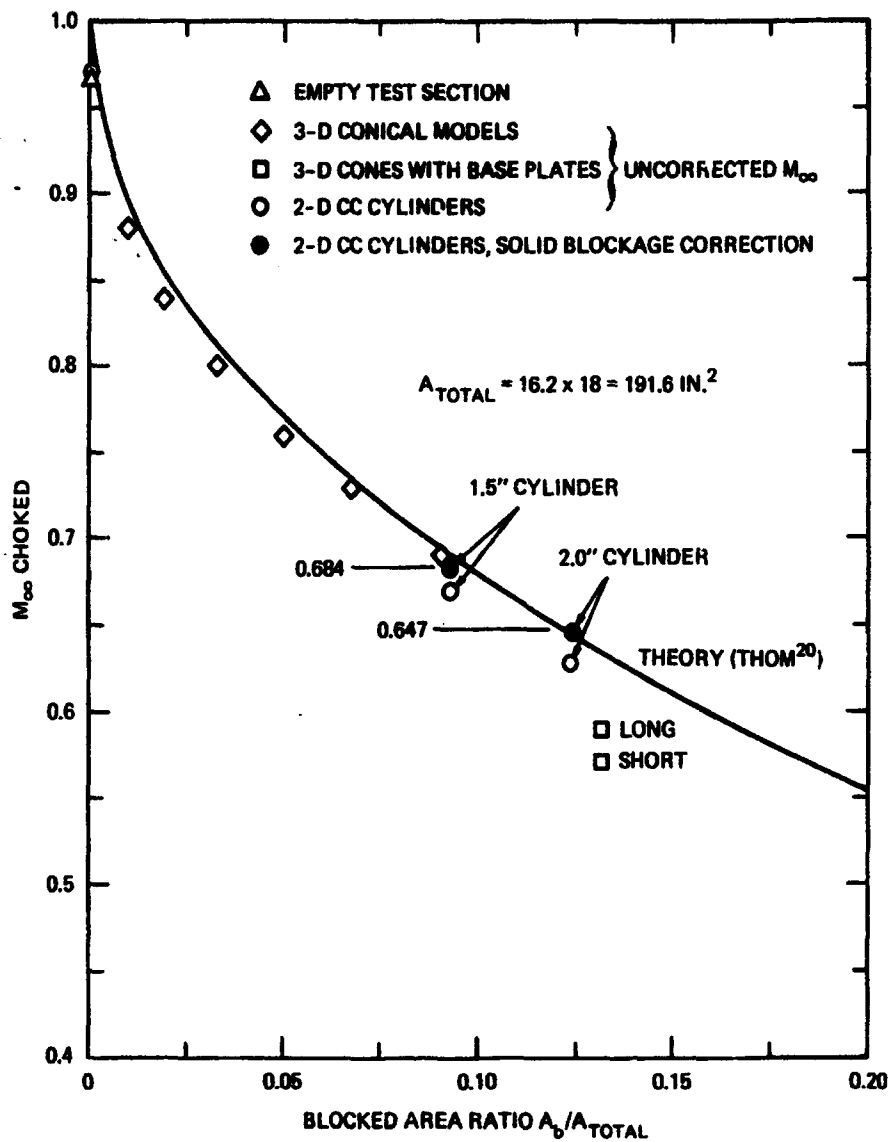


Figure 17 - Choking Mach Number-Comparison of Theory and Experiment

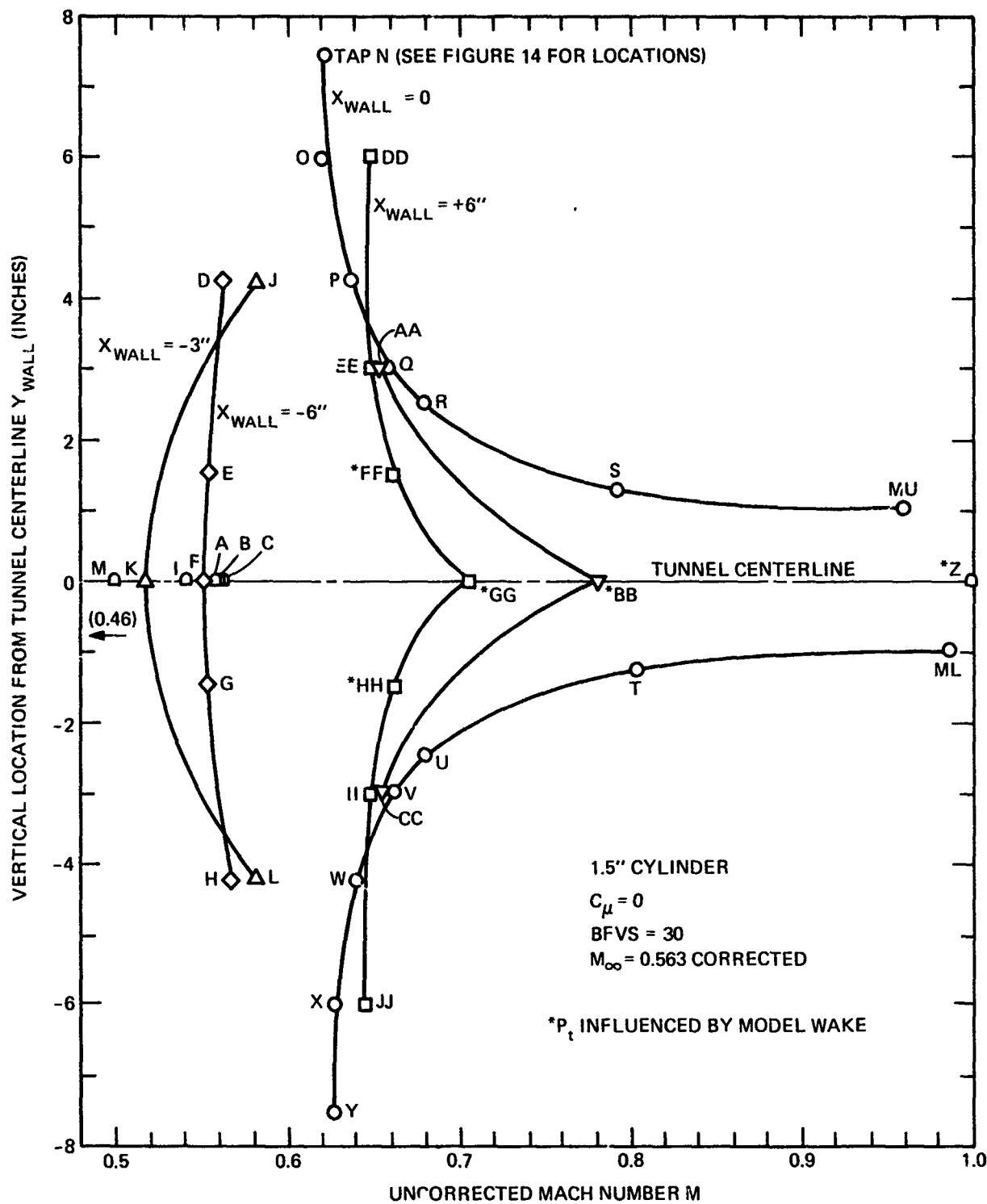


Figure 18 - Mach Number Distributions, Tunnel Unchoked

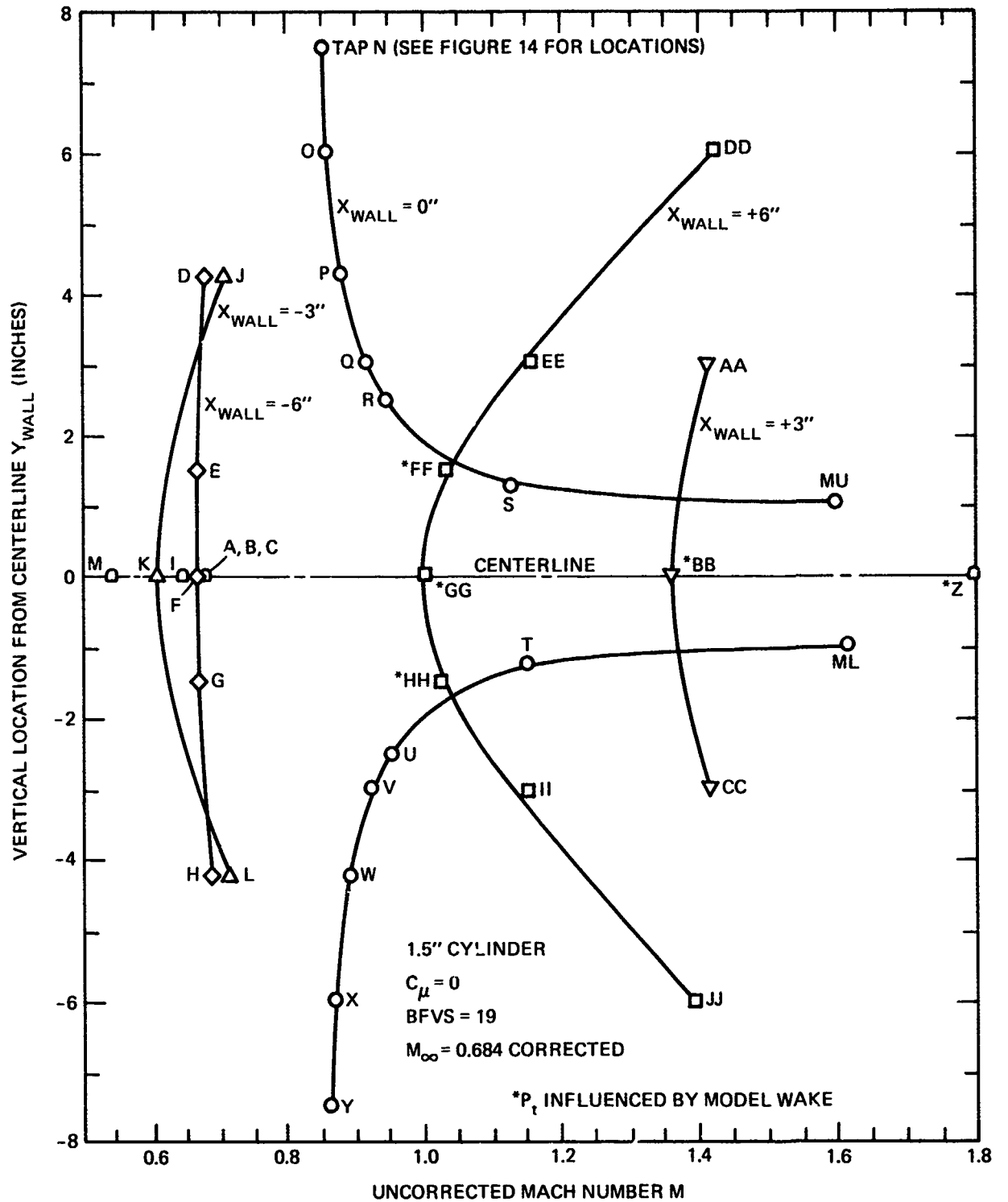


Figure 19 - Mach Number Distributions, Tunnel Choked

the taps downstream of the model. Note that a sonic line developed at the throat formed by the model and the tunnel floor and ceiling and that flow downstream of that line expanded supersonically (see Stations +3" and +6"). The development of this effect with increased butterfly opening (decreased BFVS) appears in Figures 20 and 21. Downstream taps AA and DD expanded to supersonic flow very rapidly as soon as the choked butterfly setting was reached, and then immediately reached some constant supersonic value. All other taps at the model station and upstream assumed constant values without noticeable expansion. This is confirmation that choking occurred and the maximum free-stream Mach number was reached for the given model thickness.

EFFECTS OF MODEL BLOWING

Figure 22 shows the effects of both subsonic and supersonic (choked slot) tangential model blowing on free-stream Mach number corrected for solid blockage only. A slight increase in M_{∞} was noted with blowing when the tunnel was below choking, but no apparent change in choking Mach number occurred for either model. Unfortunately, a primary blockage-related effect of blowing is not presented in this figure, i.e., the wake-reducing property of the energy-adding jet, which should produce a noticeable change in corrected M_{∞} . (Earlier, Englar⁷ confirmed drag reduction with smaller amounts of blowing.) Figure 23 shows blowing effect on the model upper surface local Mach number and on a selected downstream tap as a function of butterfly setting. The downstream tap showed the same slight effect as seen on M_{∞} in Figure 22. The model surface tap showed the characteristic property of circulation control, increasing the local Mach number and circulation over the model, even in supersonic flow. However, blowing with a choked slot was clearly less effective; this phenomenon was the primary objective in the proposed follow-on tests.

CONCLUSIONS FROM BLOCKAGE TESTS

Tests on the two circular cylinders have shown that the desired free-stream Mach number of 0.9 cannot be reached with the model thicknesses tested. (Figure 17 indicates that 0.96 inch is the maximum thickness allowable for that speed.) Using the Thom criteria²⁰ that meaningful tests should not be run within 0.03 of the tunnel choking Mach number, the maximum test Mach number should be no greater than 0.654 for a 1.5-inch-thick model and no greater than 0.617 for a 2-inch model. If the desired test Mach number were reduced to 0.60, a model with 2.19-inch thickness could be employed; this would result in a sufficiently large model to enable taking detailed data in the bluff trailing edge region. It is felt that a thickness of 0.96 inch is prohibitively small to enclose the necessary measuring equipment and that the corresponding slot height would produce such a thin jet sheet that accurate measurements would be very difficult. Also, it was determined that maximum run time for

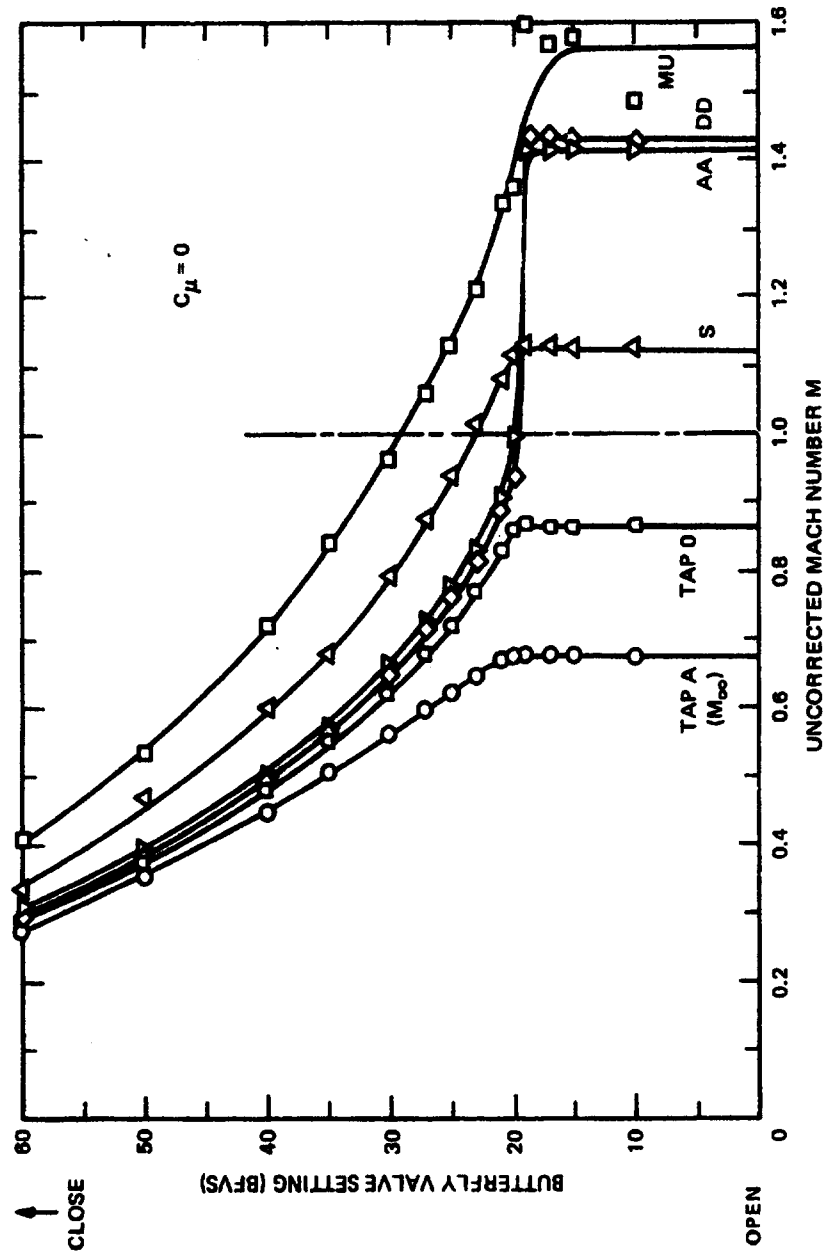


Figure 20 - Mach Number Variation at Selected Taps with Butterfly Valve Variation, 1.5-Inch Cylinder

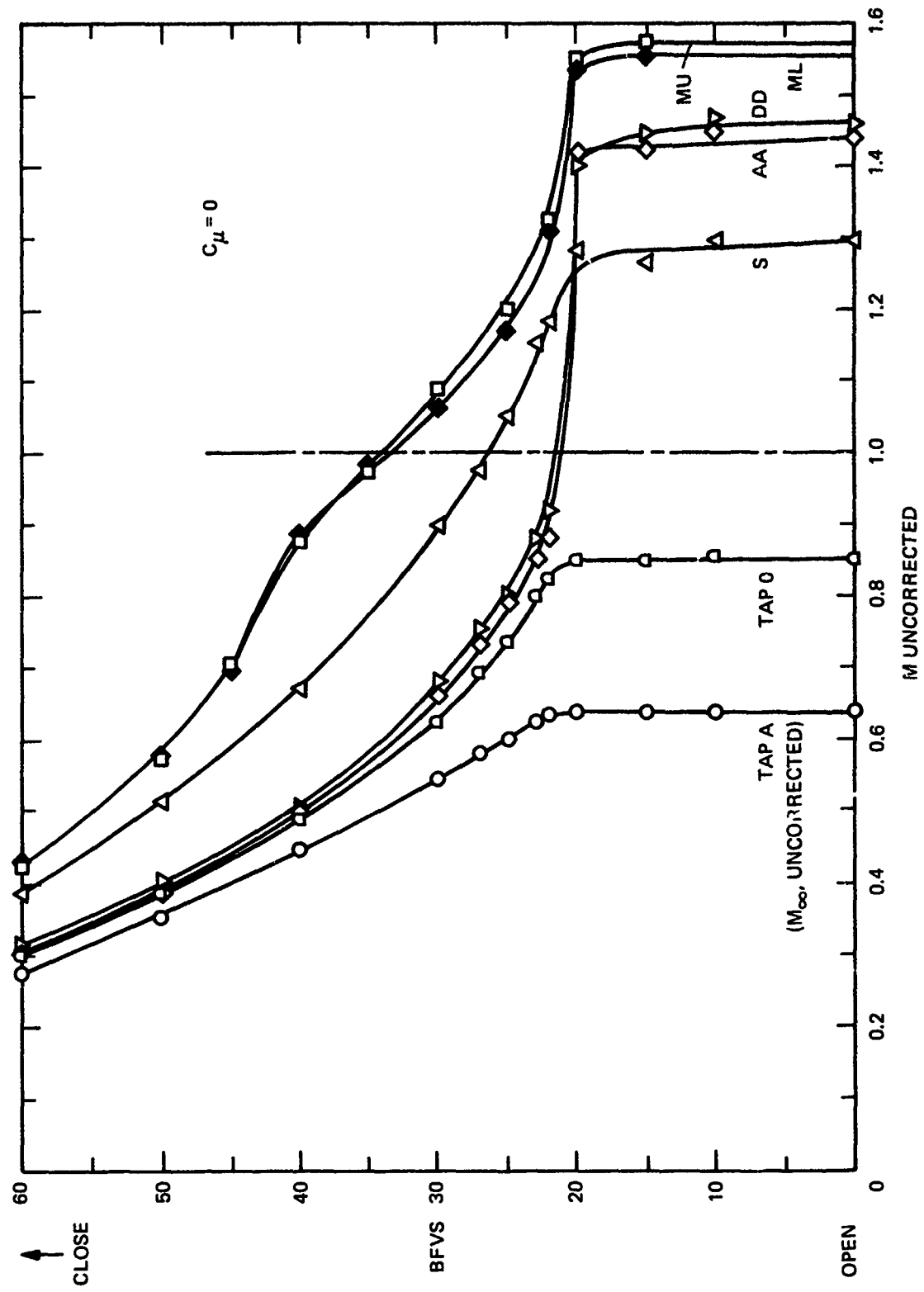
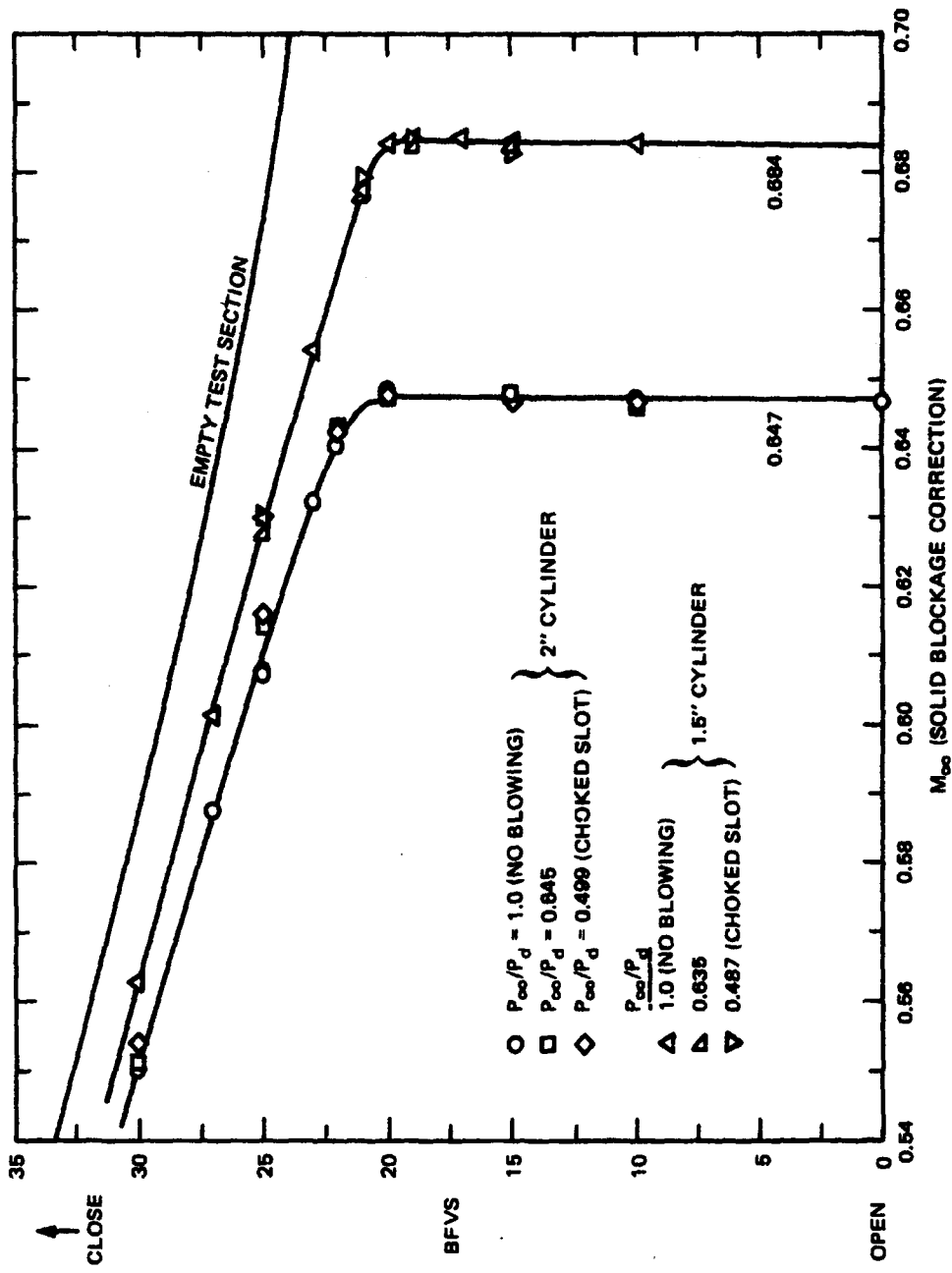


Figure 21 - Mach Number Variation at Selected Taps with Butterfly Valve Variation, 2.0-Inch Cylinder



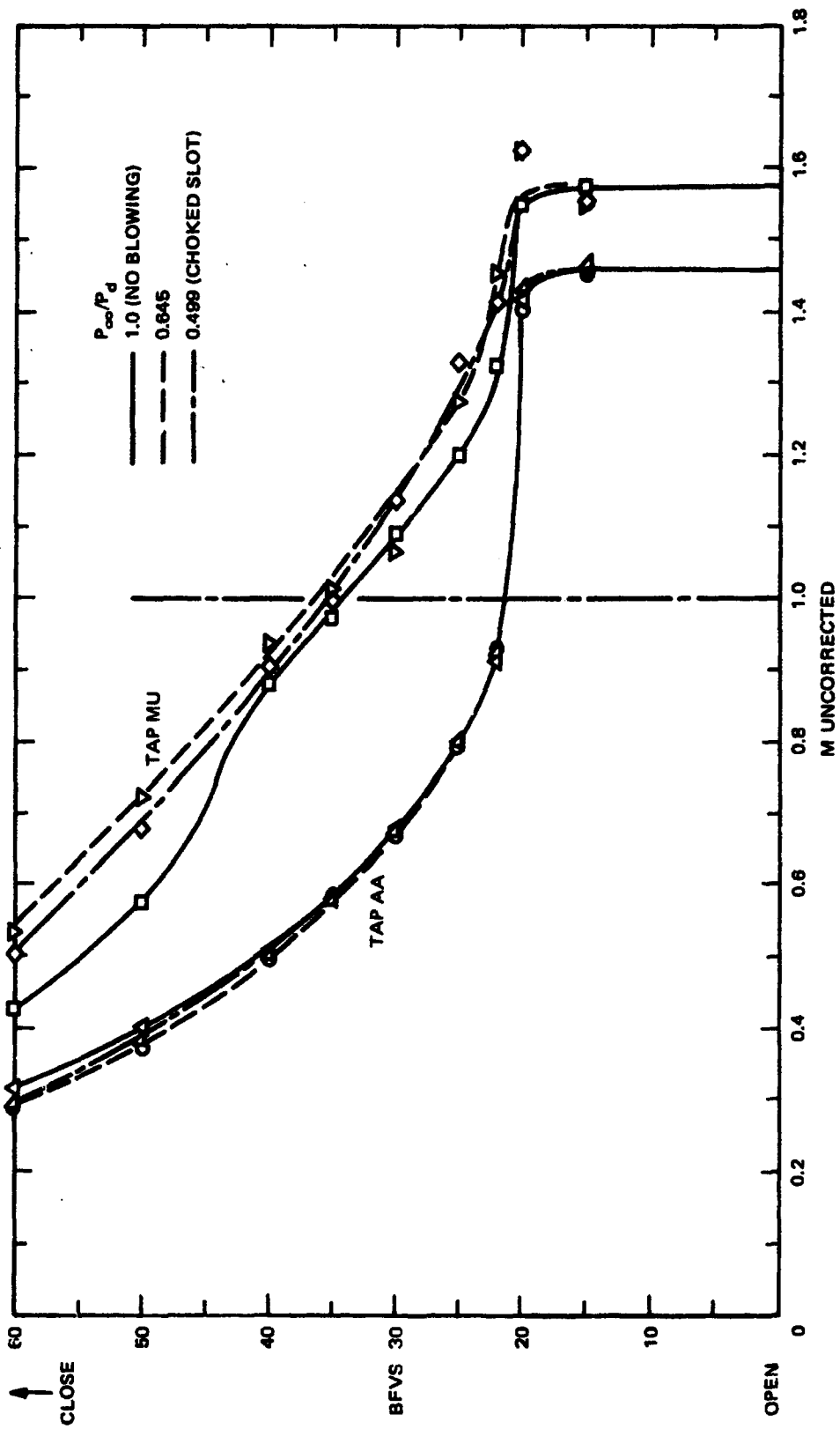


Figure 23 - Effect of Model Blowing on Two Local Taps, 2-Inch Cylinder

the in-draft tunnel was 10 seconds; half of that time was required to establish uniform flow and stabilized pressure in the data-recording system. Past experience in subsonic flow tests of blown models indicates that the maximum remaining time of 5 seconds would be insufficient to set the desired model blowing conditions and trigger the data recording scannivalves. It was thus concluded that the proposed transonic detailed tests could not be conducted in the NSRDC 18- x 18-inch tunnel on a model of sufficient size to acquire the desired information.

ALTERNATIVE TEST

As an alternative to the transonic tunnel, a 15- x 20-inch subsonic tunnel was available. Although a maximum free-stream dynamic pressure of only 60 psf (roughly 225 ft/sec or $M_\infty \doteq 0.2$) was available and thus appreciable free-stream compressibility effects could not be studied, it was still felt that the subsonic free stream would provide an external flow which would allow the jet detachment study to be conducted. The external pressure distribution and upstream boundary layer would provide a significant improvement over the static tests already discussed, and all the desired tests previously mentioned could still be run in the subsonic stream. While construction of a suitable model with 2-inch maximum thickness was underway (similar to the airfoil of Figure 12), the calibration of a hot film shear stress probe was conducted, as discussed next.

HOT FILM SHEAR STRESS PROBE CALIBRATION

An important aspect of the proposed tests is the accurate measurement of the wall shear stress along the trailing edge, primarily to locate the point of jet separation from the surface. The instrument chosen for the task in this case must meet the following criteria:

1. Produce no flow disturbance since this could easily cause premature jet separation.
2. Be applicable to curved surfaces with rather small radii, unlike an airfoil upper surface.
3. Have rapid dynamic response.
4. Be independent of the assumption of uniform static pressure across the boundary layer.

SHEAR STRESS MEASURING DEVICES

Several instruments are available for measuring shear stress in a fluid flow, but most are not applicable in this case because they cannot meet either Criterion 1 or 2 given above. A brief discussion follows.

An accepted method for determining the wall shearing stress is derived from a knowledge of the velocity gradient in the local boundary layer, where

$$\tau_w = \left(\mu \frac{du}{dy} \right)_w \quad (7)$$

This gradient has been determined experimentally in a number of ways (see, for example, Sturek and Danberg¹⁹ and Liepmann and colleagues^{21,22}). The usual device is a probe (hot wire, pitot tube, etc.) immersed within the boundary layer and traversed to yield the gradient. The main drawback is the disturbance of the flow produced by the probe and primarily the fact that the probe accuracy is least near the wall where the velocity gradient is steepest. This can be avoided by use of the floating element²³ which is a mechanical or electric balance that is actually part of the surface of the wall. No disturbance is produced and no calibration is needed, but the balance is quite complex and application to a cylindrical surface of small radius would be difficult.

Another type of surface probe can be constructed by attaching a razor blade flat against the wall so that its sharp edge almost covers a static pressure tap in the wall.²⁴ This converts the static tap into a total probe of very small disturbance; however, the static pressure at the exact edge of the blade must be known, and this usually involves the assumption that a value measured at the surface is constant across the sampled layer. That assumption may be invalidated by surface curvature effects of CC trailing edges; moreover, the dynamic response is low, and the device might be difficult to construct on a curved surface. Similar surface probes such as Stanton and Preston tubes have similar drawbacks; in addition, all three devices must be calibrated.

Fage and Falkner²⁵ developed a technique whereby a hot wire is embedded in a surface groove and shear stress measured as a function of heat transfer from it. This avoids the flow disturbance problem, and the very rapid response time is in itself an aid to flow diagnosis under unsteady conditions. The flush-mounted hot film probe is an up-dated version of the device developed by Bellhouse and Schultz;²⁶ it is commercially available, small, readily

²¹Liepmann, H. A. and A. Roshko, "Elements of Gasdynamics," John Wiley and Sons, Inc., New York, 1967

²²Liepmann, H. A. and G. T. Skinner, "Shearing-Stress Measurements by Use of a Heated Element," Nov 1954, NACA Technical Note 3268.

²³Dhawan, S., "Direct Measurements of Skin Friction," 1953, NACA Report 1121.

²⁴Pai, B. R. and J. H. Whitelaw, "Simplification of the Razor Blade Technique and its Application to the Measurement of Wall-Shear Stress in Wall-Jet Flows," The Aeronautical Quarterly, Vol. XX, Part 4, pp. 355-364, Nov 1969.

²⁵Fage, A. and V. M. Falkner, "Relation Between Heat Transfer and Surface Friction for Laminar Flow," 1931, Aeronautical Research Council R & M 1408.

²⁶Bellhouse, B. J. and D. L. Schultz, "Determination of Mean and Dynamic Skin Friction, Separation, and Transition in Low-Speed Flow with a Thin-Film Heated Element," Journal of Fluid Mechanics, Vol. 24, Part 2, pp. 379-400, Feb 1966.

mounted even in curved surfaces, and compatible with conventional hot wire anemometer equipment. The one drawback is that each probe must be individually calibrated because of the uniqueness of the sensing element.

CALIBRATION TECHNIQUE

Similar to the hot wire, the hot film probe operates on the relationship between heat transferred from the probe to a flow field in which it is immersed and the shear stress (diffusion of vorticity) acting at the wall boundary of that flow. This relationship, a refinement of King's law for convective heat transfer,^{22,25,26} expresses the electrical power required to maintain a constant probe temperature as a linear function of the cube root of the wall shearing stress:

$$\frac{i^2 R}{T_w - T_0} = A \tau_w^{1/3} + B \quad (8)$$

or in simpler form for fluids of near-constant temperature,

$$E_b^2 = A_1 \tau_w^{1/3} + B_1 \quad (9)$$

where $i^2 R$ = power supplied to the sensor (equal to Q_w , the heat loss from it)

E_b = bridge voltage of the anemometer

τ_w and T_w = shear stress and temperature at the wall

T_0 = free-stream reference temperature

A, A_1, B and B_1 = constants of proportionality for a given probe

Because of the complexity of the convective heat transfer equations as well as the problems produced by heat conduction or leaks to the probe substrate from the sensor, it is not feasible or practical to theoretically determine the constants in Equations (8) or (9) for a given probe, and thus an individual calibration must be conducted.

The probe chosen for use in this paper, a DISA Subminiature Type 55A92, was selected primarily because of its small size; it has a nickel film sputtered on the end of a quartz rod 0.083 inch in diameter and 0.43 inch long. The hot film was installed as the fourth arm of a Wheatstone bridge which composed the main circuitry of a Thermo-Systems Model 1010 Constant Temperature Anemometer (CTA). Figure 24 shows the probe and a schematic of the CTA. In operation of the system, constant temperature in the probe sensor is maintained by setting a fixed resistance with the adjustable R_4 resistance deck. As heat transfer from the probe varies with flow conditions, so also do bridge voltage and current. The voltage is

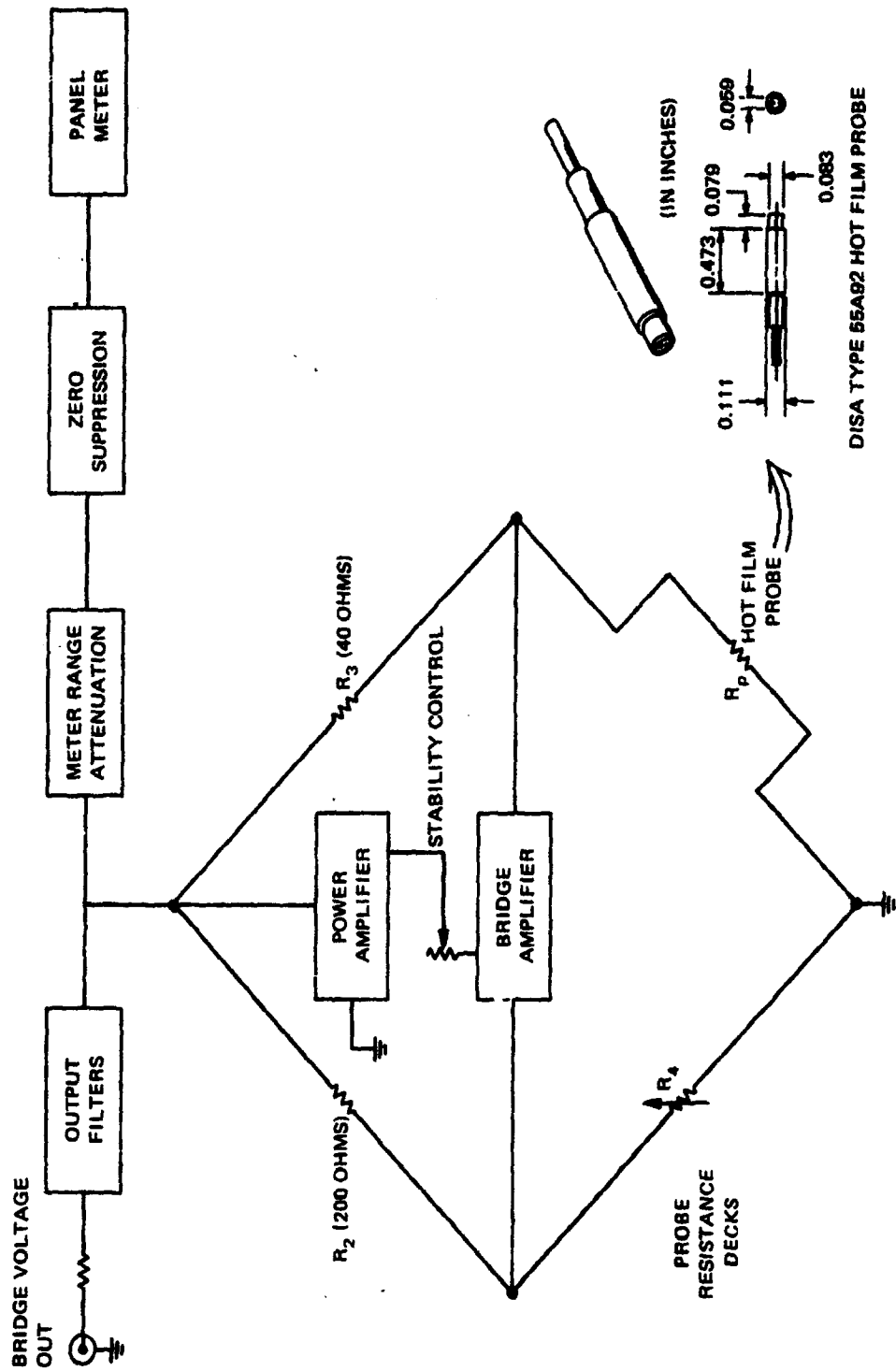


Figure 24 - Details of Anemometer Circuitry

amplified and monitored during the calibration; current and dissipated power can be calculated from knowledge of the fixed resistance. The voltage is internally and automatically adjusted to maintain the set bridge balance, and thus no temperature fluctuations occur in the probe. This feature makes the system relatively simple compared to the constant current anemometer and allows greater sensitivity; this is especially useful for dynamic measurements of unsteady conditions.

The actual calibration of the system is not a particularly simple matter, however. Equations (8) and (9) were derived and experimentally verified²² for subsonic laminar flows, and the criterion was developed that for the equations and laminar flow calibrations to hold in turbulent flow for a given probe, the following inequality must hold^{22,26,27} to ensure that the thermal sublayer downstream of the hot film is much smaller (thinner) than the laminar sublayer:

$$1 \ll \frac{Q_w L_s}{\lambda \Delta T} < \frac{P_R}{C_f}$$

or

(10)

$$1 \ll \frac{i^2 R}{T_w - T_0} \frac{L_s}{\lambda} < \frac{P_R}{C_f}$$

The same assurance is made by another experimentally developed criterion:

$$\frac{L_s U_T}{\nu P_R} < K$$

(11)

where $K = 64$ from Brown²⁸ and $K = 32$ from Pope²⁹ (for less than 4-percent error in shear stress). By using a comparison between hot film calibrations and skin friction measurements made by floating element balance, Owen and Bellhouse³⁰ showed that data up to $M_\infty = 4.5$

²⁷Geremia, J. O., "Experiments on the Calibration of Flush Mounted Hot Film Sensors," in "DISA Information, Measurement, and Analysis," No. 13, May 1972.

²⁸Brown, G. L., "Theory and Application of Heated Films for Skin Friction Measurement," Paper 18, Proceedings of the 1967 Heat Transfer and Fluid Mechanics Institute, pp. 361-381, Jun 1967.

²⁹Pope, R. J., "Skin Friction Measurements in Laminar and Turbulent Flows Using Heated Thin Film Gages," AIAA Journal, Vol. 10, No. 6, pp. 729-780, Jun 1972.

³⁰Owen, F. K. and B. J. Bellhouse, "Skin Friction Measurement at Supersonic Speeds," AIAA Journal, Vol. 8, No. 7, pp. 1358-1360, Jul 1970.

agree very closely with a calibration made in a subsonic laminar boundary layer. Similar work by Laufer and McClellan³¹ at speeds up to $M_\infty = 4.5$ showed independence from free-stream Mach number for a hot wire anemometer (but dependence on Reynolds number based on conditions behind the detached bow shock on the wire; this would not be a factor for a flush-mounted probe).

The calibration itself must be conducted in a flow condition where very accurate determination of the shear stress can be made and which will not differ markedly from the actual application of the probe (i.e., the constants of Equations (8) and (9) must be valid for both the calibration flow and the actual test condition). Flow over a flat plate immediately suggests itself for the calibration flow, but the factor of curvature of the trailing edge of the CC model implies that the flat plate boundary layer calibration (zero pressure gradient) will probably not be valid for the test conditions (pressure gradient a function of arc length and curvature). Bellhouse and Schultz²⁶ and Geremia²⁷ suggest the use of fully developed pipe flow, where the wall shearing stress is linearly proportional to pressure drop over a known distance for both laminar and turbulent flow (see Schlichting³² and Kuethe and Schetzer³³):

$$\tau_w = \frac{\Delta p}{X} \frac{R_{\text{pipe}}}{2} \quad (12)$$

Geremia²⁷ used a single pipe with the probe inserted from the outside of the pipe and protruding slightly into the inner surface; it is considered to be flush mounted (not interfering with the flow) if the protrusion is an order of magnitude less than the expected thickness of the laminar sublayer. For the case of water flowing in a 4-inch-diameter pipe with a 0.083-inch-diameter probe installed, the allowable protrusion was 0.0005 inch. The calibrated probe, however, was to be used in applications other than the pipe; thus it was installed on a flat plate and tested in a towing tank facility to check validity of the calibration. The measured shear stress, determined by using the pipe calibration, agreed quite well with skin friction data from other experiments, and it was concluded that the pipe calibration held in environments other than the pipe if the same range of shear stress was involved.

Bellhouse and Schultz²⁶ suggest a setup that, in the case of the present test, would allow a calibration of the probe in the actual test configuration. Their use of an annular

³¹ Laufer, J. and R. McClellan, "Measurements of Heat Transfer from Fine Wires in Supersonic Flows," *Journal of Fluid Mechanics*, Vol. 1, Part 3, pp. 276-289, Sep 1956.

³² Schlichting, H., "Boundary Layer Theory," 6th ed. McGraw Hill, New York, 1968.

³³ Kuethe, A. M. and J. D. Schetzer, "Foundations of Aerodynamics," 2nd ed. John Wiley and Sons, Inc., New York, 1964.

tunnel, consisting of two concentric pipes with flow in the annulus between them, allows the inner pipe to simulate the proposed model trailing edge cylinder. Thus the probe can be calibrated in the same physical geometry as the actual application. However, the two flow conditions are not identical (one is axial, one circumferential), but Reference 26 indicates good agreement for differing flows if inequality, Equation (11), holds and data are within the same shear stress range. These investigators also report²⁶ that although a probe installed in a flat plate could protrude up to 0.003 inch in turbulent flow without affecting the probe calibration, the same protrusion in laminar flow caused noticeable changes.

CALIBRATION APPARATUS AND PROCEDURE

An annular calibration tunnel was constructed by using an 8-foot length of aluminum hand-polished pipe (outer diameter 2 inches) to serve as the inner surface of the annulus. The DISA 55A92 hot film probe was mounted in a removable plug which was machined to fit the trailing edge cylinder of the subsonic two-dimensional model (also to have a 2-inch diameter). This mounting plug was interchangeable between the trailing edge cylinder and the annulus inner pipe. An iron-constantan thermocouple was also installed in the plug to measure temperature of the surface 1/8 inch from the center of the hot film. A static pressure tap was located in the inner pipe at the same longitudinal station as the film but offset 45 degrees around the cylinder. Two outer aluminum 8-foot pipes were prepared in order to produce two different annular channel heights: a 3-inch OD pipe with 1/8-inch wall thickness gave a channel height d_3 of 3/8-inch (2.80 inch² annulus area) and a 4-inch OD pipe with 1/8-inch wall gave an annulus height d_4 of 7/8 inch (7.90 inch² area).

There was a twofold reason for constructing two channels: (1) to produce different velocity ranges in the pipes and thus extend the range of shear stress attainable and (2) to confirm that the pipe flow determination of shear stress, Equation (12), in single pipes was valid for annuli (if it were not, the two different annuli should yield unlike calibrations). The outer pipes were pressure tapped in a plane which was rotated 45 degrees from the hot film probe when the two pipes were attached by means of tension and set screws located on the opposite side of the inner pipe from the probe. Figure 25 shows a schematic of the setup. The annular tunnel thus constructed was faired with circular cross-section inlets for smooth flow at the entrance and inserted at the downstream side into a 4-foot-long plenum chamber of 6-inch ID. The chamber, in turn, was joined to the inlet side of an ILG Type PE-6 Centrifugal Blower, thus forming an indraft tunnel where the pulsations from the driving unit would be downstream of the calibration section and isolated by the settling chamber formed by the plenum.

In initial operation of the system, the blower rapidly evacuated the plenum, which could not be resupplied at the same rate because of the small area of the annular tunnel. Thus the

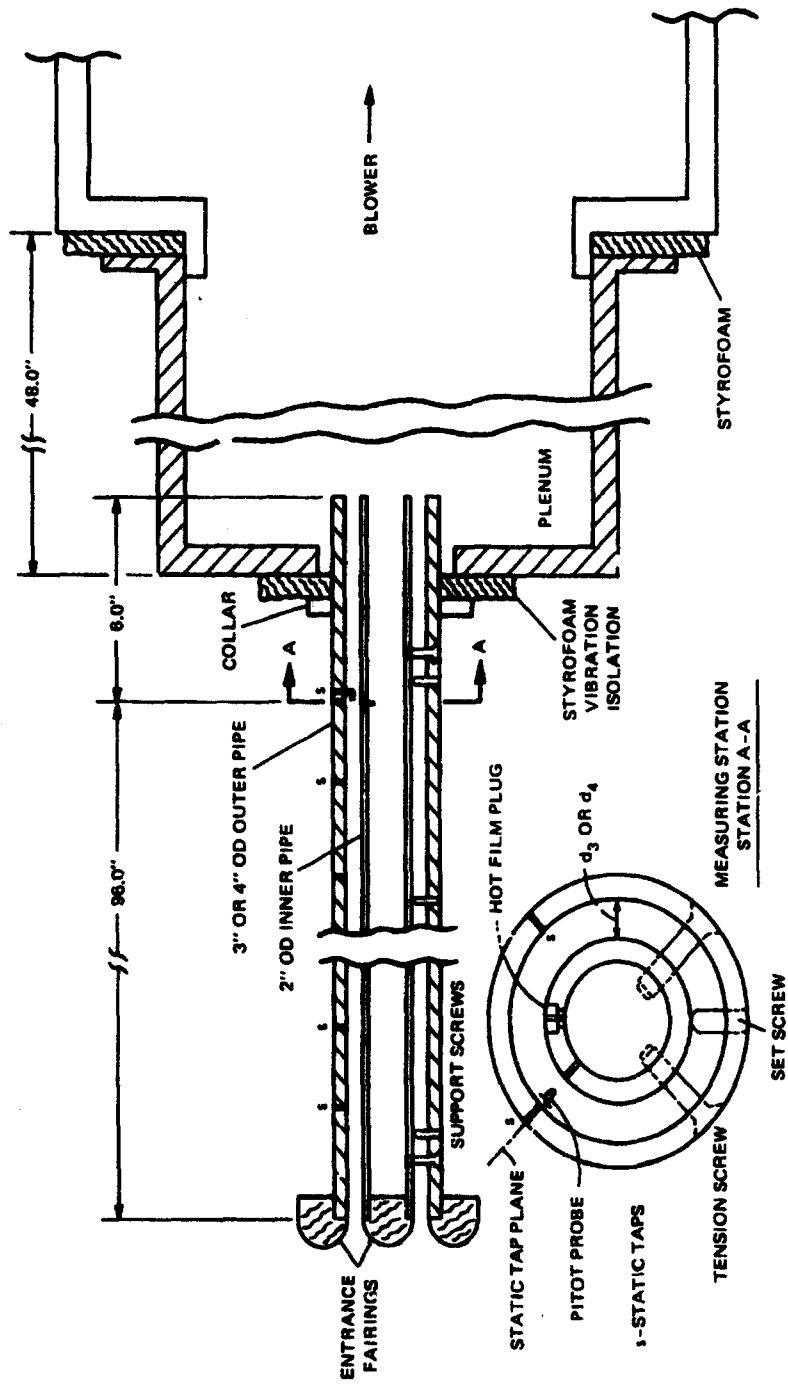


Figure 25 - Details of Annular Calibration Tunnel

centrifugal blower had to operate against a large pressure rise between the plenum and the ambient pressure at the blower exit (a condition of poor efficiency for the unit), and hence velocity through the calibration section was limited. To compensate for this, a second PE-6 blower was installed in series with the first, with its inlet connected to the exhaust side of the first. The pressure rise across the initial blower was thus considerably reduced, its operating efficiency greatly improved, and a much higher velocity achieved in the annulus. Figure 26 depicts the setup. The dynamic pressure at the measuring station was measured with a total head probe located at the center of the annulus channel and at the same longitudinal location as the static tap in the inner pipe. Two additional static taps were located in the outer pipe to verify uniform static pressure around the annulus at the measuring station. Figure 27 presents velocity, dynamic pressure, and Reynolds number based on diameter (i.e., the effective annulus height between the inner and outer pipes) as a function of the blower speed. Since the transition from laminar to turbulent flow in pipes occurs at approximately $2000 \leq Re_d \leq 13,000$, it is seen that almost all the calibration data were for turbulent flow.

The calibration procedure consisted of setting the hot film probe at a given overheat ratio and varying blower rpm and thus the velocity, pressure drop, and shear stress at the probe. Setting a constant overheat ratio (R/R_0) is equivalent to setting the probe at a fixed operating film temperature; the two are related by the equation

$$\frac{R - R_0}{R_0} = \alpha_T (T - T_0) \quad (13)$$

where α_T = temperature coefficient of resistance
 R_0 and T_0 = cold (or free-stream reference) resistance and temperature
 R and T = heated (or operating) resistance and temperature

The linear relation, Equation (13), is different for each probe and the coefficient α_T is supplied by the manufacturer; the value for the present hot film was 0.0051/degree C.

Figure 28 presents sample static pressure distributions taken along the inner walls of both the 3- and 4-inch OD outer pipes for several blower speeds. The shear stress at the probe station is directly proportional to the slope of these curves once the flow has become fully developed (at which point the curves should become linear). Geremia²⁷ indicates that for turbulent flow, this should occur at approximately 25 to 40 diameters (annulus heights) downstream of the inlet and for laminar flow, between 150 and 300 diameters. As can be seen, the pressure distribution became linear a considerable distance upstream of the probe for both pipes and thus Equation (12) should be valid in all cases.

A range of overheat ratios from 1.1 to 1.8 was set for the 3-inch pipe annulus and 1.6 to 1.8 for the 4-inch pipe; data were taken for a range of blower speeds from 250 to 3000



**INLET, ANNULAR TUNNEL, WEIGHTS,
AND PRESSURE TAPS**



CENTRIFUGAL BLOWERS IN SERIES



**JUNCTION OF ANNULAR TUNNEL
AND PLENUM**



**PROBE AND THERMOCOUPLE IN-
STALLED IN PLUG IN INNER PIPE**

Figure 26 – Annular Tunnel Calibration Setup

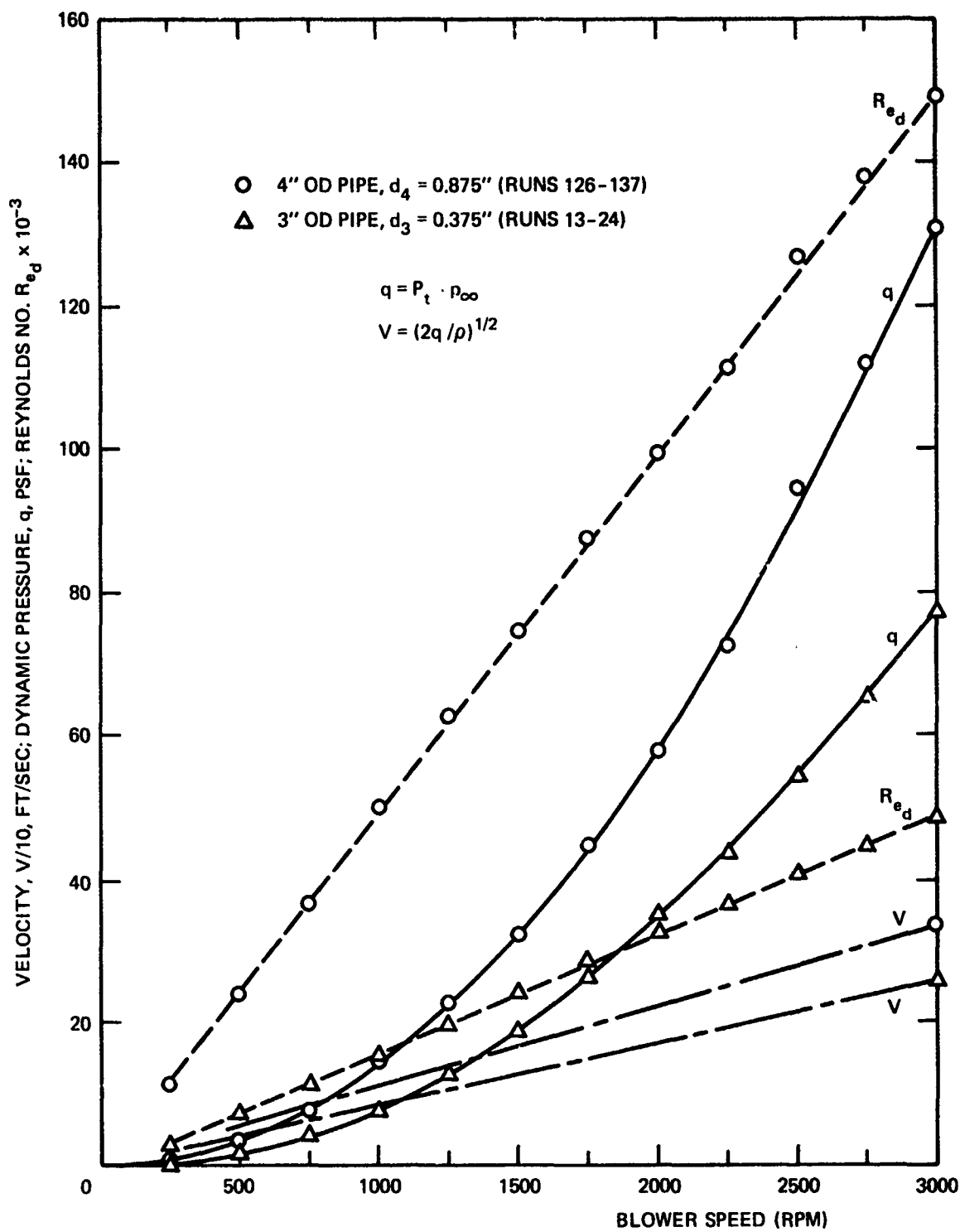


Figure 27 - Velocity, Dynamic Pressure, and Reynolds Number at the Calibration Station as a Function of Blower RPM

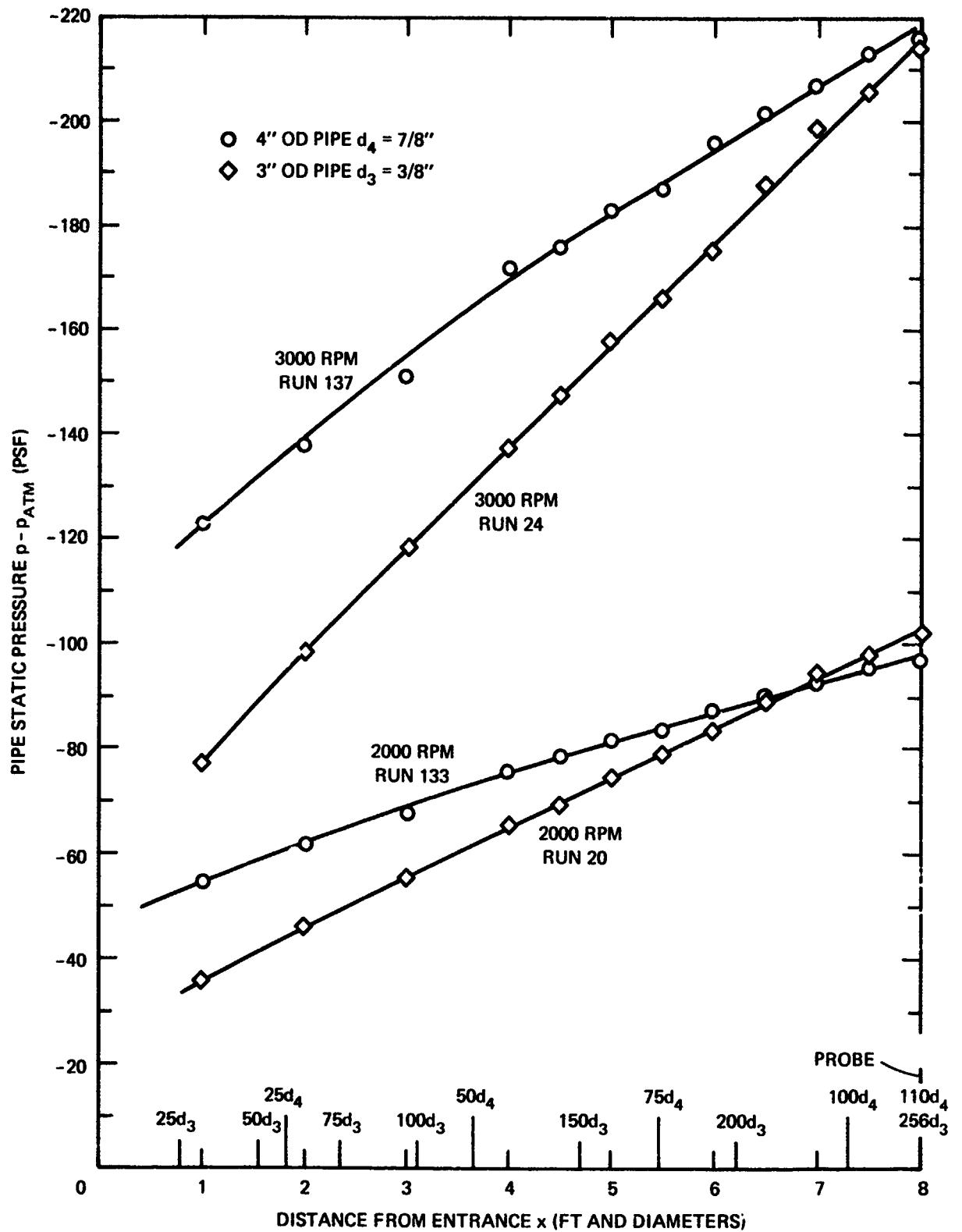


Figure 28 - Static Pressure Drop in Annulus Channel

rpm. Before each overheat ratio was set, probe cold resistance and temperature were recorded. For each data run (different rpm and constant R/R_0) the following were recorded: bridge voltage, barometric pressure, ambient temperature, and temperature from the thermocouple mounted in the hot film plug. All pipe static pressures and total pressure were automatically recorded on a 48-port scannivalve with a ± 1 -psid transducer installed. Data were computer-reduced by XDS 930 with paper tape input from the scannivalve unit. Bridge current could be readily calculated from the input data and thus the voltage at the sensor could be determined as follows (see Figure 24):

$$I_b = E_b / (R_p + R_3) \quad (14)$$

$$R = R_p - R_{leads} \quad (15)$$

$$E_s = I_b R \quad (16)$$

where probe and sensor resistance differ only by the connecting lead resistance of 1.0 ohm. From Equation (13), the sensor cold resistance, operating temperature, and power dissipation were

$$R_0 = R_{p0} - R_{leads} \quad (17)$$

$$T_s = (R - R_0) / R_0 \alpha_T + T_0 \quad (18)$$

$$\frac{P_s}{\Delta T} = \frac{I_b^2 R}{T_s - T_0} \quad (19)$$

CALIBRATION RESULTS AND DISCUSSION

Results from the calibration runs were initially plotted in terms of sensor voltage as a function of shear stress. Figure 29 shows this relationship for the 3-inch outer pipe and an overheat ratio of 1.2. All data for this and following calibration data were polynomial curve fit for powers up to 3, i.e.:

$$(E_s^2) = a (\tau_w^{1/3})^3 + b (\tau_w^{1/3})^2 + c (\tau_w^{1/3}) + d \quad (20)$$

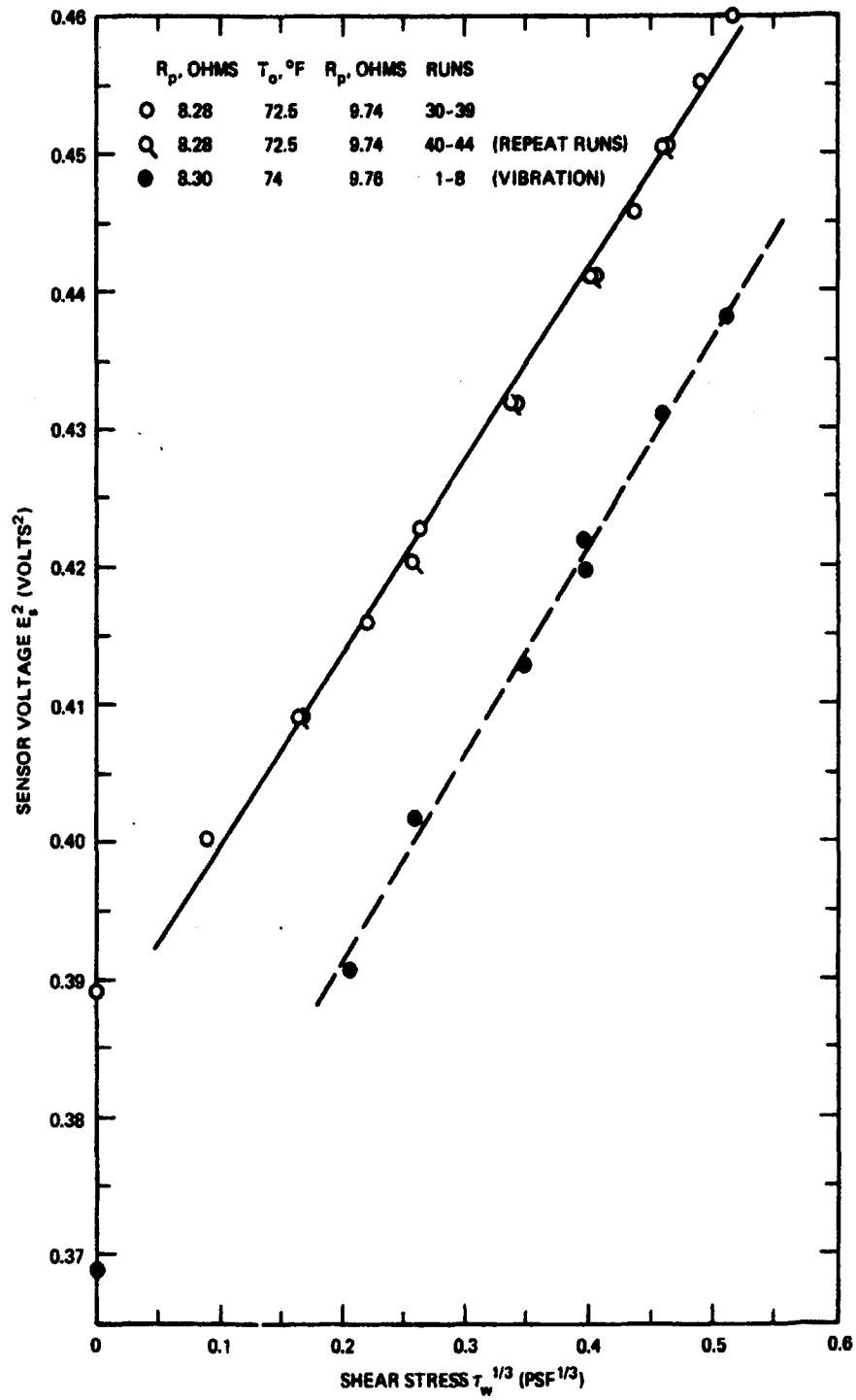


Figure 29 - Sensor Voltage as a Function of Shear Stress, $R/R_0 = 1.2$ (3-Inch OD Pipe)

and in almost every case the best fit was a linear one, as predicted by Equation (9). It would be expected from Figure 29 that the two curves should coincide since they are for the same overheat condition. For data represented by the lower curve, however, a serious vibration was noticed in the 8-foot outer pipe, and its frequency appeared to increase with blower rpm. As blowers, plenum, and pipes were all rigidly interconnected, considerable unbalance was noted in the two blowers. It was surmised that blower vibration had affected the boundary layer in the annulus and caused a fluctuating disturbance at the probe. Thick styrofoam insulation was inserted between the blower and plenum, between the plenum and annulus collar (see Figures 25 and 26), and between the annulus and wooden mounting supports. In addition, 25-pound weights were suspended from the pipes at the mounting supports to tie the system down. The vibrations in the pipe could no longer be detected, and the upper curve of Figure 29 then resulted.

Figure 30 exhibits a similar difference before and after vibration isolation for $R/R_0 = 1.6$, but another trend is also evident. The circles and flagged repeat points were run on the same day, but the triangles and flagged repeat data were run at a later date at the same overheat ratio. The change in slope is disturbing. It was noted that although R/R_0 was constant, the cold temperatures differed by 2 degrees F and the cold probe resistances were 8.24 and 8.28 ohms, thus causing the operating probe resistance to be 12.58 and 12.64 ohms, respectively, for the lower and upper curves. Thus, for a constant overheat ratio, the hot film was operating at different temperatures.

Figure 31 confirms that a deliberate change in R/R_0 did indeed change the calibration curve slope for the 3-inch pipe. Accordingly, it was decided to hold probe operating temperature and resistance constant instead of overheat ratio based on cold resistance. For this condition, Figure 32 shows the results for the 4-inch OD pipe, where probe resistance was constant at 14.09 ohms. The two curves are parallel but do not coincide. It was noted that repeat data for the circles fell closer to the triangle curve. The cause of the discrepancy in agreement was again apparently the change in cold temperature. Figure 33 depicts the change in cold resistance with cold temperature, where a relatively small change in temperature can produce enough difference in R_{p0} to cause significant change in overheat ratio. Figure 34 shows that the same problem causes disagreement when data for the two different cylinders are compared. It is thus concluded that Equation (9) is sufficiently affected by even small temperature changes of only a few degrees to render it questionable for calibration purposes.

Data for all calibration runs were then replotted in terms of Equation (8). Figure 35 presents the data of Figure 30 in terms of power dissipated. Again the discrepancy in the rerun data at different cold temperature and resistance is present but somewhat reduced. In terms of error evaluation, note that at the higher rpm portion of the curves, the discrepancy in the dependent variable between the upper and lower curves of Figure 30 is larger than for

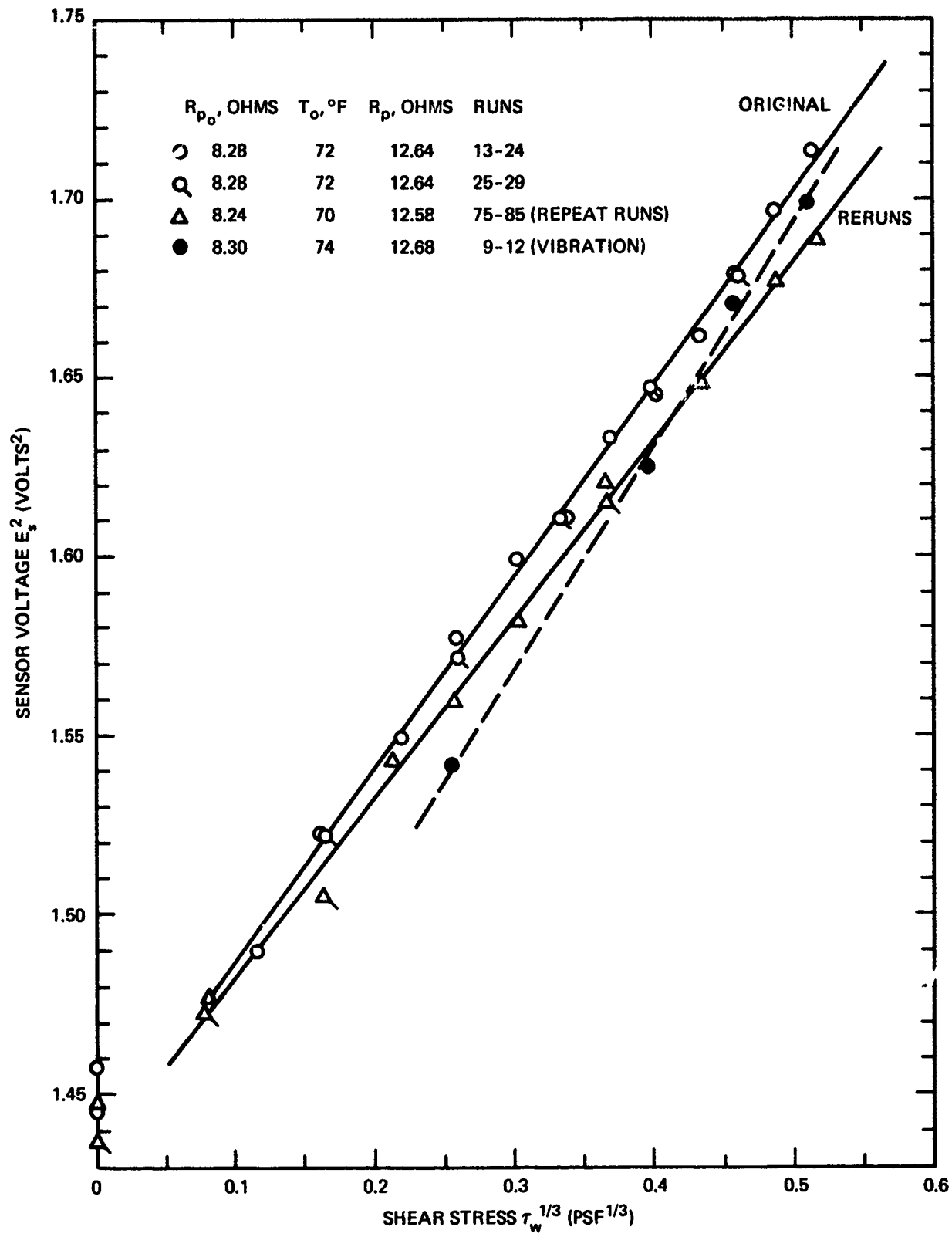


Figure 30 -- Sensor Voltage as a Function of Shear Stress, $R/R_0 = 1.6$ (3-Inch OD Pipe)

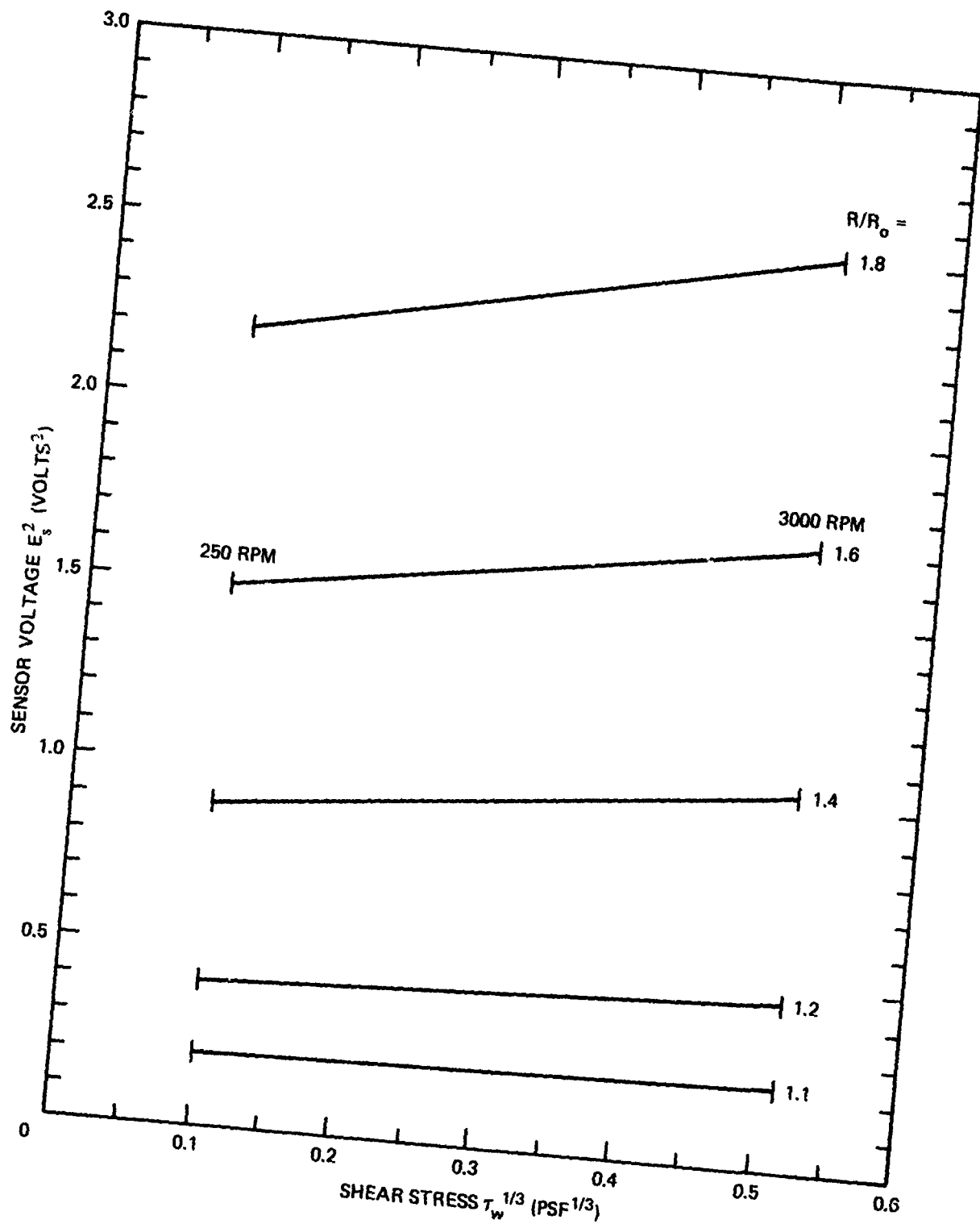


Figure 31 - Sensor Voltage as a Function of Shear Stress for Five Overheat Ratios (3-Inch OD Pipe)

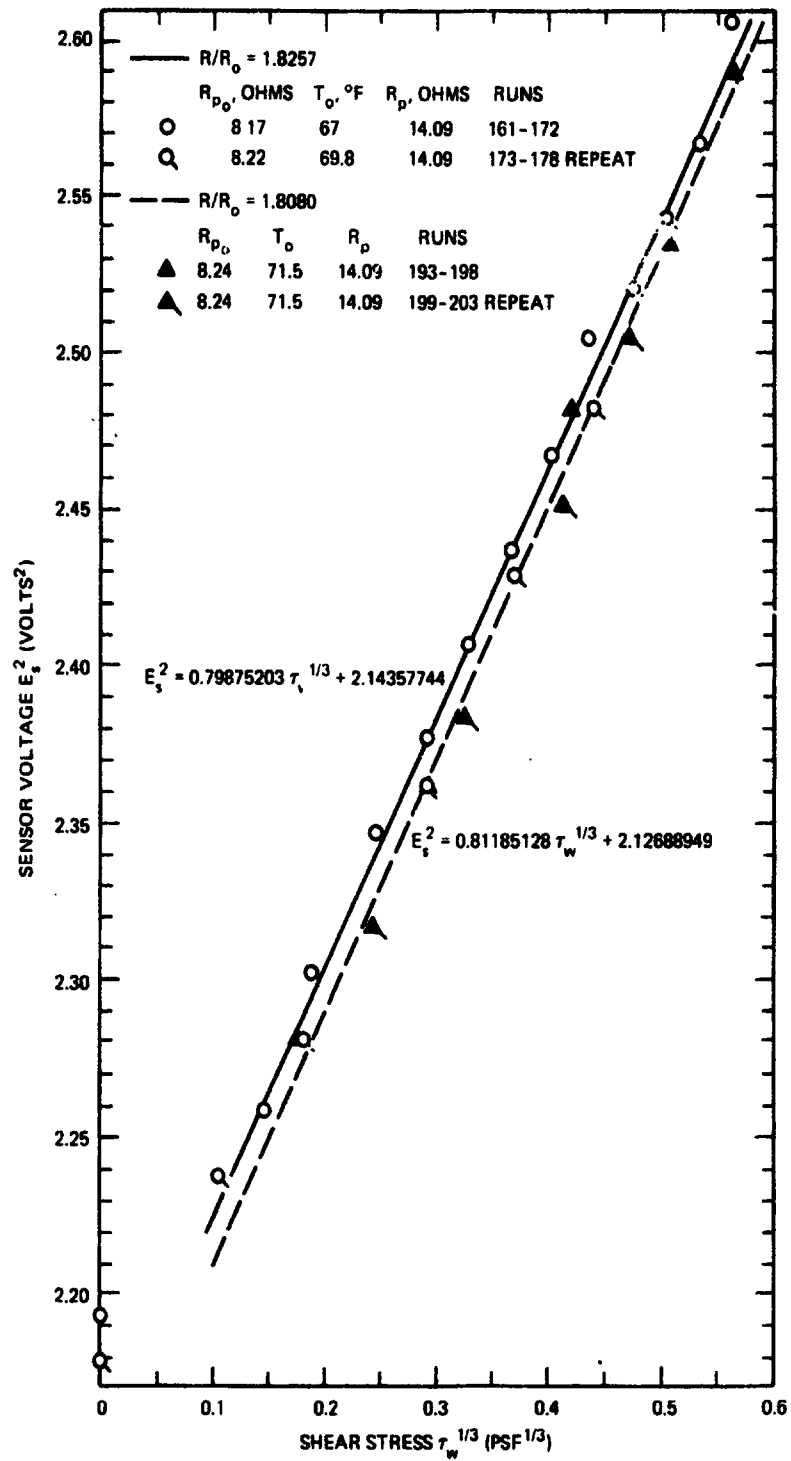


Figure 32 - Sensor Voltage as a Function of Shear Stress (4-Inch OD Pipe)

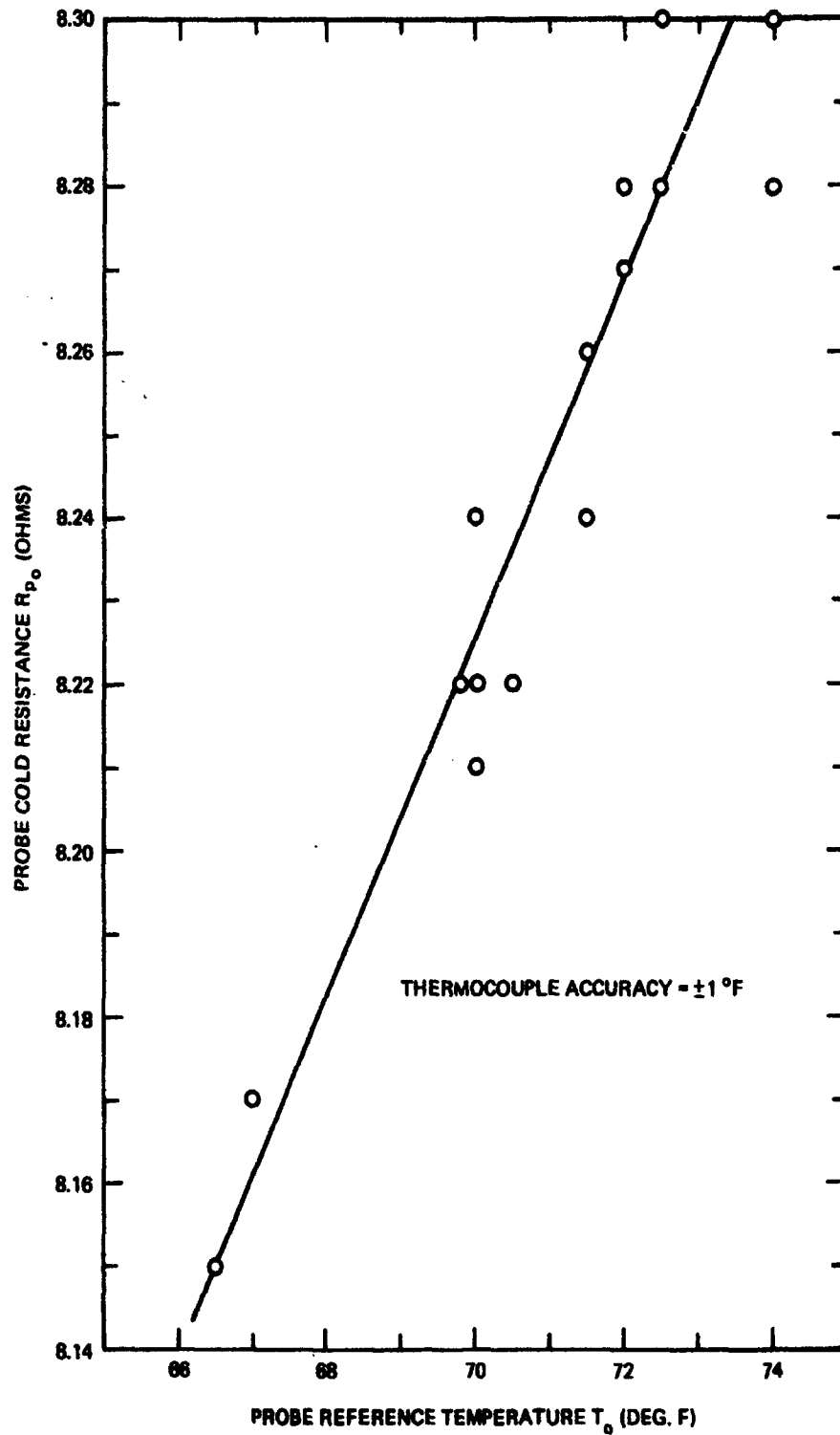


Figure 33 - Variation of Probe Cold Resistance with Temperature

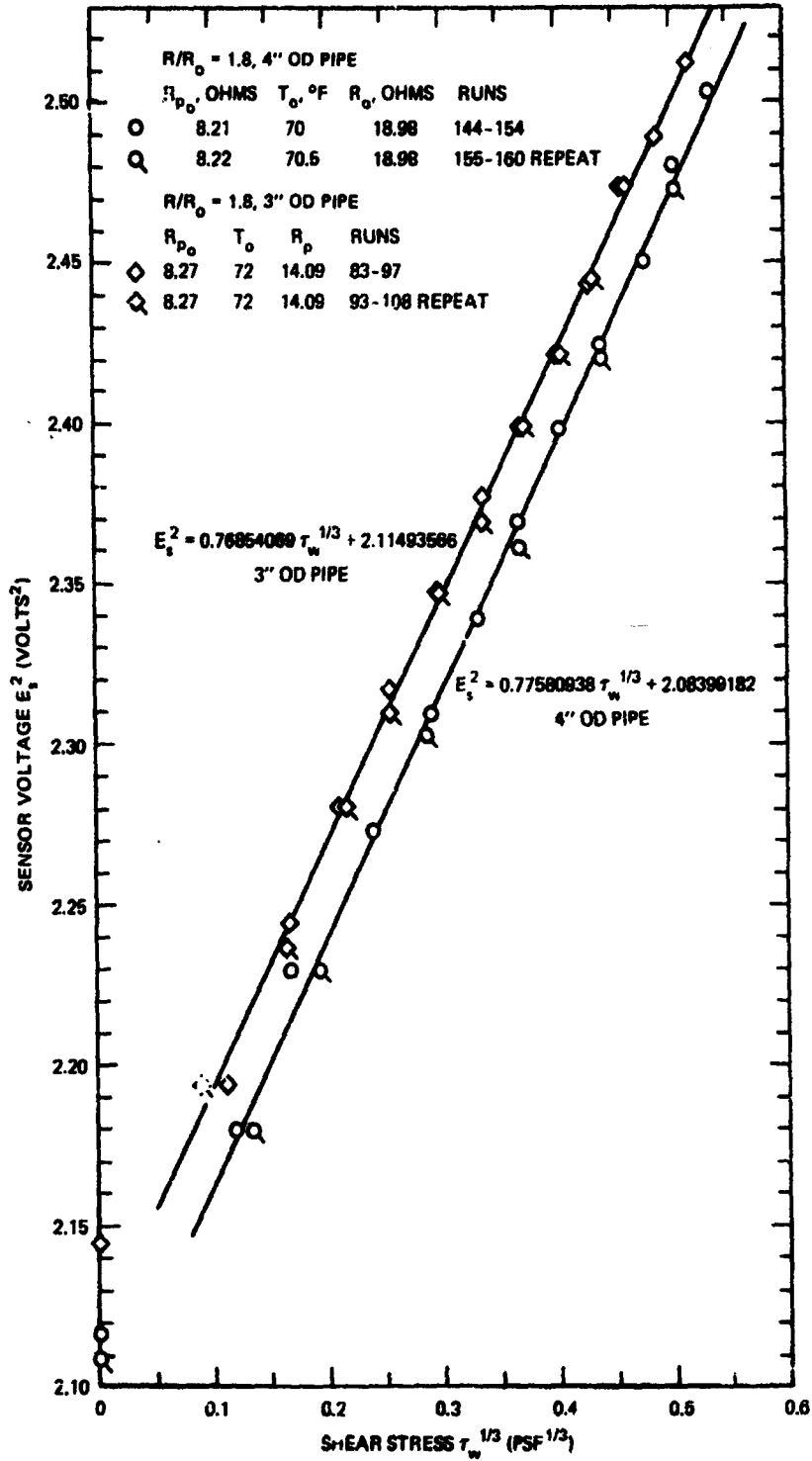


Figure 34 - Comparison of Voltage-Shear Stress Relationship for 3- and 4-Inch OD Pipes, R/R_o = 1.8

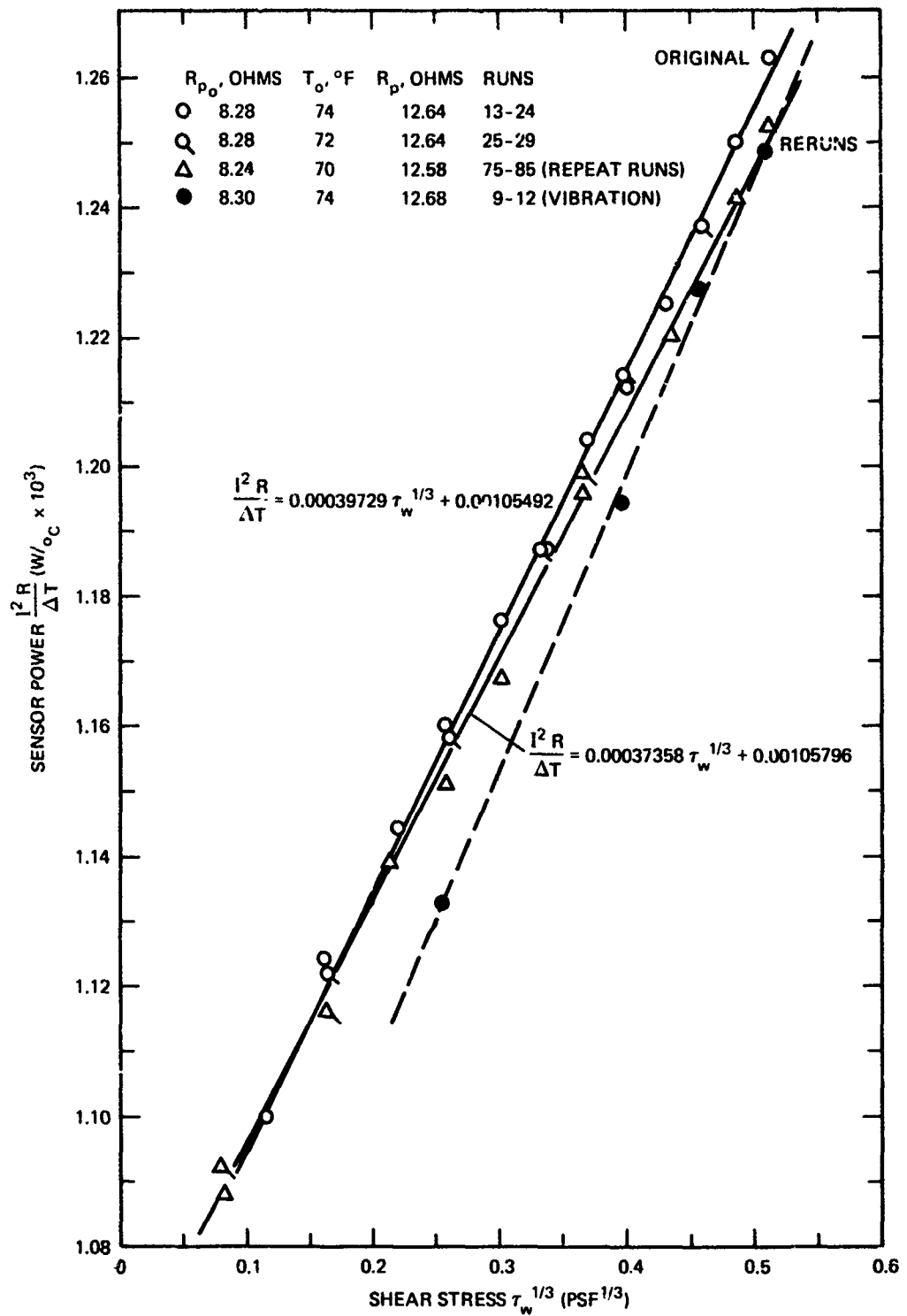


Figure 35 – Sensor Dissipated Power versus Shear Stress, $R/R_0 = 1.6$ (3-Inch OD Pipe)

Figure 35. For example, for a value of $\tau_w^{1/3} = 0.5$ produced by the same test rpm in all cases, the discrepancy in the dependent variable between the upper and lower solid curves of Figure 30 was 1.11 percent, compared to 0.72 percent from Figure 35. Although neither error appears large at first glance, it must be remembered that the calibration curves are to be used in the reverse manner as above. In other words, $\tau_w^{1/3}$ will be the dependent variable, and thus the discrepancy in τ_w will be the cube of the above.

Figure 36 compares the power dissipation curve for the 3- and 4-inch cylinders; the agreement is quite good compared to Figure 34. Also shown is the linear curve fit for the combined power data for both cylinders. Since these data were for a high overheat ratio of 1.8 (Figure 31 shows the increased sensitivity of the system as higher overheat ratios are used, i.e., more range in the recorded variable E_b over the range of $\tau_w^{1/3}$, and thus less error caused by reading inaccuracies) and since the agreement was quite good, it was decided to use this calibration in the follow-on two-dimensional model test. Thus the shear stress would be calculated from:

$$\frac{I_b^2 R}{T_s - T_0} = 0.00037458 \tau_w^{1/3} + 0.00102780 \quad (21)$$

The validity of this calibration for both laminar and turbulent flow measurements is seen from the following data, which satisfies Equation (11) in all cases and meets the more restrictive value $K \leq 32$ in all but two cases. ($L_s = 0.0059$ inch.)

RPM	τ_w (pst)	U_T (fps)	$(L_s U_T)/P_R \nu$
250	0.002	0.97	0.43
500	0.007	1.74	7.77
750	0.015	2.52	11.23
1000	0.023	3.11	13.85
1500	0.050	4.63	20.66
2000	0.082	5.95	26.50
2500	0.125	7.33	32.69
3000	0.169	8.53	38.03

SUBSONIC TWO-DIMENSIONAL INVESTIGATIONS

When the proposed transonic tests proved unfeasible, subsonic two-dimensional testing was undertaken as an alternative to determine essentially the same items as described under the transonic investigations. In the absence of the compressible flow field, it was felt that

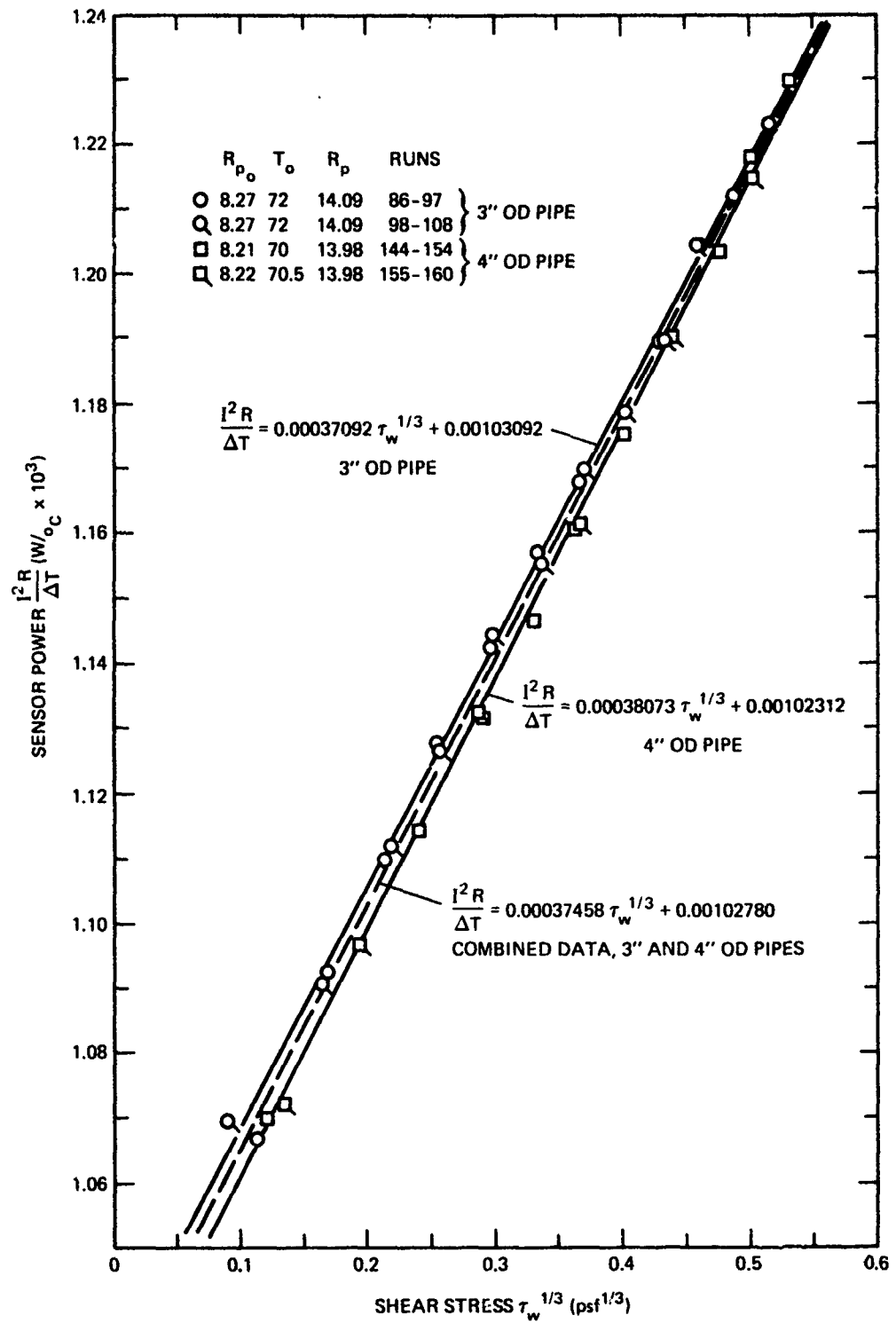


Figure 36 - Comparison of Sensor Power-Shear Stress Relationship for 3- and 4-Inch OD Pipes, $R/R_0 = 1.8$

the factors which produced the specific differences in transonic performance of the two CC ellipses would not be observable. Thus it was decided to use a flat aft surface airfoil terminating in a circular cylinder rather than an elliptical trailing edge. As previously, the emphasis would still be on the characteristics of the high-speed Coanda jet, with primary goals to investigate:

1. Effect of variation in the parameters h/R and pressure ratio P_d/P_∞ (or M_j).
2. Choked nozzle detachment criteria (effects of shock-induced recompression, external flow field, and parameters of Item 1).
3. Jet separation criteria for choked and unchoked flow and dependence on Items 1 and 2 and normal pressure gradient across the jet.
4. Subsonic lifting performance of the flat aft surface CC airfoil.

A brief discussion will shed more light on the importance of the dimensionless parameters involved. In addition to the model geometric parameters, the momentum coefficient and Reynolds number deserve consideration. The momentum coefficient can be written in another form similar to Equation (1) as

$$C_\mu = \frac{\dot{m}V_j}{q_\infty S} = \frac{2\rho_j h b V_j^2}{\rho_\infty V_\infty^2 b c} = 2 \frac{\rho_j}{\rho_\infty} \frac{h}{c} \left(\frac{V_j}{V_\infty} \right)^2 \quad (22)$$

The parameter h/c is related to the slot height-to-radius ratio of Item 1 above by using the geometric parameter R/c ; the velocity ratio is a function of the pressure ratio. Thus, the ratio of jet-to-free-stream Mach number becomes involved, and it appears the Reynolds number need be considered since both density and velocity ratios appear in Equation (22). For strictly incompressible jet velocities, at which most previous circulation control detailed experimentation has been conducted, the velocity ratio was frequently on the order of 2 or less, the density ratio was approximately unity, and the jet Reynolds number was low. The effect of the upper surface boundary layer and mixing with the wall jet would be expected to be appreciable. However, with near-sonic velocities and velocity ratios of 8 or more, one might expect strong dominance of the wall jet over viscous effects attributable to the boundary layer; thus the geometric parameters, i. e. pressure ratio and jet Mach number, and the static pressure variation across the jet take on more importance. It was for this reason that Items 1, 2, and 3 above were deemed important objectives of the high velocity wall jet investigation.

MODEL

The two-dimensional model was constructed with the intention of creating as large an airfoil as possible in order to facilitate trailing edge measurements while staying within the constraints imposed by the limitations of the 15- x 20- (width x height) inch tunnel. Whereas

physical blockage was no longer a problem with regard to test section choking, it was still an important consideration relative to the correction factors which must be applied to free-stream dynamic pressure for both solid and wake blockage. However, as Englar and Williams³⁴ point out, these are of secondary importance to the errors which can occur because of lift interference (induced camber or streamline curvature) caused on high lift models by floor and ceiling limitations and the resulting changes in lift, pitching moment, and effective incidence.

From nose to midchord, the model is a geometric uncambered ellipse with coordinates based on a 20-percent thickness-to-chord ratio; Figure 37 shows the details. The overall model is 11.0 inches long, 2.2 inches thick, has a trailing edge cylinder diameter of 2.0 inches, and a slot height adjustment range from 0 to 0.20 inches. This yields the following geometric parameters:

$$t/c = 0.20$$

$$R/c = 0.091$$

$$h/R = 0.0 \text{ to } 0.20$$

$$h/c = 0.0 \text{ to } 0.0182$$

$$(x/c)_{\text{slot}} = 0.91$$

The leading edge was made of finely finished and sealed mahogany, and the plates and spar forming the plenum were of stainless steel. The trailing edge cylinder consisted of aluminum tubing with a 2-inch OD and a 1/4-inch wall; it was hand-finished to ensure uniformity and smoothness. The cylinder was positioned in the airfoil by a stainless steel spar embedded in a filler of epoxy which was cast to the contour of the cylinder. The ends of the cylinder protruded through slightly oversized holes in the 1-inch-thick plexiglass tunnel walls and were attached to the wall by semicircular clamps. When loosened, the clamps allowed the trailing edge to be rotated to position the measuring probes. Thin neoprene tubing was laid in a groove in the epoxy cylinder seat so that when the clamps were tightened, the cylinder compressed the tubing and formed a pressure seal against leaks from the plenum. Installed in the cylinder near midspan were the plug containing the thermocouple and hot film probe calibrated in the previous section, 30 static pressure taps evenly spaced around the cylinder, five spanwise taps to monitor two-dimensionality, and the flat plate static pressure probe.

This last mentioned device was a pie-shaped segment made of 1/8-inch stainless steel machined and located as shown in Figure 38. The included angle between the edges was

³⁴ Englar, R. J. and R. M. Williams, "Test Techniques for High Lift Two-Dimensional Airfoils with Boundary Layer and Circulation Control for Application to Rotary Wing Aircraft," Canadian Aeronautics and Space Journal, Vol. 19, No. 3, pp. 93-108, Mar 1973.

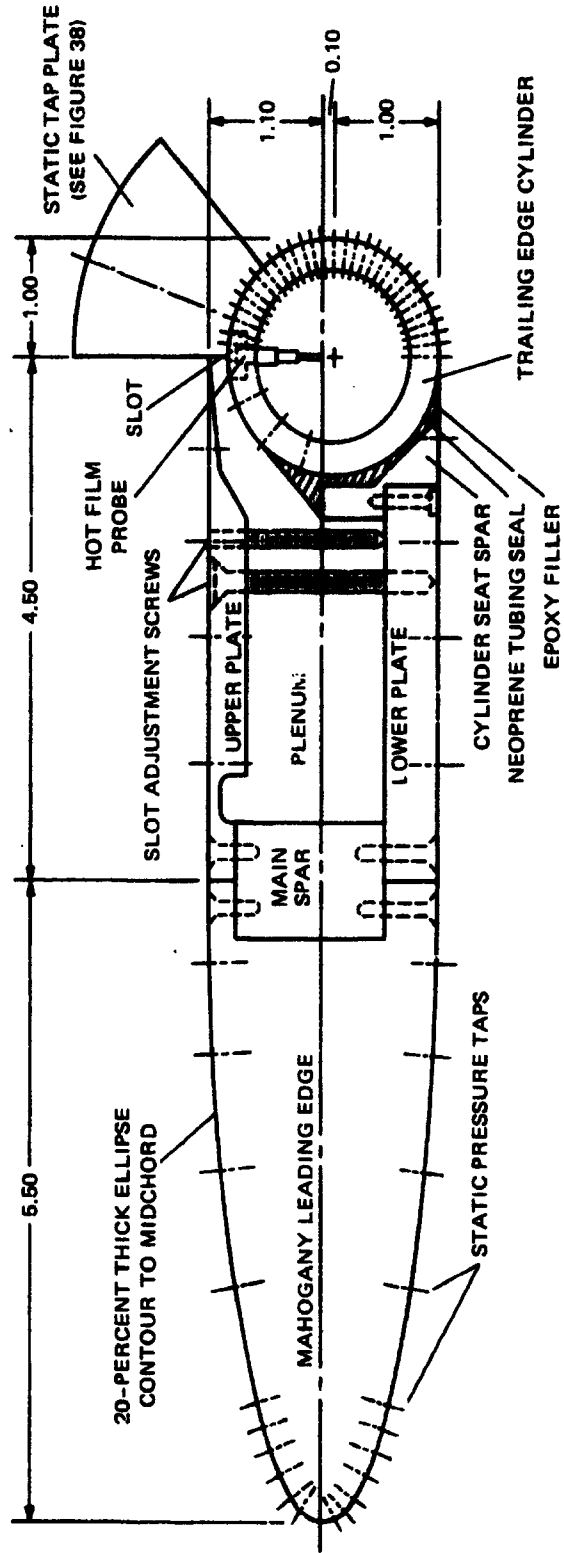


Figure 37 — Details of Two-Dimensional Subsonic Model

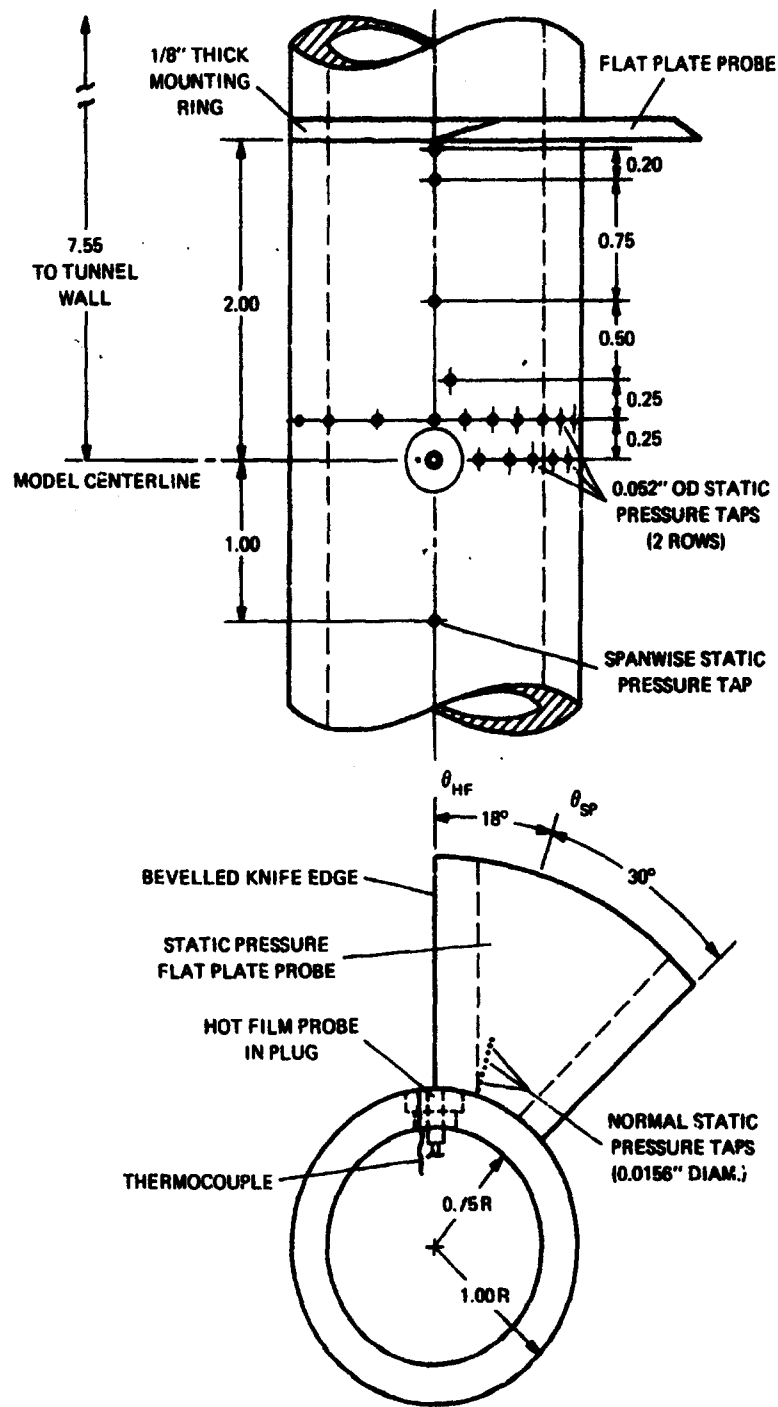


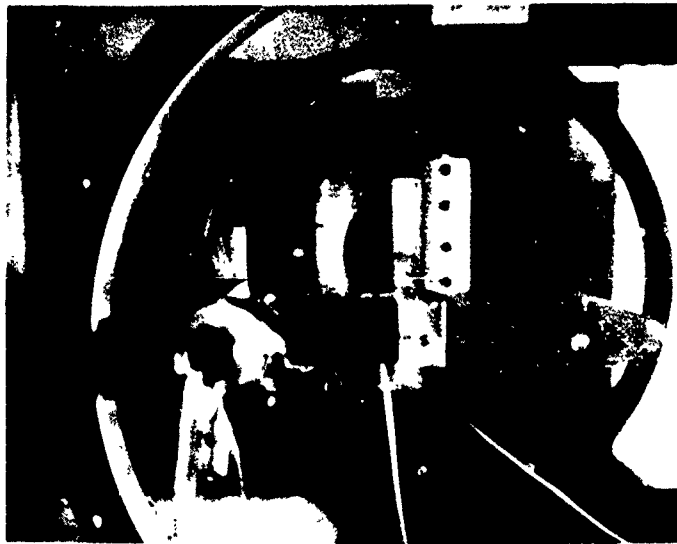
Figure 38 - Trailing Edge Cylinder and Static Probe Detail

48 degrees and the far side (i.e., outboard of the midspan) of each edge was finished to a fine knife edge. Nine 0.0156-inch-diameter static taps were embedded in a row in the near side of the plate and located along a radius 18 degrees rearward of the blade leading edge. The plate was part of a 2-inch-diameter ring which fastened 2.00 inch outboard of the model centerline and became part of the cylinder itself. The probe thus rotated with the cylinder. The cylinder surface static taps were located every 6 degrees for 180 degrees, with the first starting at the hot film location. These taps were staggered in two rows 1/4 inch apart to avoid intersection. Three additional taps were located 24, 48, and 72 degrees ahead of the hot film—these were inside the plenum itself until the cylinder was rotated. When they rotated far enough to be out of the plenum, the connecting tubing was unclamped. The tubing on those taps downstream which rotated into the plenum was then clamped off to avoid exposing the sensitive low range pressure transducers to the high plenum pressure. Thirty-one static taps were also located around the model circumference at midspan to record airfoil pressure distributions and determine lift, and nine additional spanwise taps monitored two-dimensionality. The pressure tubing for these taps led out of the model through a rectangular hole in the tunnel wall which was also the air supply entrance. The tubes were then hooked to connectors in the wall of a 6-inch ID pressure plenum which acted as a settling chamber before the supply air entered the model. The trailing edge taps as well as the hot film cable and thermocouple wiring led out the cylinder directly through the wall without going through the plenum. Figure 39 shows the model installed in the tunnel and details of the measuring apparatus.

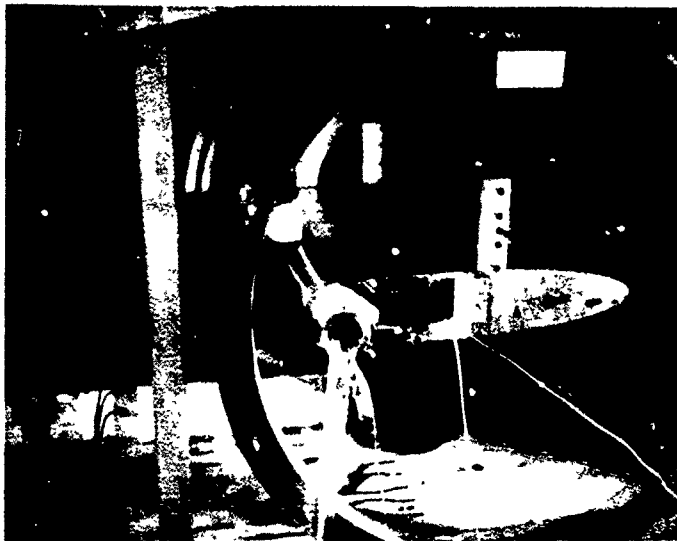
TEST APPARATUS AND TECHNIQUE

The test apparatus and high lift model test technique were similar to those developed during previous NSRDC CC airfoil tests (see, for example, Englar^{4,5} and primarily Englar and Williams³⁴). The visual display of pressure data on four 48-tube manometers gave much on-line information on the test results and acted as a valuable tool in setting up desired flow conditions. Data for all runs were recorded automatically by a three-gang scannivalve (48 ports on each) readout; it transferred the data to punched paper tape for computer reduction and plotting and printed an on-line listing of all unreduced pressures. This gave high data accuracy since a ± 1 -psid transducer range was represented by $\pm 10,000$ counts on the scannivalve output; considering some electronic shift and scatter, this still gave accuracies to better than ± 0.001 psi. Figure 40 shows this equipment.

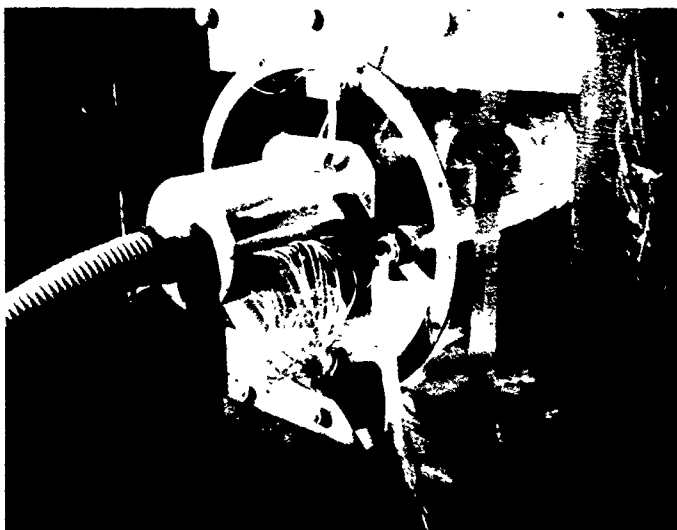
A very difficult part of all two-dimensional tests is to ensure that the flow is as nearly two-dimensional as possible. As indicated by Englar and Williams,³⁴ this is especially difficult in high lift blown airfoil tests because the severe adverse pressure gradient downstream of the jet reacts with the tunnel wall boundary layer and produces separation of the latter in the



CLOSEUP SHOWING STATIC PROBE
FROM OUTBOARD SIDE AND WALL
PLENUM CHAMBERS



TRAILING EDGE AND
PLENUM DETAIL



AIR SUPPLY PLENUM AND
PRESSURE TAP CONNECTIONS

Figure 39 – Model Installation in the 15- x 20-Inch Tunnel



OSCILLOSCOPE, ANEMOMETRY CONSOLE, AND TUNNEL CONTROL CONSOLE

PRESSURE GAGES, MANOMETER BOARDS, SCANNIVALVE AUTOMATIC READOUT, PAPER TAPE PUNCH, AND ON-LINE DATA LISTER

OVERVIEW SHOWING EQUIPMENT AND TEST SECTION

Figure 40 - Subsonic Two-Dimensional Test Setup and Equipment

form of very strong shed vorticity. This induces a strong downwash field (very much like a finite wing tip vortex) which varies across the span and causes the effective incidence to be far from the geometrically set value. To solve the problem, separate plenum chambers were installed that connected to a high pressure air supply and blew tangentially along the tunnel walls. When this wall blowing was properly adjusted, the boundary layer was energized and separation prevented (see Figure 39).

For monitoring purposes, cotton tufts were located along the tunnel walls and floor and spanwise static taps were located on the model upper surface and trailing edge. The system was found to work quite effectively. For the present tests, with section lift coefficients up to 7.5, spanwise static pressure over the mid-60 percent of the span was found to vary less than 0.9 percent from the centerline value with wall blowing properly adjusted. At the same conditions, the static taps located between 2 and 5 percent span from the tunnel wall were a maximum of 10.2 percent lower than the centerline value. These deviations were considerably reduced for smaller lift coefficients.

The blowing quantities needed to define C_{μ} were determined both theoretically and experimentally. As is almost universally the case, the jet velocity was calculated by assuming an isentropic expansion to free-stream static pressure; it was thus a function of only pressure ratio and temperature:

$$V_j^2 = 2gR_1 T_d \left(\frac{\gamma}{\gamma - 1} \right) \left[1 - \left(\frac{P_{\infty}}{P_d} \right)^{\frac{\gamma - 1}{\gamma}} \right] \quad (23)$$

(It is realized that a more exact value is obtainable by expanding to local static pressure at the slot exit, but this is, in part, a function of airfoil geometry as well, and thus C_{μ} would vary from airfoil to airfoil for the same duct pressure and slot height.) The mass flux (\dot{m}) is measured experimentally with a flowmeter in the line preceding the airfoil plenum.

In this test, two devices were used. For higher mass flows (i.e., larger slot heights and pressures), a venturimeter with a 1.5-inch-diameter throat was placed in the line. This became very insensitive to the low Δp across it for low mass flow and was replaced with a 1.401-inch-diameter orifice plate. This was quite sensitive to pressure differential across it, but was less useful at high \dot{m} because of the smaller throat area and turbulence shed from its sharp lip. Thus, the two devices had to be interchanged when significant slot height changes were made. Because of higher pressures, it was also necessary to replace the low pressure transducer recording the trailing edge static taps with a ± 10 -psid device capable of handling the very high suction caused by the high jet velocities.

The experimental investigation was conducted in essentially three phases:

1. Static tests (no free stream) were performed to generate data for comparison with the previous static tests cited in the jet detachment literature review.

2. To investigate the effect of h/R and P_d/P_∞ on jet separation or detachment, slot height variation was investigated in dynamic runs with duct pressure varying from zero to above choked. These runs were also intended to identify several promising test conditions for the detailed trailing edge investigation, Item 3.

3. The trailing edge flow field was surveyed for several differing conditions by positioning the rotatable cylinder at a large number of stations. (This would enable location of the jet separation point if not detached.)

To accomplish the above, some 488 data runs were made, the results of which will be discussed in the next section.

RESULTS AND DISCUSSION OF SUBSONIC INVESTIGATIONS

After rather extensive checkout of the data recording and reduction systems (pressure tests involve the tedious process of confirming proper tubing hookups, leak-checking all connections, checking electronic recording equipment, and running sample cases to test the bookkeeping of the data reduction computer program), the model slot height was set to 0.100 inch and a series of runs begun with no free stream. (A previous check of the 0.200-inch slot height setting indicated that the large slot area thus produced would not allow choked duct pressures to be run because of a limit of 2 lb/sec mass flow from the air supply system. Thus $h = 0.100$ inch was the largest value run; as can be seen from Figure 9, this somewhat restricts the possibility of reaching the boundary of the detachment curves.) Of primary interest in these runs were the trailing edge pressure measurements for comparison with previous static work. In addition, some dynamic runs were made with the static pressure flat plate probe installed so that normal pressure gradients across the jet with and without free-stream influence could be studied.

STATIC TESTS (NO FREE STREAM) AND DYNAMIC TESTS WITH STATIC PROBE INSTALLED

Production data runs for both $h = 0.100$ and 0.050 inch were completed for $q_\infty = 0$ and 20 psf; here the trailing edge probes (hot film and static pressure) were set at a given angle from the slot lip (θ_{HF} was always 18 degrees upstream of θ_{SP}) and a range of duct pressures was run. Figure 41 depicts the static pressure distributions around the trailing edge cylinder for a duct pressure of 10 in. Hg (4.91 psig) at three different probe settings. The pressure coefficient C'_p differs from the conventional notation $(P - P_\infty)/q_\infty$ in that the denominator is the difference between jet total and exit static pressures, which would be jet dynamic pressure

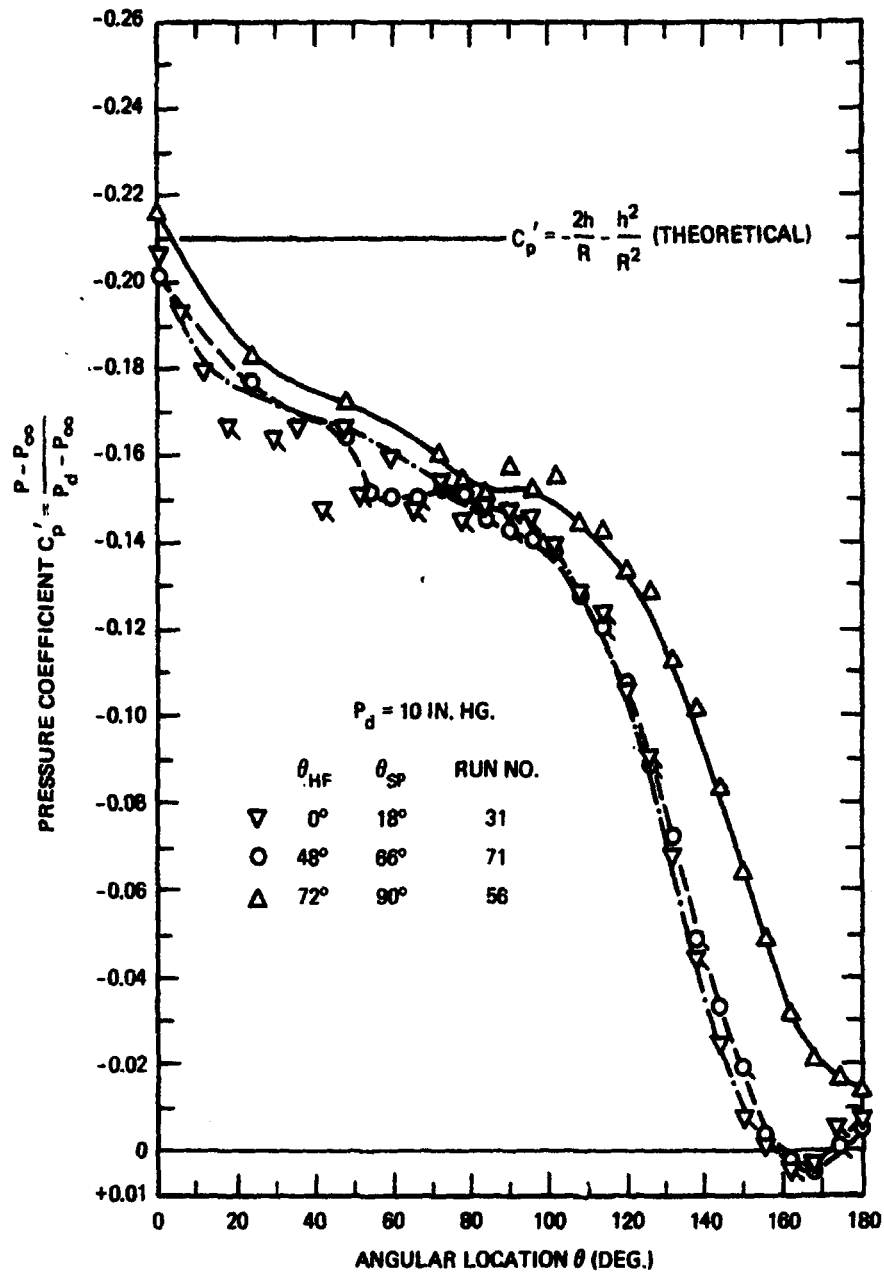


Figure 41 - Trailing Edge Static Pressure Distribution with No Free Stream, $h = 0.100$ Inch, $q_\infty = 0$

were it not for compressibility effects. Two trends were apparent in the data. For pressures located downstream of the hot film, it was noted that every other tap (flagged) dropped below or rose above the previous one rather than producing a smooth curve. (This is much more evident in Figure 42.) It was noted that each of these lower or higher valued taps was in a line behind the hot film probe (see Figure 38). Even though the probe had been installed by using a microscope and no protrusion could be felt or seen, a very thin tuft of cotton held immediately downstream of it showed a thin vortex trailing aft into the plane of the taps. Thus, these taps were considered invalid, and they will be omitted in most of the following data. However, on the basis of the criteria given for allowable protrusion of the hot film,²⁶ it is assumed that the shear stress data remain valid. The second item of note in Figure 41 is the fact that the curve for $\theta_{HF} = 72$ degrees did not coincide with the other two; this is felt to be caused by the static pressure probe and will be discussed in a later paragraph.

Figure 42 compares static pressure data for a relatively low pressure (1.98 in. Hg) and a choked pressure (33.50 in. Hg) at $\theta_{HF} = 0$ degree. The choked curve ($P_d/P_{\infty} = 2.11$, $M_1 = 1.09$) showed a jagged rise and fall in pressure immediately downstream of the slot, followed by convergence to a smooth curve at a higher pressure than the other. These waves are apparently the expansion-compression waves of a supersonic flow, and the eventual pressure rise is thus compression-induced. It is apparent, however, that no strong recompression shock formed since there was no evidence of a sudden pressure rise with continued high pressure behind it. (The flagged static taps behind the hot film probe were noticeably different from the other taps in this figure, because of probe disturbance as mentioned above.)

Similar static pressure curves for $h = 0.050$ inch and $q_{\infty} = 0$ are shown in Figure 43. At lower duct pressure, the curves coincided downstream, but the irregularities in the curves again formed near and above choked pressure. However, in all cases for $h = 0.050$ inch, the jet turned a full 180 degrees statically as indicated by the negative C'_p on the bottom of the cylinder. This was not the case for $h = 0.100$ inch (Figures 41 and 42); C'_p became zero and then positive between 140 and 175 degrees, indicating a separation bubble and less effective Coanda turning with the larger slot height. This may well have been caused by the much greater flow entrainment into the jet at the same duct pressure (but higher C_{μ})—the larger mixing losses are probably sufficient to cause a reduction in wall jet velocity and thus its kinetic energy (proportional to V_j^3). It is interesting to note that in all these figures (41–43), the theoretical C'_p derived by Roderick¹⁵ for incompressible inviscid flow

$$C'_p = -\frac{2h}{R} - \frac{h^2}{R^2} \quad (24)$$

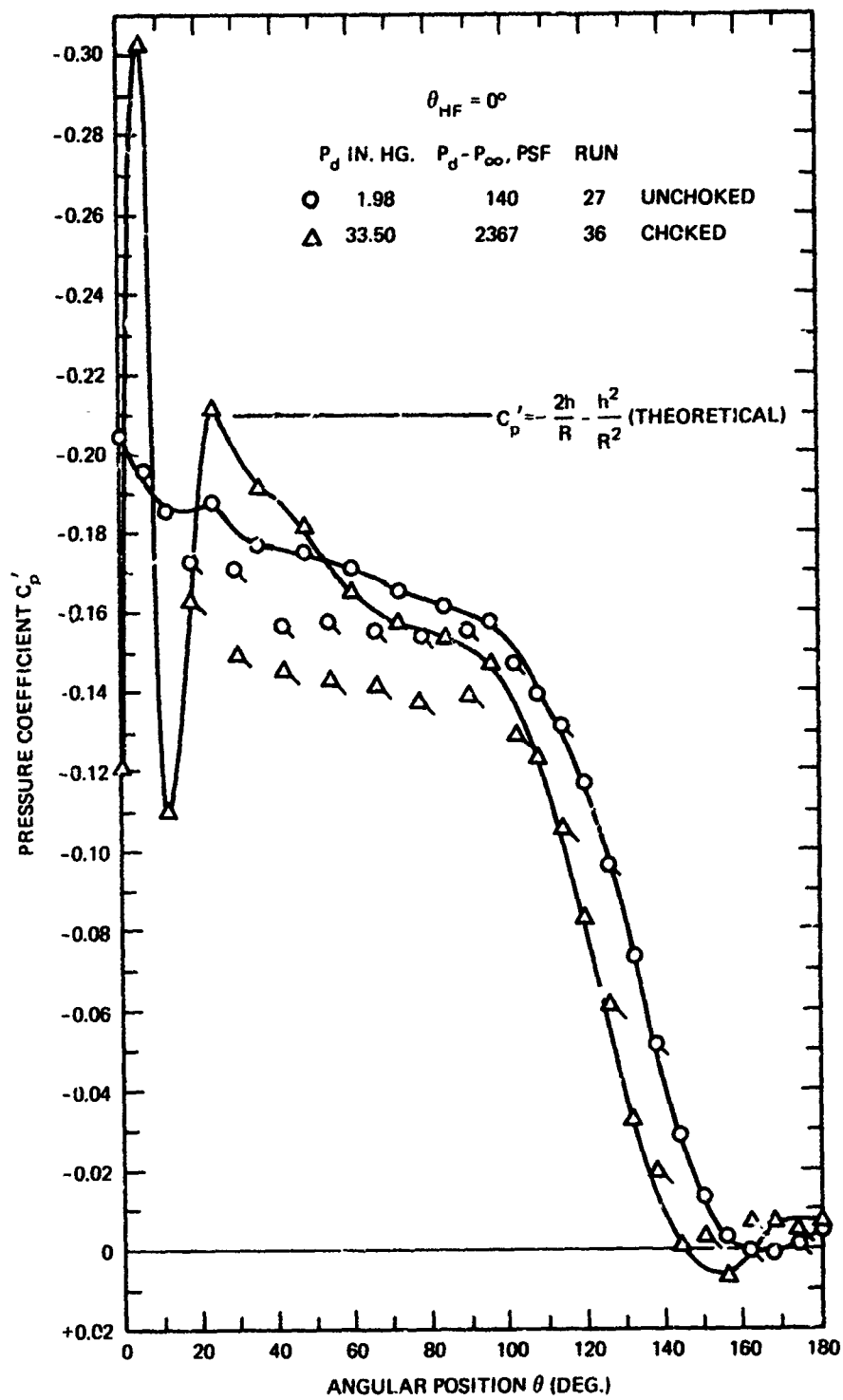


Figure 42 – Trailing Edge Static Pressure Distributions for Choked and Unchoked Slot with No Free Stream, $h = 0.100$ Inch, $q_\infty = 0$

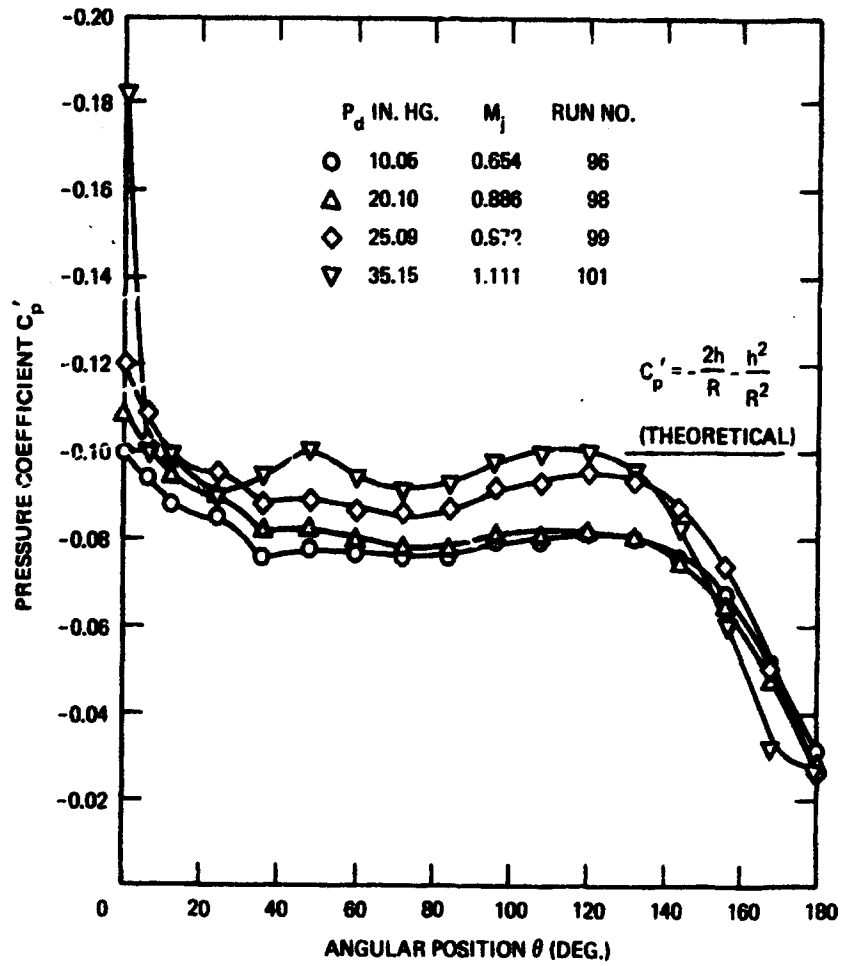


Figure 43 - Trailing Edge Static Pressure Distributions with No Free Stream, $h = 0.050$ Inch, $q_{\infty} = 0$

appears to be valid near the slot for the low pressure cases but not for the high pressures. Flow entrainment and viscous effects precluded good agreement downstream of the slot.

Figure 44 presents the normal static pressure across the jet for $q_\infty = 0$ at three probe locations. The $y = 0$ values were taken from surface static taps on the cylinder ($y_0 = 0.270$ inch is the outermost tap). The fact that the static probe data converge fairly smoothly to the surface values indicates that the corner flow where the probe intersects the cylinder caused little disturbance. The pressure rose rapidly away from the surface and the approximate location of the jet sheet edge can be seen for the three locations when C_p' nears zero. The triangles show that the data are repeatable for other pressures, but it was found that disagreement occurs above choking. Figure 45 presents similar data for $q_\infty = 22$ psf. In addition to the much larger negative pressures which occurred because of the external pressure distribution produced by the free stream, note that the upper distributions converged to constant values other than zero outside of the jet (which of course was due to the curving streamlines of the external flow). Figures 44 and 45 point out two very important facts: (1) there is a significant difference in the jet normal pressure distributions over a Coanda surface in the static and dynamic cases and any attempt to use static results to predict properties of a CC airfoil in a free stream could be very misleading and (2) static pressure across the jet is definitely not constant and the use of the conventional boundary layer assumption of constant static pressure could invalidate the analysis.

It is interesting to note that this pressure differential across the jet can be predicted fairly well by some simple analyses. For inviscid, incompressible flow, Kind³⁵ and Dunham³⁶ both integrate the centrifugal force-pressure balance across the jet, assume that the streamlines are concentric with the circular cylinder, and obtain

$$P_{0j} - P_{ij} = \frac{\dot{m}V_j}{R + \frac{h}{2}} \quad (25)$$

or in terms of C_μ ,

$$P_{0j} - P_{ij} = \frac{C_\mu q_\infty c}{R + \frac{h}{2}}$$

³⁵Kind, R. J., "A Proposed Method of Circulation Control," Ph.D. Thesis, Clare College, Cambridge University, 1967.

³⁶Dunham, J., "Circulation Control Applied to a Circular Cylinder," Jul 1967, National Gas Turbine Establishment Report 287. (AD821-006)

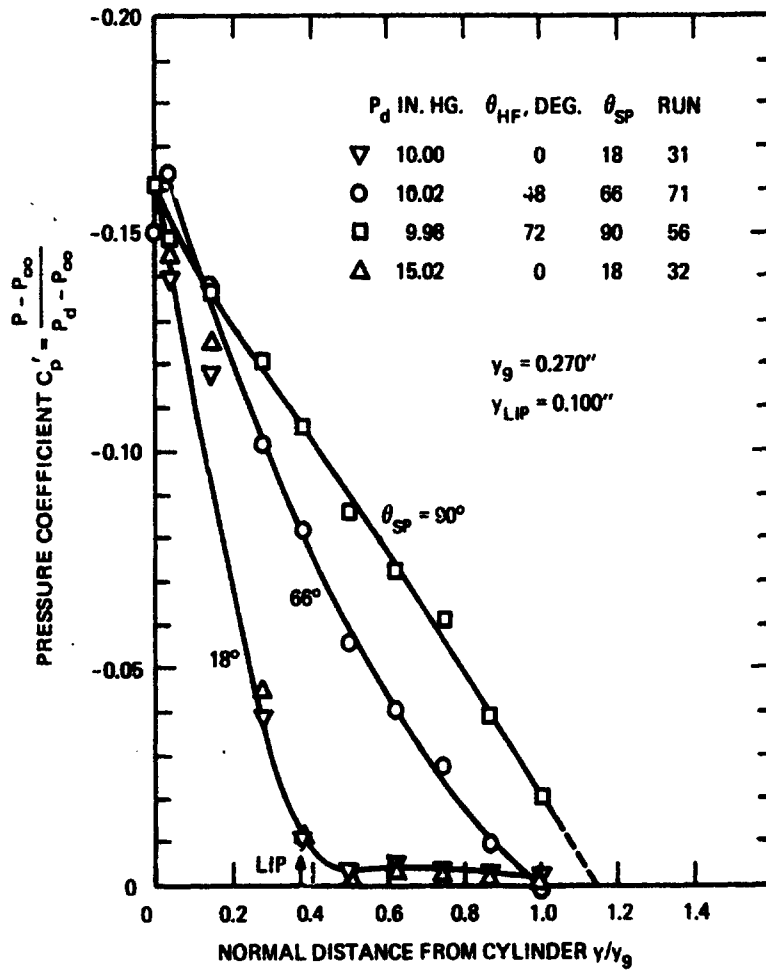


Figure 44 - Normal Static Pressure Variation across Jet, $h = 0.100$ Inch, $q_\infty = 0$

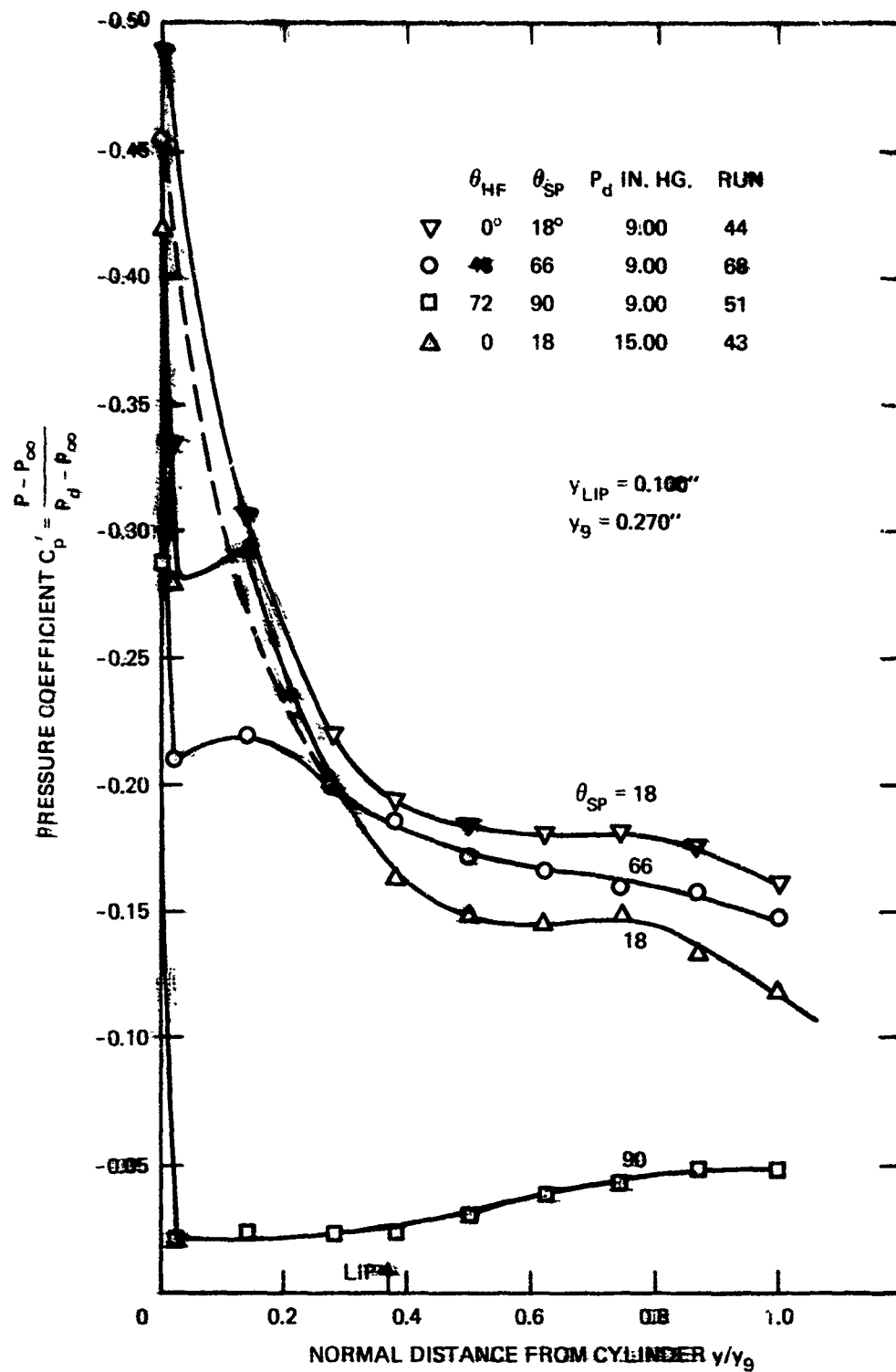


Figure 45 - Normal Static Pressure Variation across Jet, $h = 0.100$ Inch, $q_{\infty} = 22$ PSF

or

$$\Delta C_p = C_{p0j} - C_{p1j} = \frac{C_M c}{R + \frac{h}{2}} \quad (26)$$

For the top curve ($\theta_{HF} = 0$ degree, $P_d = 9$ in. Hg) in Figure 45, the nondimensional pressure difference across the jet was $\Delta C_p = 8.4$; this calculation was based on a dynamic pressure of 22 psf, $p_d - p_{\infty} = 632$ psf and the assumption that the jet outer edge occurs at $y/y_0 = 0.62$ (where $C_{p0j} = -5.0$). However, these results are for compressible flow data; use of the Prandtl-Glauert compressibility correction for the experimental jet Mach number of 0.62 reduces C_{p1j} from -13.40 to the incompressible equivalent of -10.42 , and then $\Delta C_p = 5.42$. Equation (26), with $h = 0.168$ inch at $\theta_{SP} = 18$ degrees, gives $\Delta C_p = 5.33$, only 1.7 percent different from the experimental value. Using instead Equation (5) and the above data gives

$$\frac{P_{0j} - P_{1j}}{P_{0j}} = -0.0944$$

The experimental value is -0.0965 . Thus both methods appear useful, with the stipulation, as Kind showed, that the calculation is not done in the vicinity of the jet separation. (Kind measured static pressure as the difference between total pressure from a pitot tube and dynamic pressure from a hot wire—the difference is quite small, and thus the agreement between Equation (26) and his experimental value was not as good as shown above. In addition, this measuring technique would not work in higher speed jets with compressibility effects.)

A negative result of Figure 45 is shown by the bottom three curves; there, as the wall is approached, the pressure deviates from the smooth curves. Use of a cotton tuft indicated that a very strong vortex was shed from the junction of the cylinder and the static probe face as the angle θ_{SP} was increased. This type of phenomenon had been experienced in past CC tests whenever a disturbance (foreign body, slot height spacer, surface imperfection, etc.) was present; it is apparently related to disturbing the mixing of jet and upstream boundary layer (note that Figure 44, with no external boundary layer, does not show the trend). This vortex was clearly distorting the normal pressure gradient; similar vortices had previously been found to distort the entire trailing edge wall jet flow field. When the static pressure plate was removed from the model and replaced with a 1/8-inch-thick spacer ring flush with the 2-inch OD cylinder, the vortex disappeared.

Surface shear stress as a function of duct pressure (or jet velocity) for two different positions at $q_{\infty} = 0$ is shown in Figure 46; note that the shear increased at a position 48 degrees downstream of the slot, a condition to be explained in a later section. Figure 47 depicts shear stress (nondimensionalized to give skin friction coefficient) as a function of C_{μ} for different dynamic pressures and slot heights at $\theta_{HF} = 48$ degrees. There was a noticeable difference between the data with and without the static pressure probe installed (flagged and unflagged triangles). It is also seen that a decrease in slot height produced increased skin friction (shear stress) for a constant C_{μ} ; this is because the jet velocity increases while the mass flow decreases for constant momentum flux. This implies that the kinetic energy and thus the Coanda turning should be greater for the smaller slot heights. These implications will be more clearly seen in the next section.

DYNAMIC TESTS WITH SLOT HEIGHT VARIATION

In order to isolate several cases for the detailed trailing edge studies and to observe the lift performance of the test airfoil with various slot heights, a series of dynamic (i.e., with free stream) runs was conducted for a range of duct pressures. It was expected that these would include combinations of high duct pressure and high slot height which would be indicative of jet detachment criteria in the presence of an external flow. Lift as a function of blowing is indicated in Figure 48 for a nominal free-stream dynamic pressure of 25 psf (the actual corrected value was about 27.5 to 28 psf, giving a Reynolds number based on chord of approximately 840,000). A series of four slot heights was run ($h = 0.100, 0.050, 0.025,$ and 0.013 inch), each about half of the preceding value, plus a fifth value of 0.032 inch. The results confirm the effects of slot height on Coanda turning mentioned in the previous section: decreased slot heights yield higher jet kinetic energy for constant C_{μ} and thus better Coanda turning and lift augmentation. The performance of the $h = 0.100$ -inch configuration is not as reduced as indicated; it was actually run at a lower Reynolds number ($q_{\infty} = 22$ psf and $R_c \approx 760,000$) and represents data from the earlier test phase with the trailing edge static probe still installed. The performance loss is most likely attributable to the static probe and accompanying vortex rather than to the lower Reynolds number.

Two problems should be noted which have some effect on the interpretation of Figure 48. First, the slot upper lip had deliberately been machined to a fine knife edge to prevent turbulence being shed from it; accordingly, the metal in the knife blade was thin. Under high pressures, this edge was ~~unable~~ to deflect, thus expanding the slot height as much as 80 percent for 35-in. Hg duct pressure: (this slot height increase is relatively linear with pressure). Thus in Figure 48, the upper portions of the curves actually correspond to higher h values. Second, rows of cotton tufts taped spanwise across the tunnel floor indicated that the jet sheet impinged on the floor at high pressure. The approximate points of this

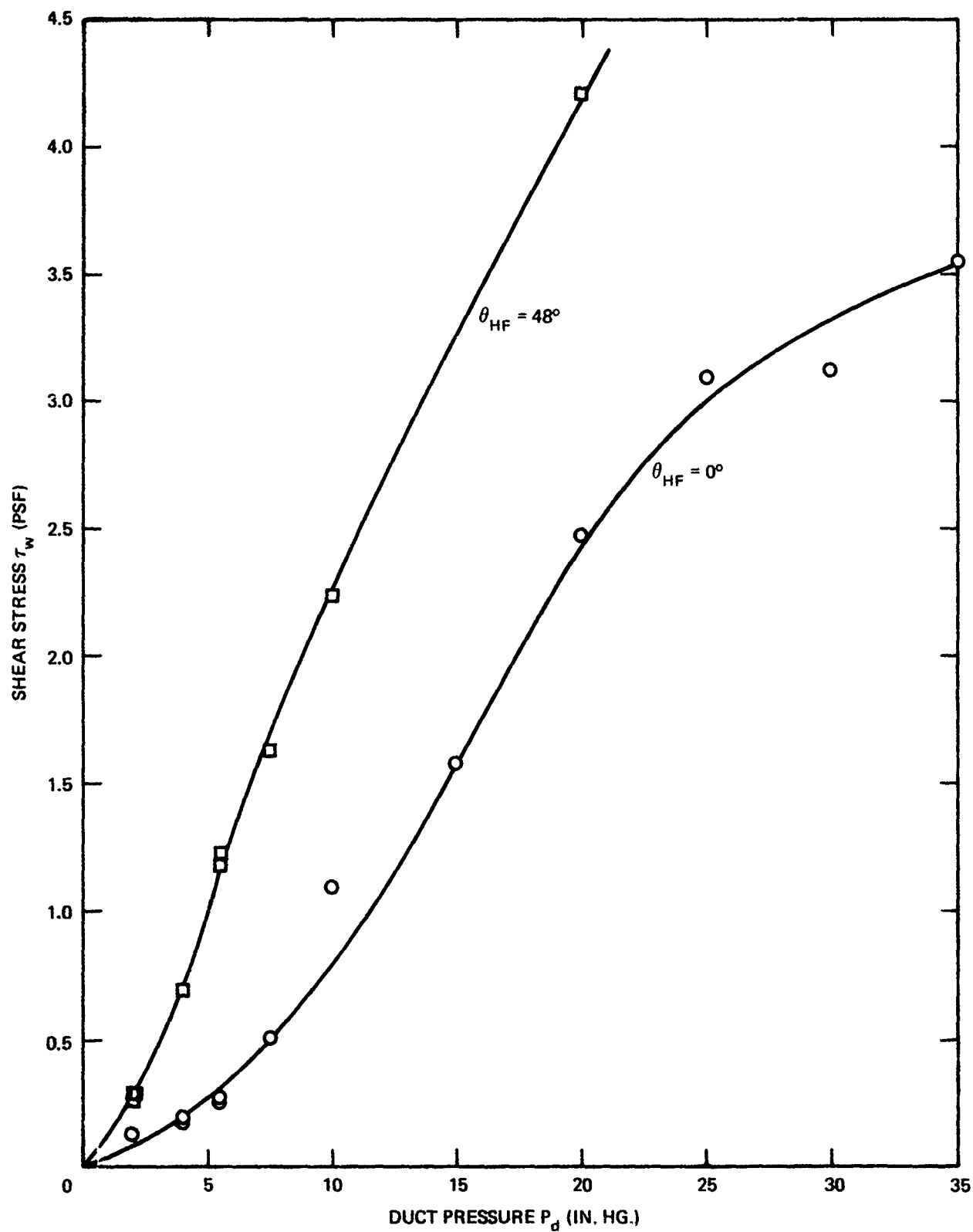


Figure 46 - Wall Shear Stress as a Function of Duct Pressure, $h = 0.050$ Inch, $q_\infty = 0$

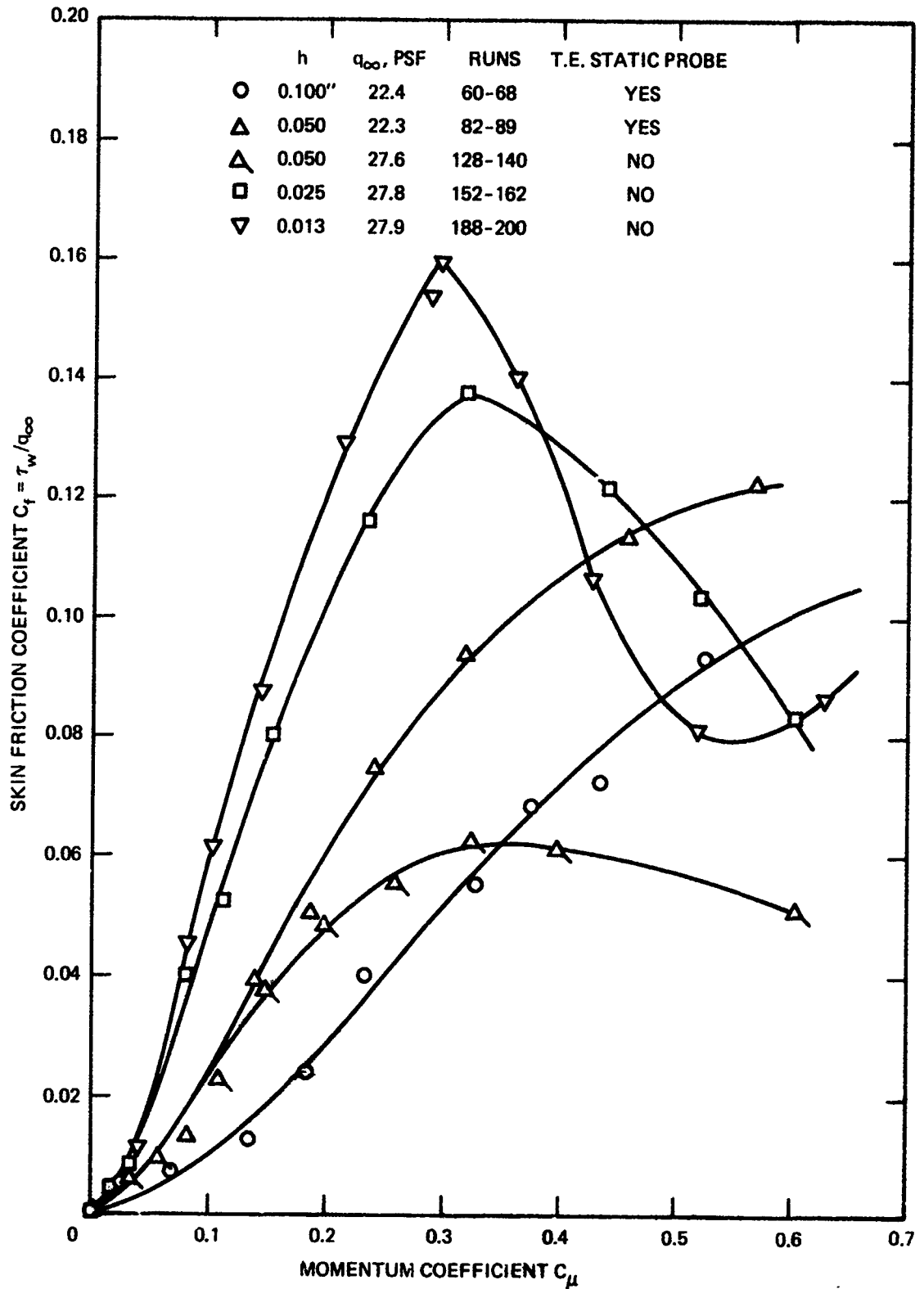


Figure 47 - Skin Friction as a Function of Blowing for Various Slot Heights, $\theta_{HF} = 48$ Degrees

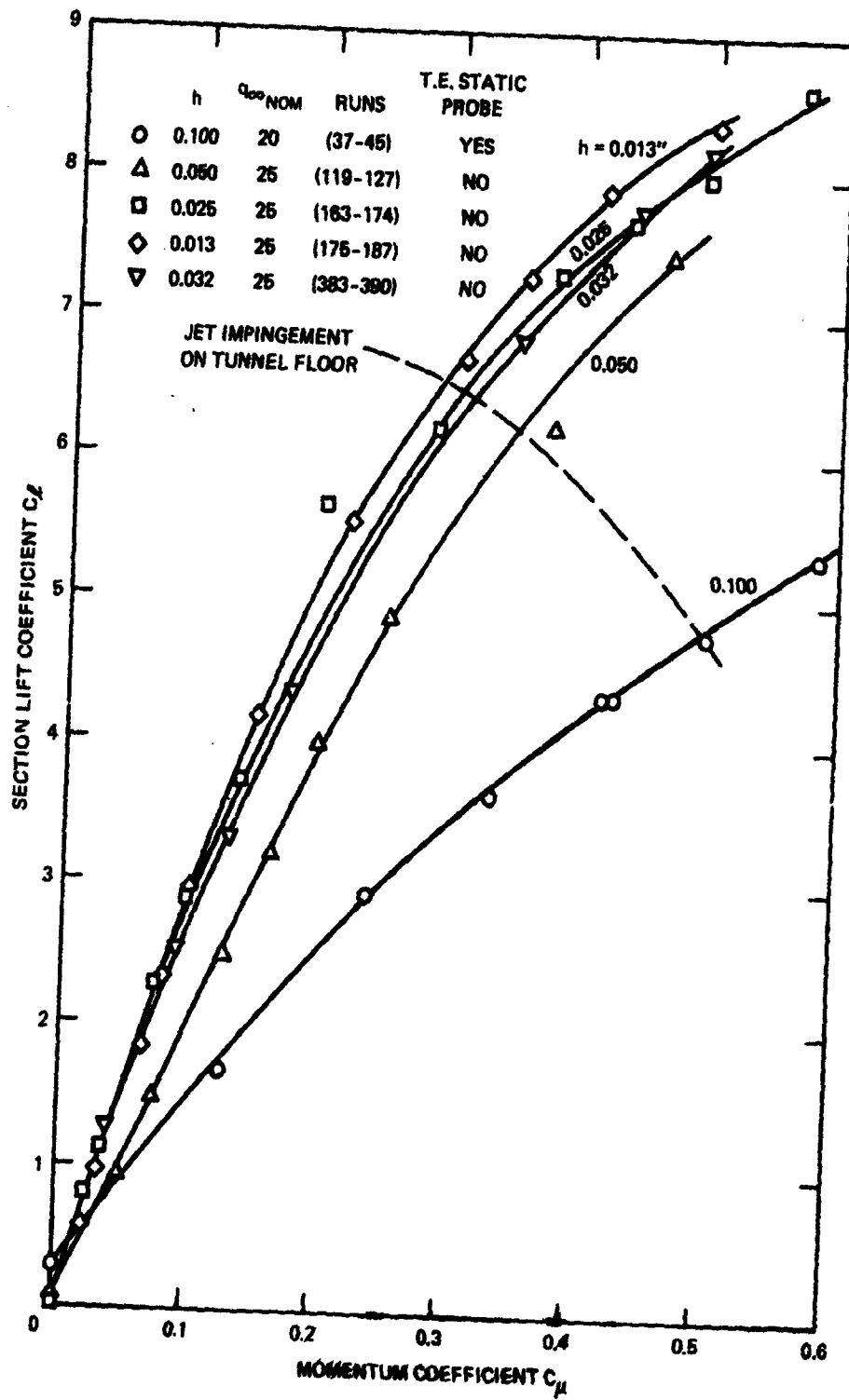


Figure 48 - Airfoil Lift as a Function of Blowing, $\alpha = 0$ Degree, $\theta_{MP} = 0$ Degree

occurrence are shown by the dashed line in Figure 48; it is not immediately obvious from the plot, but impingement occurred at lower duct pressures for the larger slot heights (larger mass flows). Although no sudden changes in the lift curves occurred at this point, it is felt that the magnitude of the higher lift data must be regarded as questionable. Nevertheless, for a C_{μ} of 0.3, a valid C_L of 6.5 is obtained for $\alpha = 0$ degree, with the associated lift augmentation, $\Delta C_L/C_{\mu}$, of over 21 (higher augmentations are obtained at lower rates of blowing). This limitation on C_{μ} with larger slot heights precluded generating data which would verify or modify the detachment criteria of Figure 9. The larger heights could not be choked without floor impingement; the smaller values could produce supersonic flow, but the system could not provide the high pressure ratios needed to cause detachment (from Figure 9 criteria).

The static pressure distributions around the ellipse are plotted for various blowing rates in Figure 49, where the trailing edge taps behind the hot film are still included; their deviation was noticeable only in the higher pressure case. The characteristic saddleback pressure distribution ended in a very high suction peak of $C_p = -20.5$. Movement of the fore and aft stagnation points toward midchord is indicative of the increase in circulation and lift. The curve for $P_d = 20.03$ in. Hg, which is above the floor impingement limitation, shows the invalid pressure buildup under the model, as indicated by $C_p \approx 1.6$, an impossible condition in unrestricted subsonic flow. Figure 50 shows similar data for $h = 0.013$ inch, where for choked blowing, the jagged dropoff in C_p is noted—the taps directly behind the hot film are then omitted. Similar data were obtained for the other three slot heights ($h = 0.100, 0.032,$ and 0.025 inch) as well as some limited data for $h = 0.006$ inch. This last value was very difficult to set properly and changed whenever the trailing edge was repositioned; thus it is not included.

Because of the two major test limitations (inadequate mass flow at high pressure and/or jet floor impingement), a condition of large slot height and duct pressure sufficiently high to produce jet detachment with or without a free stream was never reached throughout these tests. Static test maxima were $P_d/P_{\infty} = 2.356$ and $M_j = 1.178$ (based on expansion to p_{∞}) for $h = 0.025$ inch, and free-stream maxima were $P_d/P_{\infty} = 2.165$, $M_j = 1.111$; no indication of jet detachment was present.* It thus seems that jet detachment is not likely to be an operational problem on CC airfoils of trailing edge geometry presently thought to provide good subsonic performance¹¹ even at high jet velocities up to $M_j = 1.3$. Furthermore, a line of constant $P_d/P_{\infty} = 3.0$ imposed on the compressible flow data of Figure 4 indicates that lift augmentation degraded before this point. Since it is known from the above tests that $P_d/P_{\infty} = 3.0$ does

*Very recent NSRDC tests on a CC high lift fixed wing aircraft configuration without the above tunnel constraints have shown that no detachment occurs at $P_d/P_{\infty} = 2.972$ and $M_j = 1.30$ for a mean slot height of 0.021 inch and mean radius of 0.69 inch.

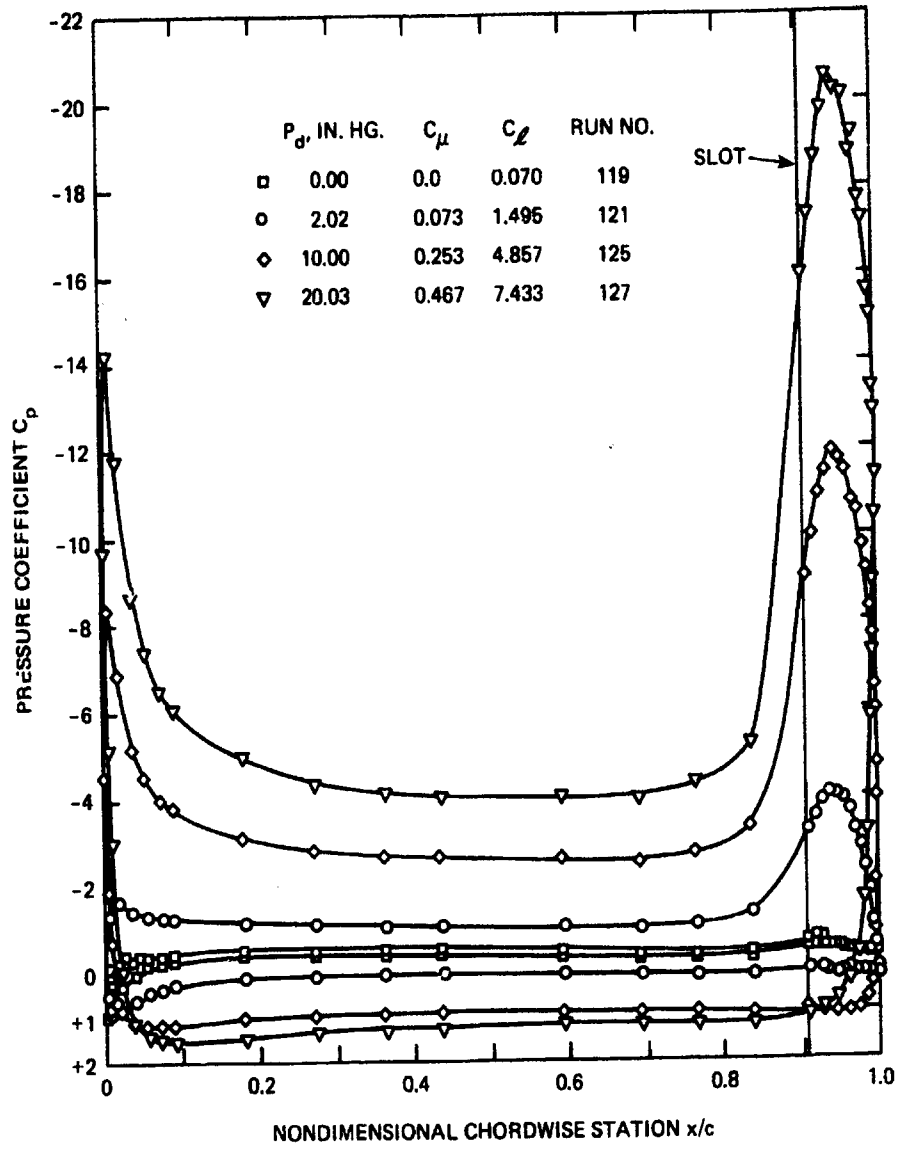


Figure 49 – Airfoil Static Pressure Distributions, $h = 0.050$ Inch, $q_\infty = 27.5$ PSF, $\alpha = 0$ Degree

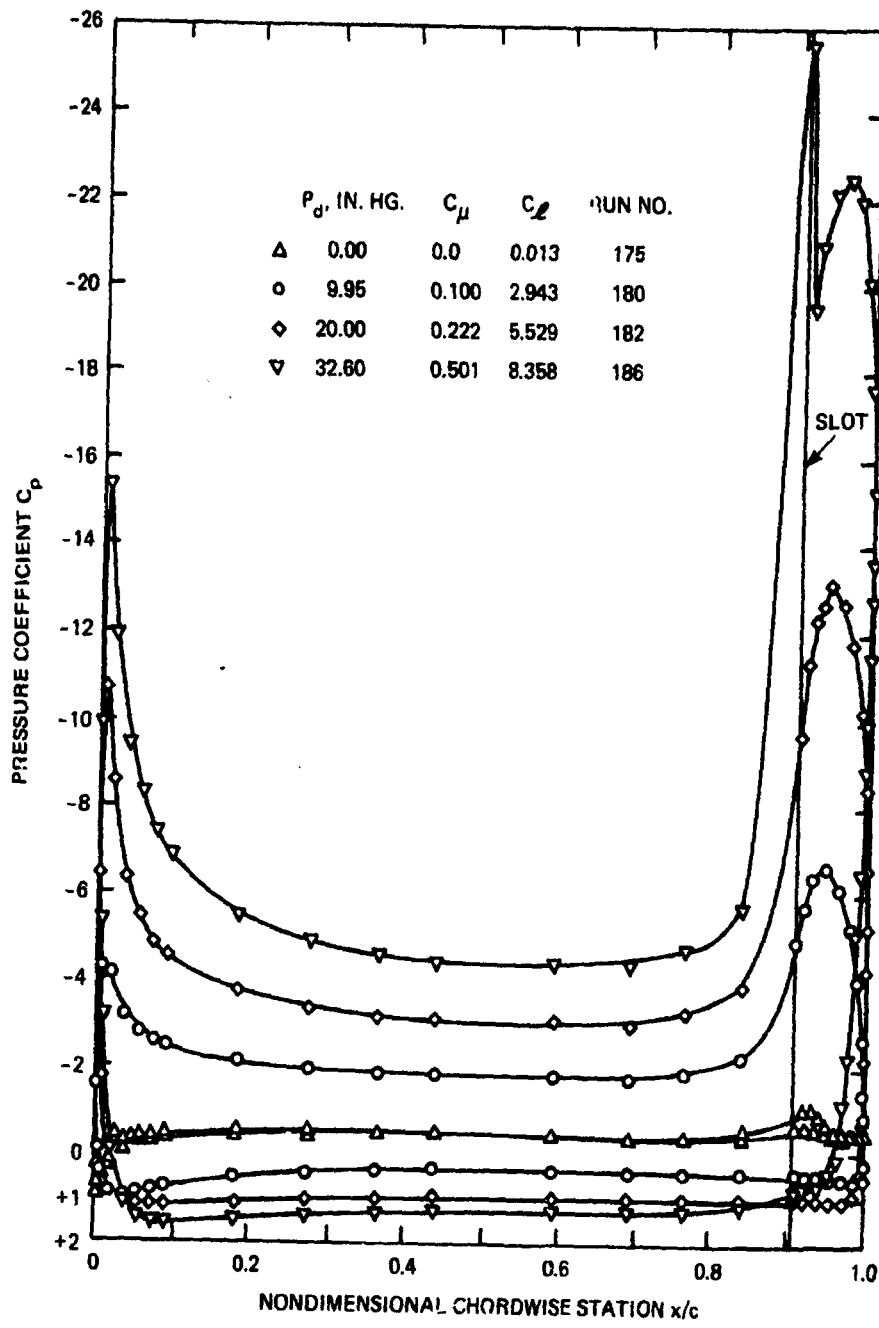


Figure 50 - Airfoil Static Pressure Distributions, $h = 0.013$ Inch, $q_\infty = 27.5$ PSF, $\alpha = 0$ Degree

not yet represent jet detachment, it must be concluded that detachment is not solely responsible for the performance loss and that compressibility effects (i.e., reduced external static pressure) seem to be involved. Operation in a compressible external flow field may be an entirely different problem than the above investigations from the detachment standpoint. Thus, the remainder of the present investigation has been concerned with the higher velocity Coanda wall jet properties (especially shear stress and separation characteristics) and not with detachment.

DETAILED TRAILING EDGE INVESTIGATIONS

The 0.013-inch slot height configuration was selected for further study because of the ability to run high duct pressures without floor impingement or mass flow limitations. It was also decided to test the $h = 0.032$ -inch configuration to determine the effect of a slot height increase, yet still allowing choked pressures. For each slot height, the test procedure consisted of rotating the trailing edge to a number of distinct positions (θ_{HF} , measured from the slot) and running four or five duct pressures at each position. These pressures would include two unchoked values (10 and 20 in. Hg), the sonic value (approximately 27.5 in. Hg depending on free-stream static pressure), and one or two supersonic values (30 and 35 in. Hg for $h = 0.013$ inch; only 30 in. Hg could be obtained for $h = 0.032$ inch). All measurements were taken with free-stream conditions of corrected dynamic pressure of 27 to 28 psf, Reynolds number approximately 840,000, and V_∞ between 152 and 156 ft/sec. The following data were recorded for each run.

1. Static pressure around the trailing edge.
2. Spanwise static pressure at the trailing edge and upper surface.
3. Free-stream temperature and total and static pressure plus barometric pressure.
4. Hot film operating voltage and resistance plus plug temperature.
5. Polaroid picture of oscilloscope displaying hot film voltage dynamic fluctuation.
6. Air line pressure and temperature and pressure differential across the orifice plate or venturimeter.
7. Duct total pressure and temperature.
8. Pressure in the tunnel wall jets.

The trailing edge static pressures as a function of angular location are presented in Figures 51 and 52 for the two slot heights. Each curve may be a composite of more than one run in that as the trailing edge was rotated, the valid taps (those not in the plane behind the hot film probe) could be positioned to take data at angles which previously had invalid pressures. Several items were noticeable for the unchoked and sonic cases. The suction peak (maximum velocity) moved downstream with increased pressure, as did the region where the lower surface pressure became constant and positive (frequently called the "separation bubble")

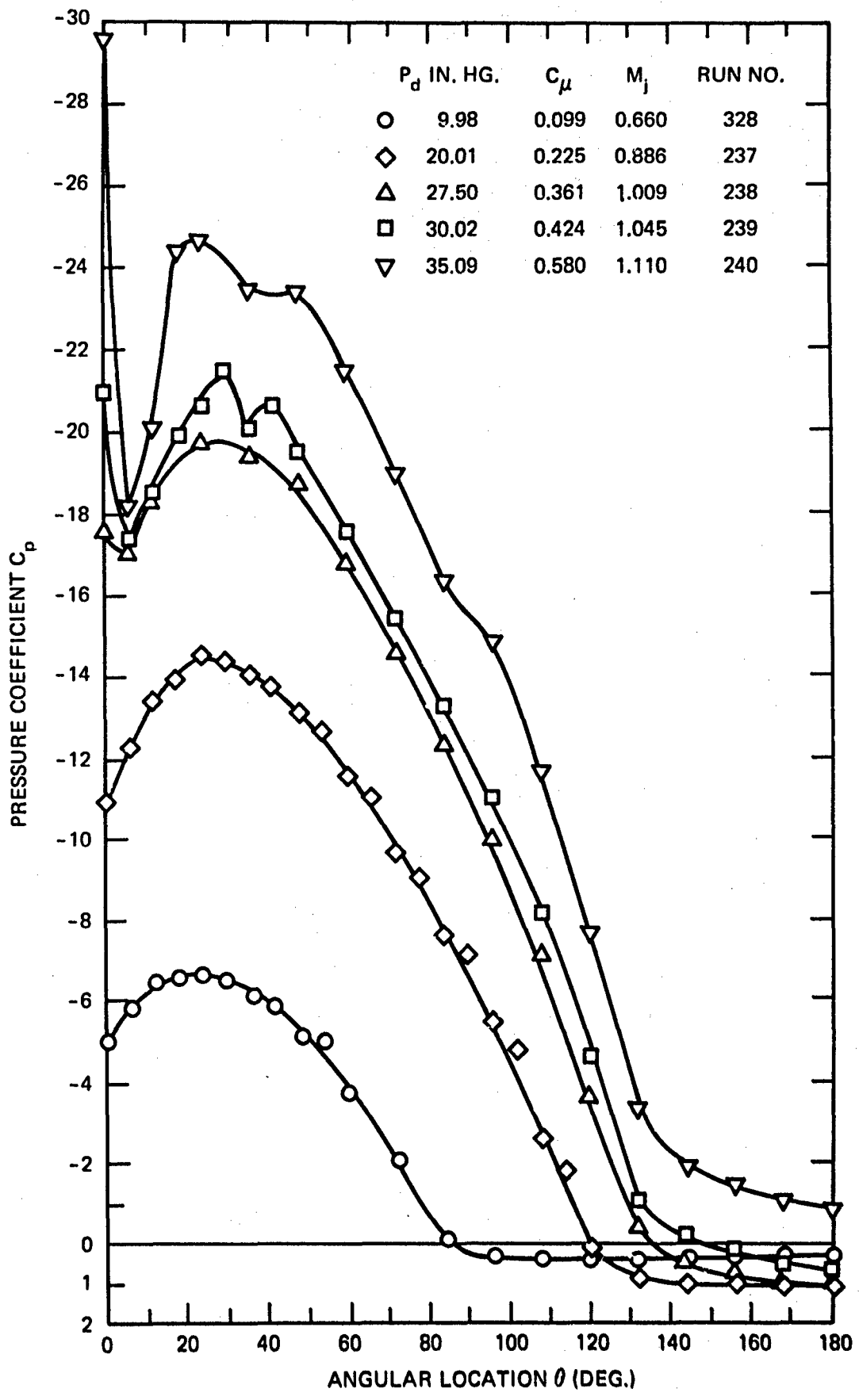


Figure 51 - Trailing Edge Pressure Distributions, $h = 0.013$ Inch, $q_{\infty} = 27.5$ PSF

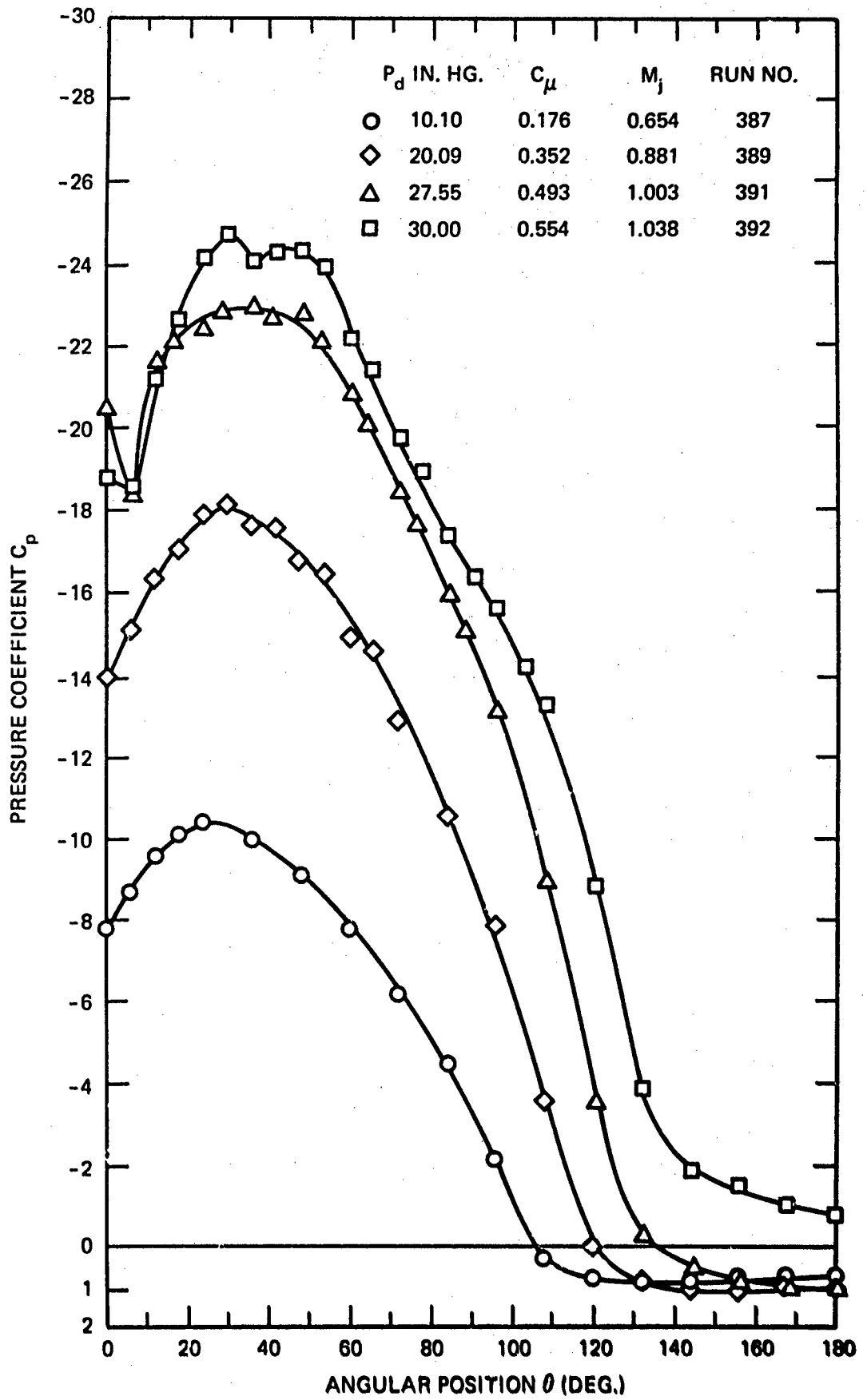


Figure 52 - Trailing Edge Pressure Distributions, $h = 0.032$ Inch, $q_{\infty} = 27.0$ PSF

although the exact separation point or stagnation point within this region is difficult to locate from static pressures alone). Surface oil flow visualization was employed in a small number of cases to locate the bubble; heavy lines of accumulation formed on either end of the region, but oil between was swept away, indicating the circulatory flow there. The suction peak movement indicates increased turning and lift augmentation; this continued to be the case even after the jet became choked. When choking occurred, the "near-slot" pressure began to display the familiar jaggedness suggestive of compression-expansion waves. However, the fact that the lower surface pressure did not reach a constant value, and in fact became more negative with increasing C_{μ} , indicates that the jet had turned through 180 degrees with the high jet pressure and had pushed the separation bubble onto the flat lower airfoil surface. To the degree investigated in these cases, jet of greater than sonic velocity appear to be quite beneficial as long as strong compressibility effects are not present. It should be noted that the jet Mach numbers calculated for each curve are based on isentropic expansions to free-stream static pressure where, in fact, the expansion is actually to the much lower static pressure at the slot exit. Thus true M_j at the slot should be larger than the values listed. It also should be noted that unlike many of the early investigations with lower C_{μ} and jet-to-free-stream velocity ratios of 2 or less, (e.g., Stone and Englar⁸), the present tests are for V_j/V_{∞} of about 7 or 8. With such a large difference between the velocities of the jet and the upper surface boundary layer, it is thus possible that the effects of viscous mixing and entrainment may have far less dominance. This could account for the good agreement in an earlier section between experiment and inviscid theory.

Shear stress measurements were taken at a selected number of trailing edge angular positions along with photographs of the fluctuating oscilloscope traces. Figures 53 and 54 present the shear stress data for the two slot heights as a function of duct pressure. The steep drop in the curves immediately downstream of the slot can apparently be explained in terms of high-speed nozzle flow. The chordwise pressure gradient was favorable for some limited distance downstream of the slot and the jet was essentially a potential core with a thin laminar boundary layer. The shear stress would thus be expected to decrease along that portion of the wall. As the pressure gradient became adverse, the flow became turbulent, resulting in a rapid increase in skin friction. Note that the suction peaks of Figures 51 and 52 nearly coincide with the points of minimum skin friction in Figures 53 and 54. (Closer agreement would probably have resulted if it had been possible to control the trailing edge probe location more precisely. It is estimated that the location is accurate to within 1 degree, but that error can produce significant scatter in the steep region of the shear stress curves for small θ . Nevertheless, it is felt that the trends shown are valid and the data reasonably correct.) The drop revealed in the curves is significant in itself--previous attempts to measure

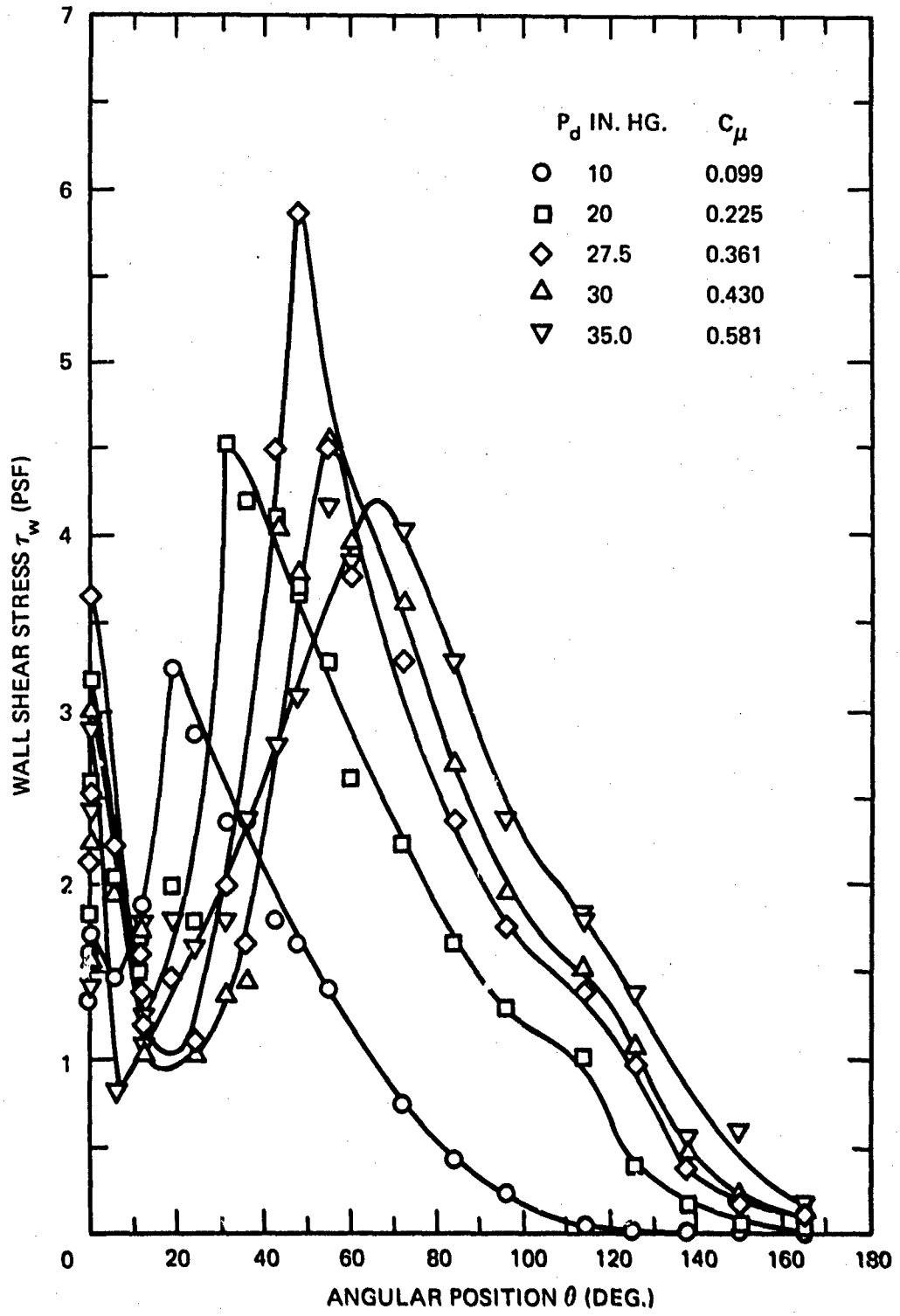


Figure 53 -- Shear Stress Distributions for Five Duct Pressures,
 $h = 0.013$ Inch, $q_\infty = 27.5$ PSF

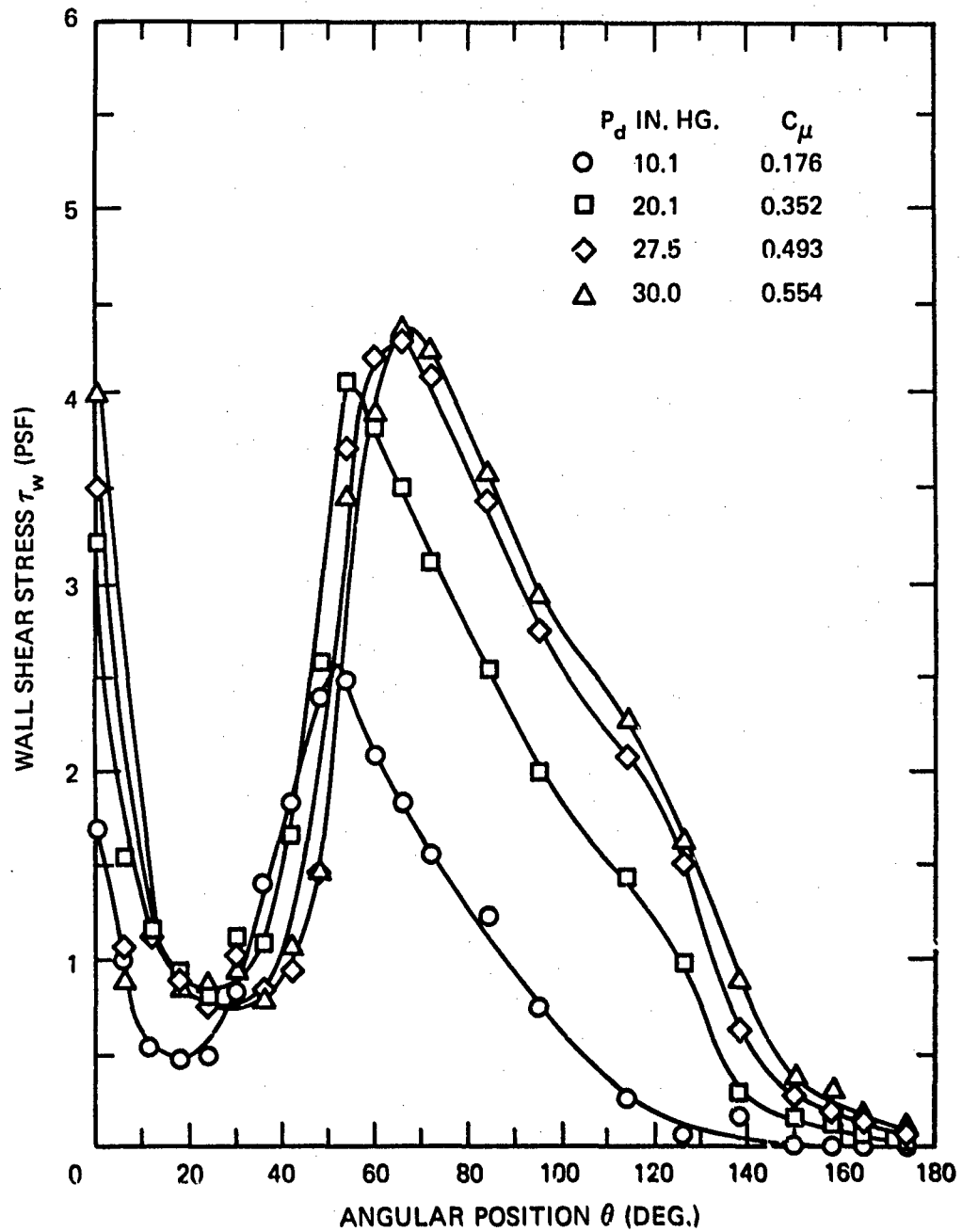


Figure 54 – Shear Stress Distributions for Four Duct Pressures, $h = 0.032$ Inch,
 $q_\infty = 27.5$ PSF

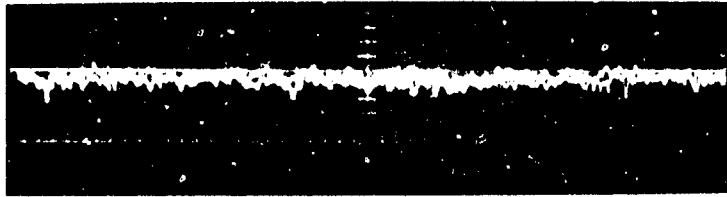
shear stress on a Coanda surface (Fernholz,³⁷ for example) have not indicated its presence primarily because of the use of such devices as Stanton tubes which were not able to accurately measure the flow details so close to both the slot and the surface.

Downstream of this shear stress minimum, the curves rose very rapidly to sharp peaks; these occurred further downstream and were of greater magnitude as duct pressure increased. For the $h = 0.013$ -inch case, it appears that the maximum peak occurred for a choked jet and that the values then dropped for supersonic flow (this result was not apparent for the $h = 0.032$ -inch data). Downstream of the peaks, the shear decreased slightly less rapidly than it rose, but eventually all curves approached very low values. The circumferential location of the point of jet separation from the trailing edge through use of the heat flux gage requires that some care be taken in interpreting the readings. The "separation bubble" usually contains a region of circulating turbulent flow and thus the true separation point is not necessarily indicated by an apparent reading of $\tau_w = 0$. These "eddies" can still cause heat loss from the hot film, and thus a zero shear reading may not be realized. Thus the shear in Figures 53 and 54 tends to stabilize at some constant low value—the jet separation point is approximately indicated by the beginning of this region. As is evident from the data, this separation point occurs further around the airfoil with an increase in duct pressure, even beyond choking.

The behavior of the flow field is more clearly indicated by the oscilloscope traces of Figure 55, which are for the $P_d = 10$ in. Hg and the $h = 0.032$ -inch curve of Figure 54. These traces of the fluctuating bridge voltage were taken at a CRT scan rate of 0.2 cm/msec (each block on the screen is 1 cm in width) and the amplitude is 0.5 V/cm. Since the mean voltage was recorded by the anemometry equipment, it was not of interest here, and thus the oscilloscope horizontal reference was not rezeroed after each run; only the trace amplitudes and fluctuations were of interest. As can be seen, the low amplitude trace at $\theta_{HF} = 0$ degree rapidly yielded to larger amplitude fluctuations as the trough of Figure 54 was approached and then gave way to large turbulence as the shear rapidly increased (i.e., θ_{HF} from 24 to 48 degrees, the beginning of the adverse pressure gradient in Figure 52). As the shear peak was reached (θ_{HF} from 48 to 54 degrees) the fluctuations began to subside and then returned to the low turbulence case (similar to $\theta_{HF} = 0$ degree) on the down side of the curve. As the separation region was reached, the frequency of the fluctuations decreased and then died out completely at very low indicated values of τ_w .

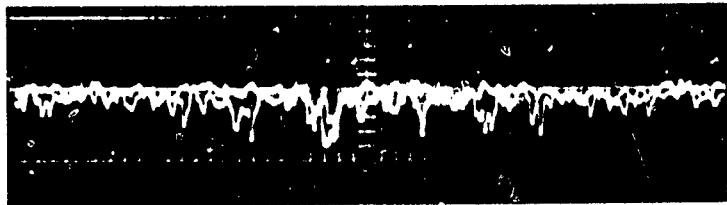
³⁷Fernholz, H. H., "The Deflection of Free Jets at Convexly Curved Walls (Coanda Effect)," National Research Council of Canada Technical Translation 1504, 1971.

Figure 55 – Oscilloscope Traces for $h = 0.032$ Inch, $P_d = 10$ In. Hg,
 $q_{\infty} = 27.5$ PSF



θ_{HF} RUN NO. τ_w , PSF

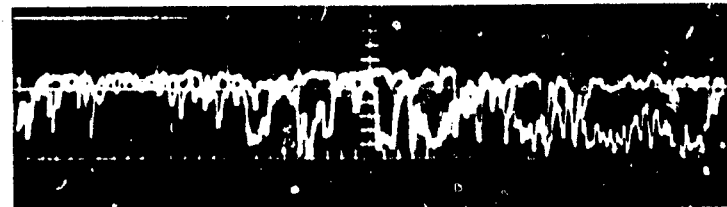
0° 387 1.6914



12° 397 0.5151



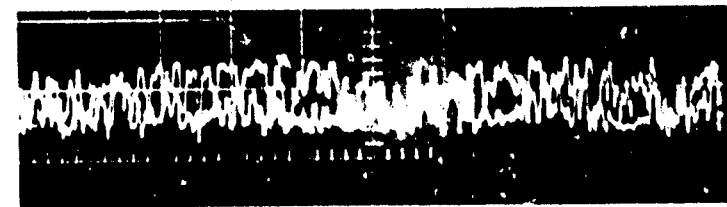
24° 405 0.4838



30° 409 0.8327

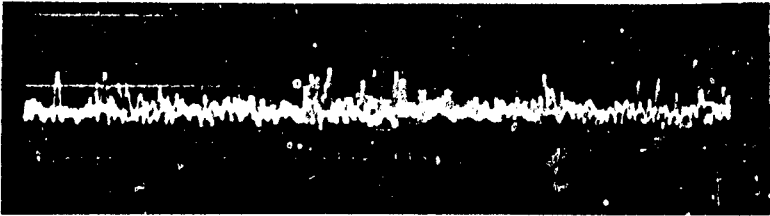
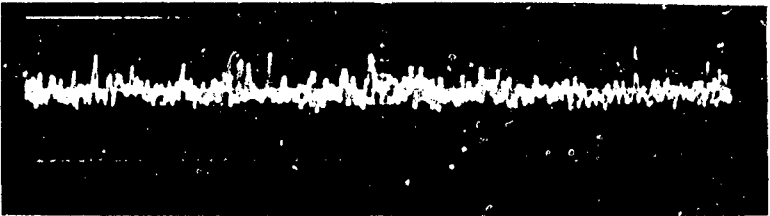
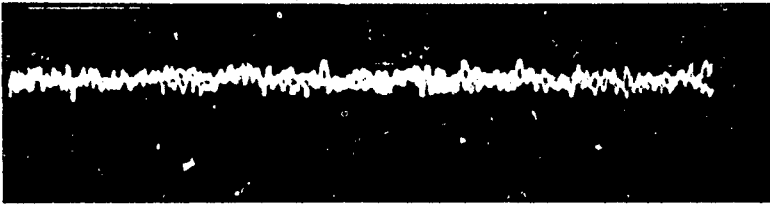
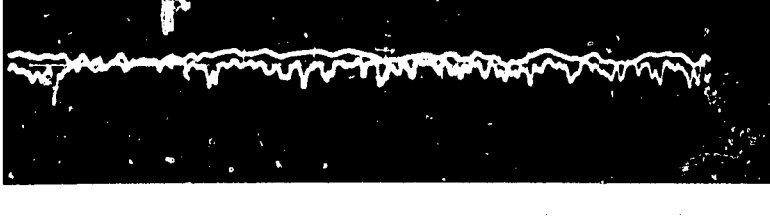

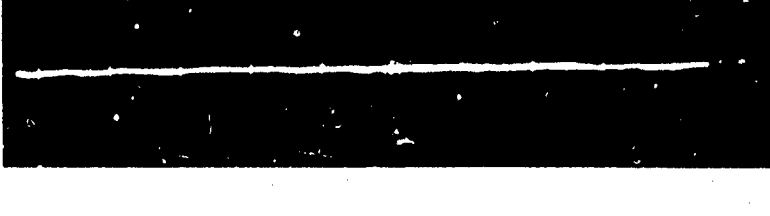


36° 413 1.3902



42° 417 1.8367

Figure 55 (Continued)

θ_{HF}	RUN NO.	τ_w , PSF	
	48°	421	2.3951
	54°	425	2.4897
	95°	453	0.7483
	126°	461	0.0658
	150°	469	0.0084
	174°	477	0.0099

If the curves of Figures 53 and 54 are plotted in terms of momentum and skin friction coefficients, the shear stress data obtained may be somewhat more usable and the results from the two slot heights compared. This is done in Figures 56 and 57, where the angular location θ is also shown in terms of arc length divided by slot height. The expected collapse of the two families of curves into one family independent of slot height did not materialize, even though there was some overlay in the regions aft of the shear peaks. This may be due in part to the incompatibility of C_μ and C_f as "universal" parameters since both parameters are based on free-stream conditions when they should in fact be based on local static pressure, density, and velocity in the jet.

A very useful result did occur, however, when the data were replotted as shown in Figure 58. Curves from Figures 56 and 57 did not allow an accurate determination of the point of zero shear stress for a constant C_μ , but the replot allowed determination of the value of C_μ required to cause the flow to turn just to separation at a given angular location. As Figure 58 shows, these values are obtained by extrapolating the curves for constant θ to $\tau_w = 0$, which is thus said to be indicative of separation.

The empirical tool thus generated is shown as Figure 59, where the separation angle for the two slot heights is plotted as a function of blowing (or, when the C_q versus C_μ relationship is known experimentally, the separation point for a given lift is known). The usefulness of this plot is realized if an attempt is made to theoretically determine pressure distributions by any proven potential flow method. Since for a bluff trailing edge, the rear stagnation point cannot normally be located theoretically, lift for a given configuration at a given incidence is not unique (i.e., the pressure distribution for any desired C_q may be generated). However, if Figure 59 is used to distinctly locate the stagnation point for a given C_μ , the inviscid C_q and the C_p distribution may then be obtained. The validity of this technique is heavily dependent on how closely the separation point from Figure 59 represents the true stagnation point—this is, of course, a function of the length of the separation bubble and the width of the jet wake behind the model. The behavior of the curves of Figure 59 as C_μ goes to zero is not certain, but they seem to become independent of slot height and probably converge almost asymptotically to the point (0,0).

CONCLUSIONS AND RECOMMENDATIONS

The present two-dimensional investigation was originally intended to probe the mechanism for reduction of performance of a CC airfoil in compressible flow. The results indicated that at least up to $M_j = 1.3$, choked Coanda jets did not prove harmful to the lift capabilities of these airfoils at low subsonic speeds, nor did the corresponding pressure ratios of 3 ever produce detachment of the jet with or without an external flow. Further conclusions from

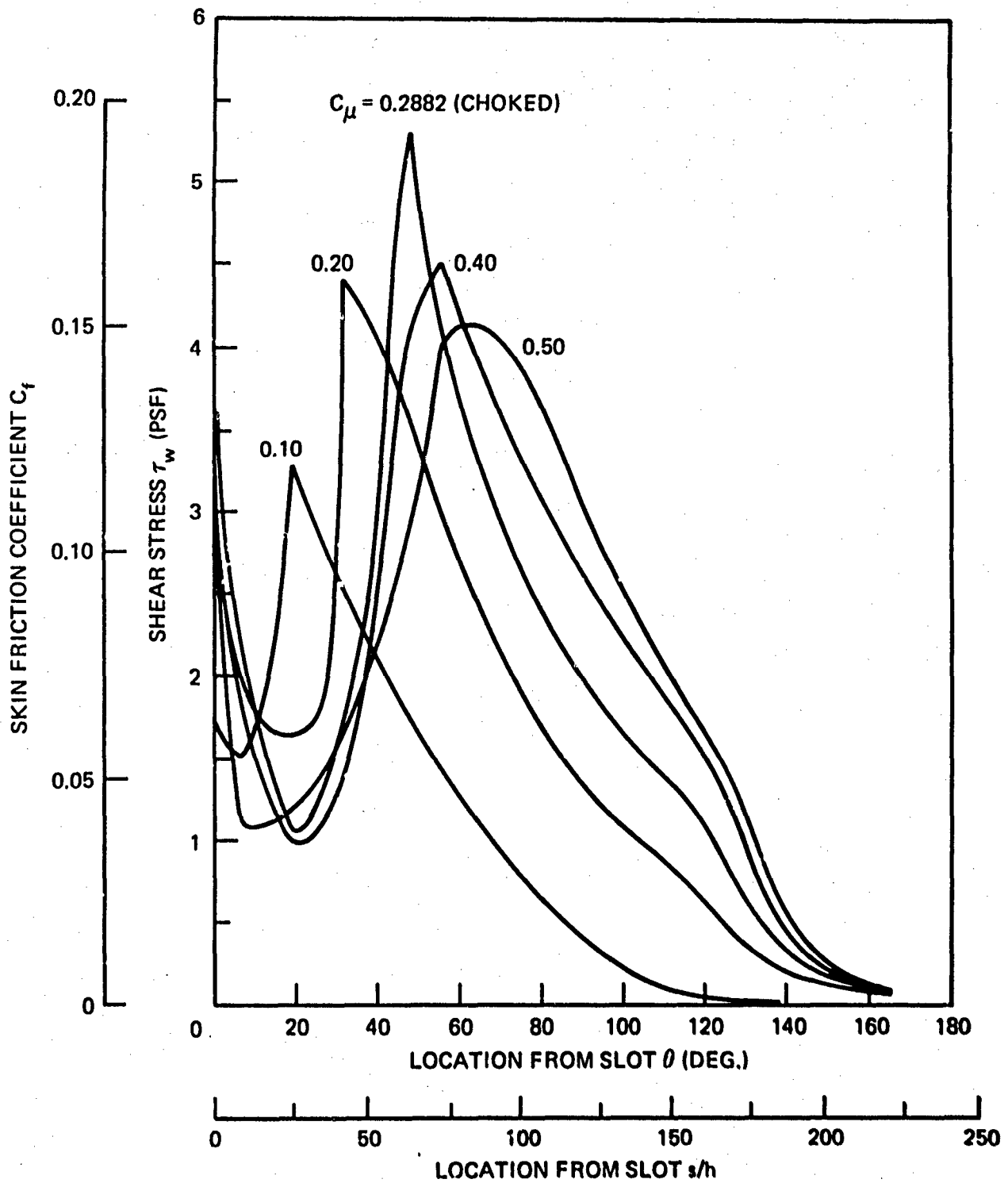


Figure 56 – Skin Friction Coefficient Distributions for Five Momentum Coefficients, $h = 0.013$ Inch, $q_\infty = 27.5$ PSF

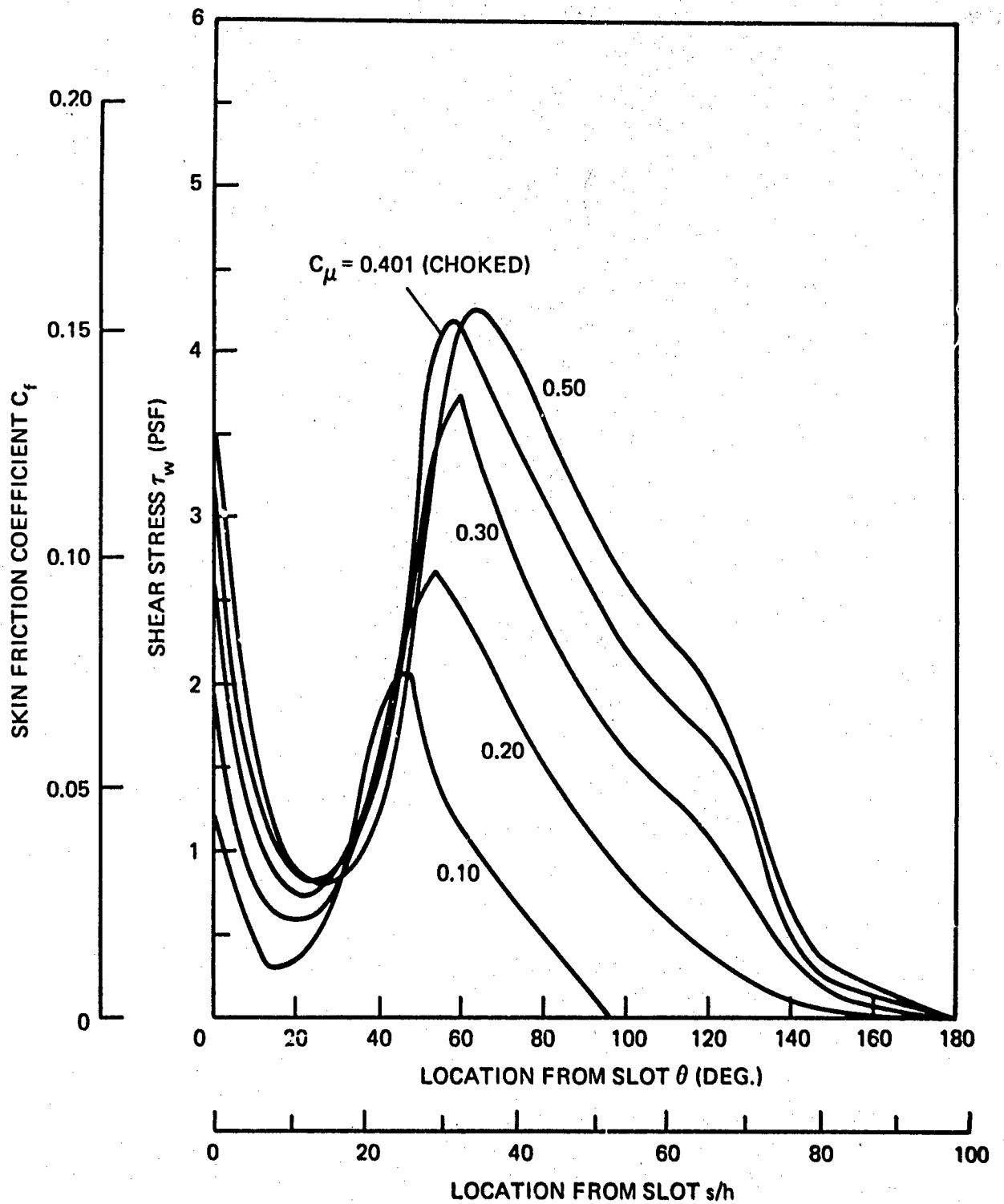


Figure 57 – Skin Friction Coefficient Distributions for Four Momentum Coefficients, $h = 0.032$ Inch, $q_\infty = 27.5$ PSF

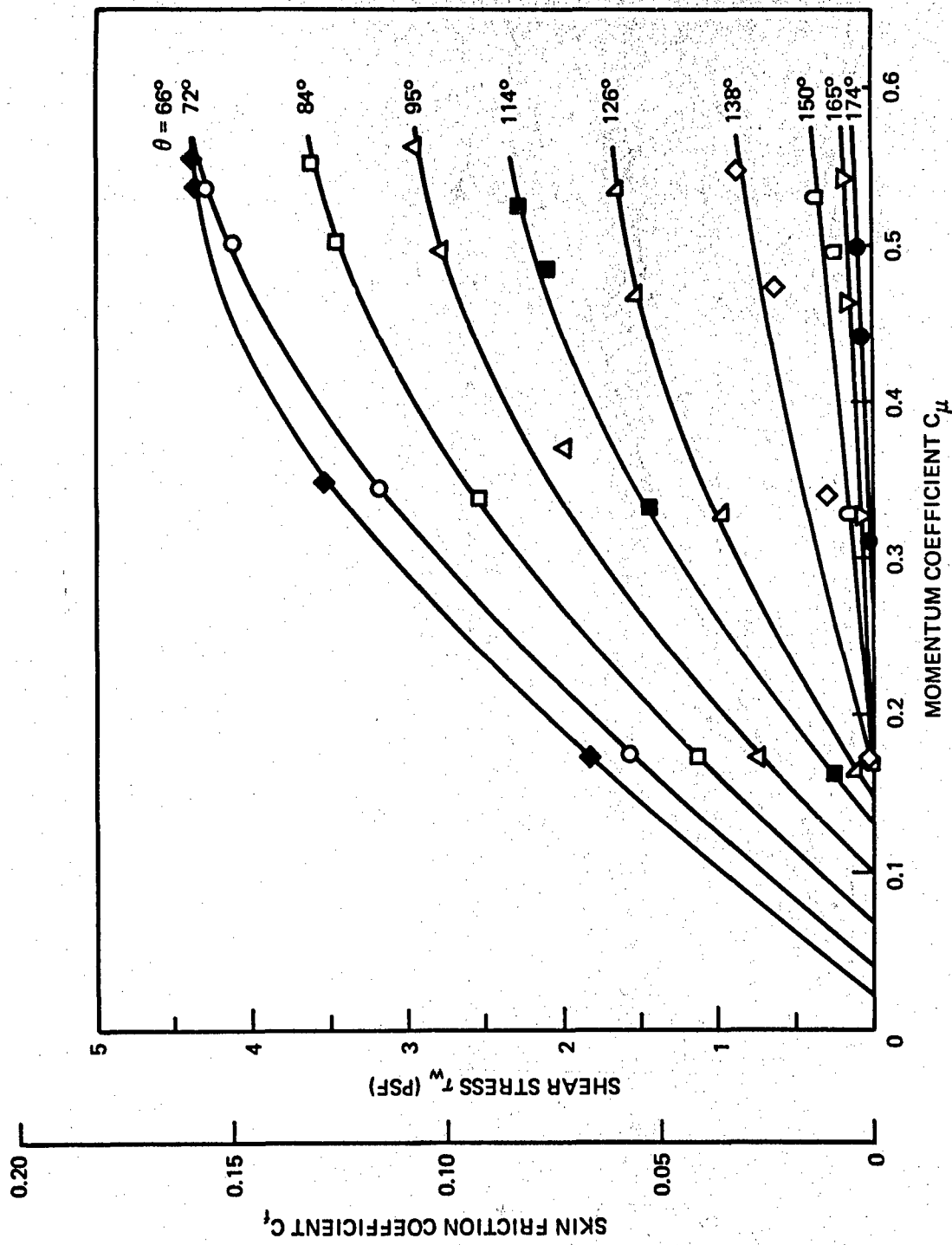


Figure 58 - Skin Friction as a Function of Blowing for Constant Angular Position, $h = 0.032$ Inch, $q_\infty = 27.5$ PSF

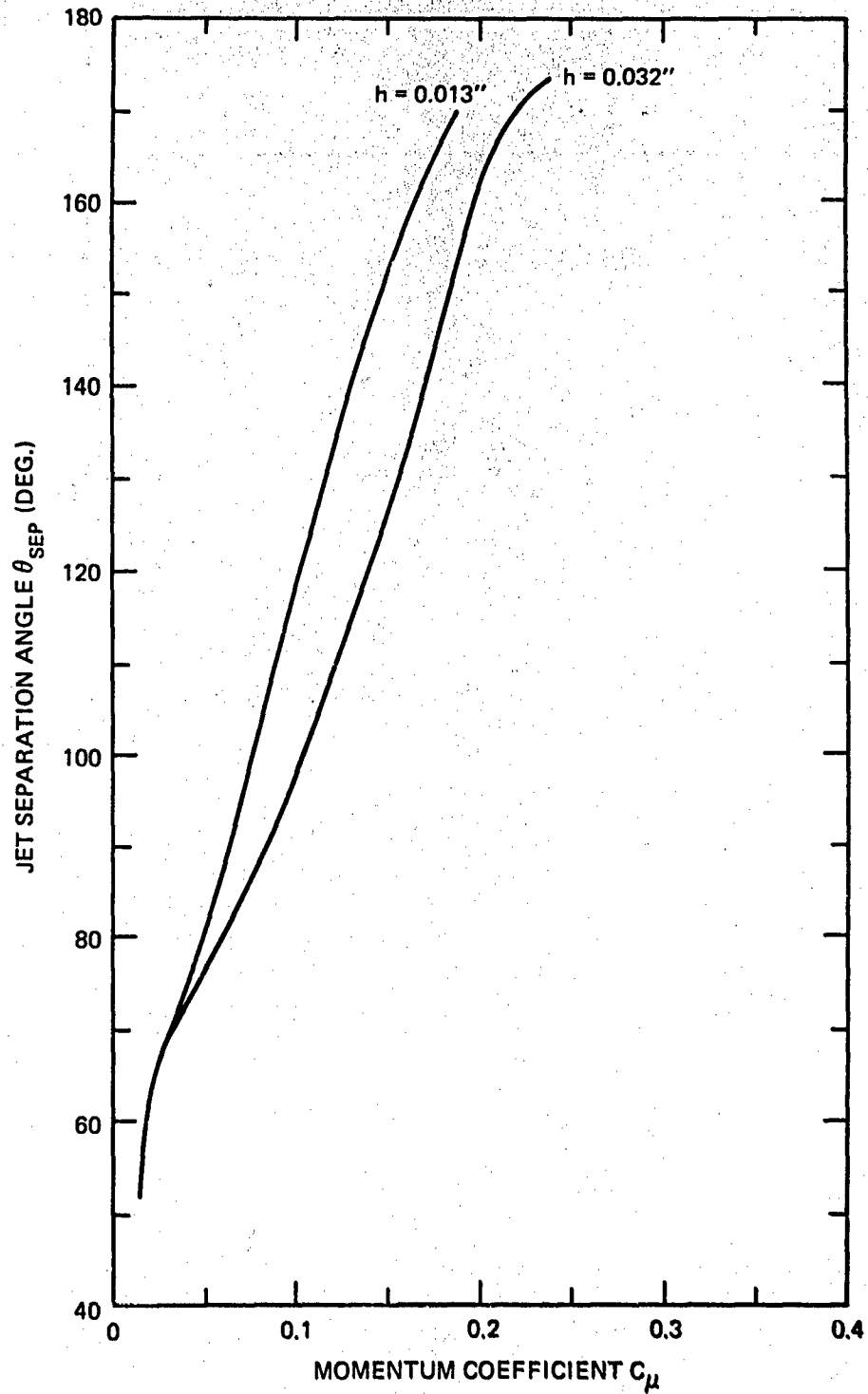


Figure 59 – Location of Jet Separation Point for Two Slot Heights as a Function of Blowing, $q_\infty = 27.5$ PSF

the test results provide new insight into the understanding of circulation control airfoils operating with high jet-to-free-stream velocity ratios:

1. Significant differences exist in both the chordwise and normal pressure distributions between static (no free stream) and dynamic operation of a Coanda trailing edge. Thus it is felt that any attempt to predict dynamic performance from static results is not valid. For this reason, the static jet detachment curves presented by various investigators are probably not accurate indications for higher pressure ratio operation since an external flow field should have considerable effect on them.

2. Contrary to the assumption made in conventional boundary layer theory, measurements indicated significant changes in static pressure across the jet.

3. As had previously been indicated, larger slot heights were found to produce reduced Coanda turning (and thus lift) for a constant C_{μ} ; this was true for both static and dynamic cases.

4. Choked and supersonic jet velocities were found to produce expansion-compression type pressure fluctuations downstream of the slot, but these damped out and had little adverse effect on airfoil lift. Above choking, peak shear stress was less than that for an unchoked jet.

5. Hot film shear stress measurements indicated a rapid drop and then a rise in skin friction just downstream of the slot because of jet inner layer laminar-to-turbulent transition. To the author's knowledge, this has never previously been shown experimentally for Coanda surfaces; previous probe devices have not been able to measure so close to the surface or the slot without flow disturbance.

6. Hot film measurements showed that the peak shear stress location, the following adverse pressure gradient, and the jet separation point all move downstream with an increase in duct pressure, even after the choking value is reached.

7. The shear stress measurements enabled a determination of jet separation point; it was then possible to correlate the theoretical airfoil pressure distributions and lift with the momentum coefficient.

The above results suggest the following areas for further research:

1. A similar investigation should be conducted in a tunnel with much larger height-to-chord ratio and increased blowing air supply so that the present test limitations can be exceeded and subsonic detachment criteria established.

2. Compressibility effects and relationship, if any, to jet detachment should be determined in a high-speed facility.

3. Extensive flow visualization (optical, such as Schlieren to locate embedded compression waves, or oil flow, etc.) should be employed in any future work.

4. Upper surface boundary layer characteristics just upstream of the slot should be investigated to increase knowledge of their relationship to the high-speed wall jet.

5. The trailing edge rotation should be mechanized so that a sweep around the entire 180 degrees could be made for each run, rather than setting each θ and duplicating the previous flow condition.

REFERENCES

1. Cheeseman, I. C. and A. R. Seed, "The Application of Circulation Control Blowing to Helicopter Rotors," Journal of the Royal Aeronautical Society, Feb and Jul 1966.
2. Wilkerson, J. B., K. R. Reader, and D. W. Linck, "The Application of Circulation Control Aerodynamics to a Helicopter Rotor Model," Paper 704, 29th Annual National Forum of the American Helicopter Society, Washington, D. C., May 1973.
3. Williams, R. M. and E. O. Rogers, "Design Considerations of Circulation Control Rotors," Paper 603, 28th Annual National Forum of the American Helicopter Society, Washington, D. C., May 1972.
4. Englar, R. J., "Two-Dimensional Subsonic Wind Tunnel Tests of Two 15-Percent Thick Circulation Control Airfoils," Aug 1971, Naval Ship Research and Development Center Tech Note AL-211. (AD 900 210L)
5. Englar, R. J., "Two-Dimensional Subsonic Wind Tunnel Tests of a Cambered 30-Percent Thick Circulation Control Airfoil," May 1972, Naval Ship Research and Development Center Tech Note AL-201. (AD 913-411L)
6. Williams, Robert M. and Harvey J. Howe, "Two-Dimensional Subsonic Wind Tunnel Tests on a 20 Percent Thick, 5 Percent Cambered Circulation Control Airfoil," Washington, D.C., Aug 1970, Naval Ship Research and Development Center Tech Note AL-176. (AD 877-764)
7. Englar, R. J., "Two-Dimensional Transonic Wind Tunnel Tests of Three 15-Percent Thick Circulation Control Airfoils," Dec 1970, Naval Ship Research and Development Center Tech Note AL-182. (AD 882-075).
8. Stone, M. B. and R. J. Englar, "Circulation Control—A Bibliography with Selected References," Jul 1973, Naval Ship Research and Development Center Report 4108.
9. Griswold, R. W., "Circulatory Jet Airfoils," United States Patent 2,885,160, 5 May 1959.
10. Kizilos, A. P. and R. E. Rose, "Experimental Investigations of Flight Control Surfaces Using Modified Air Jets," St. Paul, Minn., Nov 1969, Honeywell, Inc. Document 12055-FR1, (DDC AD 864-2716).
11. Englar, R. J. and R. M. Williams, "Design of a Circulation Control Stern Plane for Submarine Applications," Mar 1971, Naval Ship Research and Development Center Tech Note AL-200. (AD 901-198)
12. Tararine, S. and R. Dorand, "Determination Through Wind Tunnel Tests and Analytical Methods of the Optimum Deflection Devices Suitable for Use on Jet Flap Helicopter Rotor Blades," Dec 1960, European Research Office, U. S. Dept. of the Army, Report DE2013.

13. Lowry, J. G., J. M. Riebe, and J. P. Campbell, "The Jet-Augmented Flap," Paper 715, 25th Annual Meeting of the Institute of the Aeronautical Sciences, New York, Jan 1957.
14. Bailey, A. B., "Use of the Coanda Effect for the Deflection of Jet Sheets over Smoothly Curved Surfaces, Part I," Aug 1961, University of Toronto Institute of Aerophysics Tech Note 51.
15. Roderick, W. E. B., "Use of the Coanda Effect for the Deflection of Jet Sheets over Smoothly Curved Surfaces, Part II," Sep 1961, University of Toronto Institute of Aerophysics Tech Note 49.
16. Egli, W. H., "An Approximate Analysis of the Criterion for Detachment of a Supersonic Jet from the Surface of a Right Circular Cylinder," Feb 1968, Honeywell, Inc., Memorandum MR 10235.
17. Seed, A. R., "Detachment of Wall Jets from Curved Surfaces," Apr 1969, Paper published by the National Gas Turbine Establishment, Pyestock, Hants, England.
18. Bradfield, W. S. and G. E. Yale, "Small Pitot Tubes with Fast Pressure Response Time," Journal of the Aeronautical Sciences, Oct. 1951.
19. Sturek, W. B. and J. E. Danberg, "Experimental Measurements of the Supersonic Boundary Layer in a Region of Moderate Adverse Pressure Gradient," Paper 71-162, AIAA 9th Aerospace Sciences Meeting, New York, Jan 1971.
20. Thom, A., "Blockage Corrections in a Closed High-Speed Tunnel," Nov 1943, Aeronautical Research Council R & M 2033.
21. Liepmann, H. A. and A. Roshko, "Elements of Gasdynamics," John Wiley and Sons, Inc., New York, 1967.
22. Liepmann, H. A. and G. T. Skinner, "Shearing-Stress Measurements by Use of a Heated Element," Nov 1954, NACA Technical Note 3268.
23. Dhawan, S., "Direct Measurements of Skin Friction," 1953, NACA Report 1121.
24. Pai, B. R. and J. H. Whitelaw, "Simplification of the Razor Blade Technique and its Application to the Measurement of Wall-Shear Stress in Wall-Jet Flows," The Aeronautical Quarterly, Vol. XX, Part 4, pp. 355-364, Nov 1969.
25. Fage, A. and V. M. Falkner, "Relation Between Heat Transfer and Surface Friction for Laminar Flow," 1931, Aeronautical Research Council R & M 1408.
26. Bellhouse, B. J. and D. L. Schultz, "Determination of Mean and Dynamic Skin Friction, Separation, and Transition in Low-Speed Flow with a Thin-Film Heated Element," Journal of Fluid Mechanics, Vol. 24, Part 2, pp. 379-400, Feb 1966.

27. Geremia, J. O., "Experiments on the Calibration of Flush Mounted Hot Film Sensors," in "DISA Information, Measurement, and Analysis," No. 13, May 1972.
28. Brown, G. L., "Theory and Application of Heated Films for Skin Friction Measurement," Paper 18, Proceedings of the 1967 Heat Transfer and Fluid Mechanics Institute, pp. 361-381, Jun 1967.
29. Pope, R. J., "Skin Friction Measurements in Laminar and Turbulent Flows Using Heated Thin Film Gages," AIAA Journal, Vol. 10, No. 6, pp. 729-780, Jun 1972.
30. Owen, F. K. and B. J. Bellhouse, "Skin Friction Measurement at Supersonic Speeds," AIAA Journal, Vol. 8, No. 7, pp. 1358-1360, Jul 1970.
31. Laufer, J. and R. McClellan, "Measurements of Heat Transfer from Fine Wires in Supersonic Flows," Journal of Fluid Mechanics, Vol. 1, Part 3, pp. 276-289, Sep 1956.
32. Schlichting, H., "Boundary Layer Theory," 6th ed. McGraw Hill, New York, 1968.
33. Kuethe, A. M. and J. D. Schetzer, "Foundations of Aerodynamics," 2nd ed. John Wiley and Sons, Inc., New York, 1964.
34. Englar, R. J. and R. M. Williams, "Test Techniques for High Lift Two-Dimensional Airfoils with Boundary Layer and Circulation Control for Application to Rotary Wing Aircraft," Canadian Aeronautics and Space Journal, Vol. 19, No. 3, pp. 93-108, Mar 1973.
35. Kind, R. J., "A Proposed Method of Circulation Control," Ph.D. Thesis, Clare College, Cambridge University, 1967.
36. Dunham, J., "Circulation Control Applied to a Circular Cylinder," Jul 1967, National Gas Turbine Establishment Report 287. (AD 821-006)
37. Fernholz, H. H., "The Deflection of Free Jets at Convexly Curved Walls (Coanda Effect)," National Research Council of Canada Technical Translation 1504, 1971.

INITIAL DISTRIBUTION

Copies	Copies
1 OASECNAV/SPECIAL ASST (AIR)	2 NASA HQS 1 Code RAA 1 A. Gessow
1 USAAMRDL/Ft. Eustis	
1 USAAMCA/AMXAM-SM	4 NASA Ames 1 USA Air Mobility R&D Lab 1 Full-Scale Res Div 1 Tech Lib 1 M. Kelly/Lg-Scale Aerodynamics
1 CNO/077	
1 CMC/A. L. Slofkosky (AX)	
1 NAVMAT/H. G. Moore (884 CO-6)	2 NASA Langley Res Cen 1 J. P. Cambell 1 Tech Lib
1 NRL/Lib 2029	
2 ONR 1 MS 48 1 ONR 461	1 West Va U/J. Loth
1 USNA/Lib	1 Analytical Methods Inc F. Dvorak
1 NAVPGSCOL/Lib	1 Boeing Co/Vertol Div Tech Lib
1 NAVAIRDEVGEN/Tech Lib	1 Bell Aerospace Corp Bell Helicopter/Ft Worth
8 NAVAIRSYSCOM 1 AIR 03PA 1 AIR 320D 1 AIR 50174 1 AIR 5302 1 AIR 53011 1 AIR 53012 1 AIR 53014 1 AIR 54041	1 Cornell Aeronautical Lab, Inc A. Ritter/App Mechs Dept
1 NAVAIRTESTCEN/TPS	3 Gen Dyn Convair San Diego 1 Tech Lib 1 H. Yoshihara/582-00 1 E. S. Levinsky/631-00
12 DDC	1 Fairchild-Hiller/Germantown Tech Lib
1 HQS, USAFRDT-EX/Res & Tech	1 Grumman Bethpage/M. Siegel
2 USAFFDL 1 XFV/VTOL Tech Div 1 FXM/Aeromechanics Br	1 Honeywell Minneapolis R. E. Rose/Sys & Res Div
1 USAFOSR/Mechanics Div	1 Lockheed Burbank/Lib
1 FAA/V/STOL Programs (DS-22)	2 Lockheed Georgia 1 Y. T. Chin 1 Advanced Flight Services
	1 Kaman Aircraft Corp

Copies

1 Ling-Temco-Vought/Tech Lib
2 McDonnell-Douglas/Long Be
1 A. M. O. Smith/36-81
1 M. Lopez
1 Northrop A/C Hawthorne/Lib
1 Rochester Appl Sci Asso, Inc
R. P. White
1 Singer-General Precision, Inc
L. S. Galwin
2 United A/C Corp
1 Research Department
1 Sikorsky Aircraft Division

CENTER DISTRIBUTION

Copies	Code	
1	0000	CAPT M. C. Davis
10	1600	H. R. Chaplin
1	1606	S. de los Santos
1	1615	R. M. Williams
4	1619	D. G. Kirkpatrick
1	1660	J. H. Nichols
20	1660	R. J. Englar
30	5211	Reports Distribution
1	5221	Library (C)
1	5222	Library (A)
2	5223	Aviation Collection